FABRICATION AND TESTING OF COMPUTER GENERATED HOLOGRAMS USING THE MLA 150

by

Kira Purvin

A Thesis Submitted to the Faculty of the

James C. Wyant College of Optical Sciences

In Partial Fulfillment of the Requirements

For the Degree of

MASTER OF SCIENCE

In the Graduate College

THE UNIVERSITY OF ARIZONA

2021

THE UNIVERSITY OF ARIZONA
GRADUATE COLLEGE

As members of the Master's Committee, we certify that we have read the thesis prepared by **Kira Marie Purvin**, titled ***Fabrication and Testing of Computer Generated Holograms using the MLA 150*** and recommend that it be accepted as fulfilling the thesis requirement for the Master's Degree.

Professor Thomas D. Milster Date: 12/3/2021

Daewook Kim
Professor Daewook Kim Date: _____

Youngsik Kim
Professor Young Sik Kim Date: _____

_____ Date: _____

Final approval and acceptance of this thesis is contingent upon the candidate's submission of the final copies of the thesis to the Graduate College.

I hereby certify that I have read this thesis prepared under my direction and recommend that it be accepted as fulfilling the Master's requirement.

Professor Thomas D. Milster Date: 12/3/2021
Master's Thesis Committee Co-Chair
Wyant College of Optical Sciences

Signature: Daewook Kim
Email: dkim@optics.arizona.edu

Signature:
Email: yskim@optics.arizona.edu

Acknowledgements

Throughout the writing of this thesis I have received a great deal of support and assistance.

I would first like to thank my supervisor, Professor Tom Milster, whose expertise was invaluable in formulating research questions and methodology. Your countless insights pushed me to sharpen my thinking and elevated my work to a higher level of standards.

I would also like to thank my parents for their undying support of my studies as well as my closest friends and colleagues. You have always been there for me and without your support I wouldn't be where I am today.

TABLE OF CONTENTS

List of Figures

List of Tables

1 ABSTRACT

Grayscale lithography is a powerful technique that makes it possible to fabricate three-dimensional microstructures in photoresist. This thesis presents a newly developed process for achieving high quality grayscale lithography using the MLA 150 as well as initial results for various applications. Multiple photoresists including S1813, S1827 and AZ P4620 are characterized to provide a foundation for the developed fabrication process. A linearization regime is also presented that calibrates the MLA 150's nominal grayscale output such that a result displaying equally spaced gray layers is achieved. The final grayscale lithography process is applied to fabricate a computer generated hologram (CGH) for use in adaptive optics for phase retrieval. A replication process is detailed that enables the exposed patterns to be replicated in NOA61 to form a usable and semi-permanent optical element. Comparisons made between the fabricated optical elements and the original designs demonstrate the success of the fabrication process.

2 INTRODUCTION

Despite there being many lithography techniques, the modern approach to optical lithography utilizes a photomask-less lithography technology to focal-spot write the designed pattern onto the substrate via UV radiation. These maskless writers enable the fabrication of grayscale exposures without the need to fabricate multiple masks. This project details the process development for grayscale optical lithography through the use of three different types of photoresists. The material properties of photoresist and its response to UV-radiation require each individual photoresist to be characterized such that its exposure response can be measured and calibrated. Using this photoresist characterization, a linearization regime can be applied to any grayscale pattern such that the resulting exposure has equally sized gray-layers. In this thesis, a simple calibration ramp pattern is developed that serves as a metrology tool for quantifying the success of the fabrication process. The linearization regime consists of multiple MATLAB scrips that utilize the fabricated ramp profiles to isolate linearly behaving portions of the resists' total depth.

Furthermore, direct replication techniques utilizing NOA 61 allow the rapid fabrication of high-quality micro-optical elements such that each design/fabrication/testing iteration can be performed in a single day. The exposed grayscale patterns are first stamped into NOA 61 and cured under UV lights. Once the two samples are separated, the hardened NOA 61 will have the inverse of the exposed pattern stamped into it. The ability to perform highly iterative design processes on grayscale elements has allowed for its use in many applications involving the need for CGHs.

This thesis covers the fabrication of CGHs for applications in adaptive optics for phase retrieval. For the adaptive optics application, a CGH test setup is created in order to verify the successful fabrication of the CGH. A description of the test setups used as well as their detailed alignment is given. For the application in aberration correction the design process for the CGH is

outlined as well as the parameters for the CGHs future use. Overall, the developed grayscale lithography fabrication process is presented as well as its initial results for its various applications.

3 BACKGROUND

This thesis covers a broad range of topics centered around lithography. The fundamental concepts of lithography and various applications are outlined in this chapter. Lithography is first introduced, and a general procedure is given. Grayscale lithography is then presented as a specific type of lithography. Finally, the various applications discussed in this thesis are discussed.

3.1 Fundamentals of Lithography

Optical lithography as used in this thesis is the process by which specific patterns are exposed onto a photoresist-coated substrate, and then exposed areas of the resist are removed during a chemical development. Lithography specifically covers the process of defining and exposing the pattern on the substrate. Exposing a pattern into photoresist affects the resist material, such that material properties change to be less resistant to being removed during development in proportion to the light level of the exposure. The process of lithography starts with comprehensive sample preparation in order to ensure that the resist coating adequately adheres to the sample. The sample is then coated with resist via spin-coating at a specific speed and time in order to control the coating thickness. Next, the sample is loaded into a lithographic instrument that exposes the resist with ultraviolet (UV) light in a pattern on the resist surface. Finally, post-exposure processes are applied, where the sample is immersed in developer that dissolves the exposed portions of the resist. This process results in a topographical microstructure in the resist coating. Depending on the application, this microstructure can form the final product, or it can be transferred onto a more permanent material via etching or replication. In this chapter an overview of lithography procedures and relevant terms is given.

Photoresist is a key material in the optical lithography process that greatly affects the overall success of an exposure. Since it is the photoresist's chemical change that dictates the topographic change in development, it is vital to understand the process by which developed photoresist forms the microstructures being printed. Photoresists are divided into two main groups, positive-tone and negative-tone resists. Positive photoresists exhibit the behavior where exposed sections of the photoresist become soluble to the developer solution, and are the type used in this thesis. The remaining unexposed portions of the photoresist remain insoluble in the developer. Negative photoresists exhibit the behavior where the portions of the photoresist that are exposed become insoluble in developer solution. The remaining unexposed portions of the sample are soluble by the developer and dissolve [1]. Modern positive photoresists consist of diazonaphthoquinone (DNQ) molecules blended into a novolac resin. The DNQ molecules nominally impede the solubility of the resin. When exposed to UV radiation, DNQ molecules begin a rearrangement reaction and produce a carboxylic acid byproduct that increases the solubility of the solution [2]. The large difference in dissolution rates between the exposed and unexposed regions is what enables high-resolution printing in DNQ/novolac systems.

The type of developer used, as well as its application method, greatly affects the quality of the final product, since the chemical development forms the topographical patterns. Some developer methods include spray, puddle, hybrid and immersion development. Spray development involves applying a specific amount of developer over a spinning sample before rinsing and drying. Puddle development entails enough developer to be placed on the sample such that a surface bubble develops from the tension. The developer is left on the sample for the allotted time before being rinsed and dried. Hybrid development involves a process of puddle development followed by spray development. Immersion development consists of simply immersing the sample in

developer either with or without agitation for a period of time before rinsing and drying the sample. In this thesis, immersion development is used.

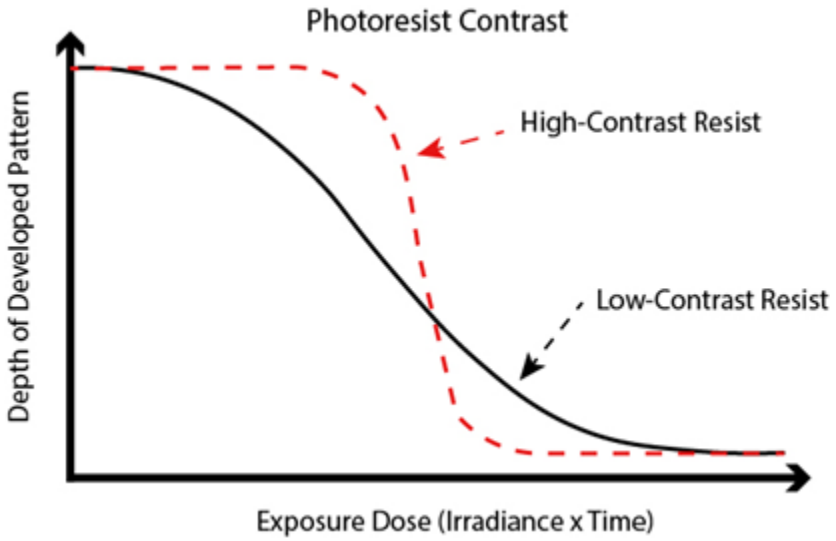

Figure 1 Chart demonstrating the response of different contrast photoresists when an increasingly higher dosage of light energy is used. Binary applications utilize a high-contrast photoresist, where there is a steep curve from minimum to maximum depth that occurs over a small dosage range. Grayscale applications utilize a low-contrast photoresist, which are characterized by a gradual change in depth over a large dosage range [3]**.**

The relationship between the exposure dosage of the lithography instrument and the resulting physical pattern depth is known as photoresist contrast. Many lithographic applications use binary exposure, where a high contrast photoresist is used, as shown in Figure 1. Photoresists that are high contrast have a small difference between the maximum and minimum depth in terms of the required dosage to achieve each. Applications, like making computer-generated holograms described in this thesis, require a grayscale exposure. Grayscale exposure utilizes a low-contrast photoresist that exhibits a gradual change in depth in relation to increasing dose. Both resist types have a minimum dose threshold, where any dose lower than the threshold will not result in any significant physical depth change after development. Likewise, going beyond a maximum exposure threshold means that the depth of the pattern has reached the maximum thickness of the

photoresist. Since the depth of the photoresist after development varies depending on which specific photoresist is used and processing conditions, exposure/dose characteristics must be determined for each type of resist and processing conditions.

3.2 Grayscale Lithography

In binary lithography, sharp-walled, two-level structures are formed in the developed pattern that are determined by exposure doses either above or below a threshold dose, as shown in Figure 1. Grayscale lithography is an evolution of binary lithography, where smooth topographical features are formed in the photoresist that are a function of a continuous exposure dose. The ideal physical profile of grayscale lithography then approaches a linear progression from zero exposure to maximum exposure. The exposure and subsequent etching of gray-scale exposures exponentially increases in difficulty in comparison to binary lithography. In this thesis, grayscale lithography is implemented with a mask-less lithography tool. The ability to change patterns constantly between design iterations as well as exposure patterns in a single pass provides much needed versatility. The resulting variable-depth steps/layers of grayscale lithography are achieved by modulating the dose through setting incident source irradiance appropriately onto each pixel. Pixelated mapping directs the variable dosage to precise locations on the photoresist-coated sample. A precise coupling of low-contrast photoresist paired with appropriate dose produces three-dimensional structures on the micro- and nanoscale. This section gives an overview of grayscale lithography applications, processes and development.

There is currently a high demand for 3D patterned substrates for applications such as LEDs, blazed gratings for waveguides, medical devices, and various diffractive optical elements [4]. While there are various methods of producing high precision 3D microstructures, such as mechanical milling, these methods can be time consuming and costly. Challenges also arise with

their limited throughput and resolution that further hinder the scalability of these methods. The need for highly scalable processes in fields such as semiconductor manufacturing have led to great improvements in the field of 3D or grayscale photolithography. The continued development of mask-less, direct-laser-writing lithography systems has enabled rapid and more affordable prototyping of diffractive optical structures.

A vital attribute of grayscale lithography is being able to precisely control the localized exposure on the coated sample. One method for accomplishing this task is the implementation of an acousto-optic modulator (AOM) and an acousto-optic deflector (AOD). AOMs enable grayscale writing by accurately controlling the source power transmitted through them. AODs are change the angle of light passing through them, which change the position of the focused spot on the sample along a scan line. Both AOMs and AODs are acousto-optical crystals linked to a piezoelectric transducer. The vibrations resulting from the electric signal in the radiofrequency range are transmitted into the crystal as sound waves that create localized cosinusoidal changes in the surrounding optical density, and, hence, refractive index. Light passing through the crystal is diffracted into an angle that is proportional to the transducer drive frequency according to Bragg diffraction. By placing an aperture on the output to limit deflected at high angles and using a binary drive envelope to the transducer signal, transmitted light can be switched on and off at very high speeds with an AOM. In addition, the power of the AOM radiofrequency signal is varied to change the diffraction efficiency into the high-angle beam, thus producing a high-speed, variable power transmission. This means that the exposure dose is defined by the AOM as it controls the laser beam intensity during scanning of the substrate. An AOD uses a similar principle, except there is no exit aperture and the power of the transducer signal is constant. By changing the AOD transducer drive frequency, the output beam is scanned over a range of angles that are then focused

into the photoresist along a line, where position along the line is proportional to the drive frequency. The main parameters affecting the lateral resolution in AOD/AOM systems pertain to the instrument itself. The wavelength (commonly 405nm) is one large factor, as well as the instrument's write mode, which is a combination of pixel size and the lens being used. The spot size for a typical grayscale lithography instrument is about 800nm in diameter [4].

While pixelated AOM/AOD grayscale lithography systems are very precise, this method is very slow when large pattern areas are required, due to the required mechanical scanning of the focus line over a two-dimensional sample. An alternative to this type of system is to use a digital micromirror device (DMD) that acts as an adjustable spatial light modulator (SLM) projection mask that images the design exposure onto the substrate [5]. While these systems are much faster than their scanning single-pixel AOM/AOD counterparts, they are limited by the resolution of the DMD. These instruments commonly have a DMD frame width of about 1000x1000 pixels, which means that larger patterns must be stitched together from individual frames. Some instruments also allow the user to isolate only the inner portion of the DMD (the inner 400x400 pixels for example), which improves exposure quality by limiting source illumination irregularities, though it does increase the write time.

3.3 Adaptive Optics Overview

Adaptive Optics is a field of optical sciences that focuses on imaging through an aberrated media. In order to correct aberrations that result from imaging through the aberration, adaptive optics (AO) systems utilize one or more deformable mirrors that change shape in order to compensate for the aberrations. The largest application of AO is in ground-based telescopes. These types of telescopes need to image through the Earth's turbulent atmosphere and therefore rely on AO systems to be able to image distant astronomical features clearly. Space telescopes

have the advantage of being able to operate outside this turbulent atmosphere. Wavelengths such as the ultra-violet bands at near-infrared wavelengths not at the atmospheric windows of the J, H or K bands and the mid and far-infrared are most commonly exploited [6]. However, the largest telescopes cannot be launched into space without great difficulty and at large cost. It has become common to follow up images and low-resolution spectra taken by space telescopes with AO-equipped ground-based telescopes that use a much larger collecting area. Adaptive Optics systems have also been applied to many fields outside of astronomy. Having evolved recently in the 1990's, AO has branched into imaging fields for applications such as imaging the human retina, as well as biological microscopy and deep-tissue imaging [7]. AO technology is important to discuss in this thesis because it is the main application of grayscale lithography presented. This section introduces the fundamental topics of adaptive optics such as common components and their uses.

In its simplest form, AO is a technology used to correct and enhance the performance of an optical system by manipulating its wavefronts. Doing so improves the final output of the system compared to a non-AO system. Here, a wavefront is defined as the surface shape associated with equal-phase points in a propagating wave. When not aberrated, an undistorted wavefront commonly takes a planar or spherical shape, though that shape can be altered through the use of optical elements. A simple positive lens changes an incident plane wavefront into a spherical wavefront and focuses light down to a point, as shown in Fig 2.

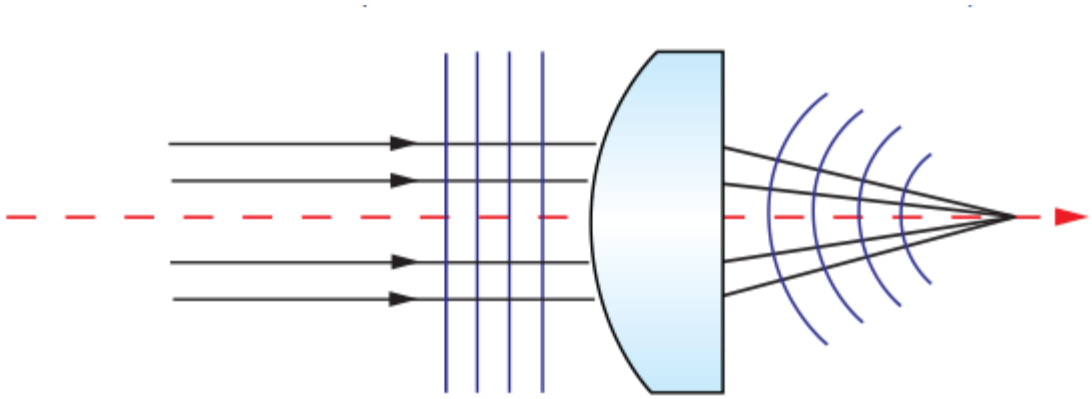

Figure 2 Positive lens manipulating an incident planar wavefront into a converging spherical wavefront [8]**.**

AO systems employ optical elements that precisely manipulate a system's wavefront, such as a deformable mirror. A deformable mirror has the advantage of being able to control the shape of a wavefront via precise and programmable control and leads to vast improvement in the system's overall performance. For this reason, AO systems are used in a wide variety of imaging and non-imaging applications in order to reduce aberrations, improve image quality and shape laser beams.

A deformable mirror is an adaptive element consisting of a controllable reflective surface, which is commonly a 12x12 array of micro-mirrors. These micro-mirrors rapidly change shape in the presence of an applied electronic signal in order to form the corrective mirror shape. When an incident aberrated wavefront reflects from the deformable mirror, its shape is corrected as shown in Figure 3.

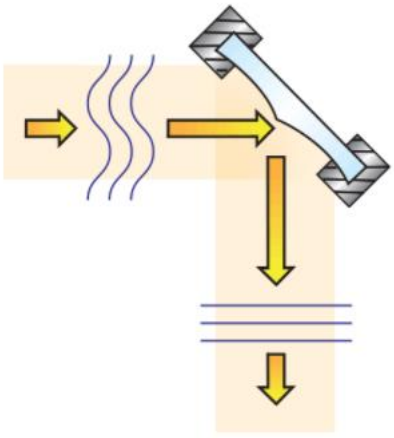

Figure 3 Deformable mirror with a correction map applied manipulates a distorted incident wavefront [8]**.**

The shape or correction map applied to the deformable mirror is pre-calculated, such that the deformable mirror (DM) is under open-loop control, or it can be iteratively calculated based on system feedback and operate under closed-loop control. An open-loop AO imaging system is shown in Figure 4 and is composed of the DM and control electronics, an imaging sensor, and other common optical elements.

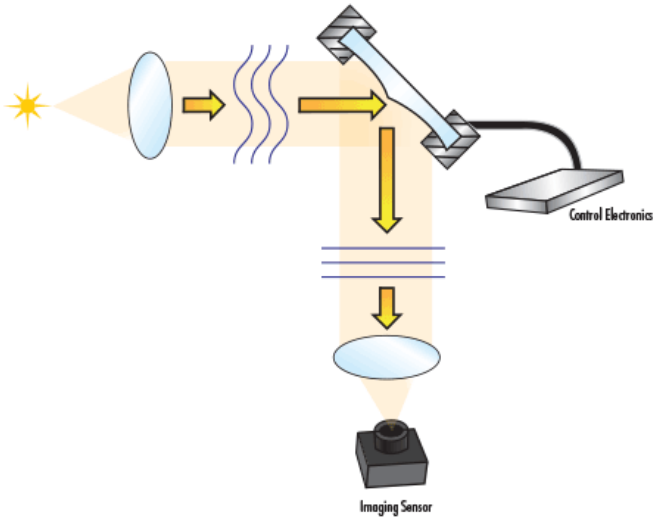

Figure 4 Simple AO imaging system operating under open loop control [8]**.**

An open-loop control configuration uses predetermined mirror shapes or correction maps that are used to correct for various aberrations in the system. This configuration is helpful if the system is known to have a specific aberration or if an element within the system is inducing a known aberration. The reverse is also correct, in that the DM can form specific shapes to induce one or more aberrations into the system. This arrangement is useful in order to see a specific aberration's impact on an optical system for tolerancing considerations.

However, if the aberration in an optical system is not well characterized or is rapidly changing, the pre-calculated correction map loses validity and usefulness. In such instances, it is necessary to have a feedback mechanism within the system from which the DM forms correction-maps in near real time. A wavefront sensor (WFS) is used as part of the feedback loop to quantify the errors that need correction. The most common wavefront sensor is a Shack-Hartmann Wavefront Sensor that is comprised of a micro lens array mounted on a CCD or CMOS detector array as depicted in Figure 5.

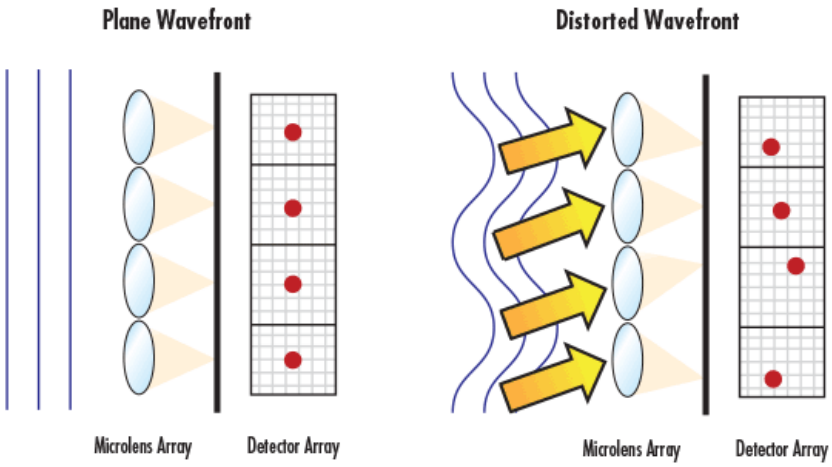

Figure 5 Interaction between an incident wavefront and the lenslet array and detector plane of a Shack Hartmann Wavefront Sensor [8]**.**

Figure 5 depicts both an incident plane wavefront (left) and distorted wavefront (right). For a perfectly planar wavefront, each lens in the lenslet array causes the light rays to focus into the center of each detector in the corresponding detector array. Since the detector array is placed at the focal plane of the lenslet array, the position of these focus spots give information about the phase tilt of each small section of the incident wavefront. When a distorted wavefront is incident on the WFS, the light focusing through the lenslet array focuses at displaced locations on the detector array. The phase of the incident distorted wavefront is then determined from analyzing the focus position from each lenslet. Once the phase of the distorted wavefront is found, this information is used to compute a correction-map and feedback to the DM in order to correct for the aberrations in the system.

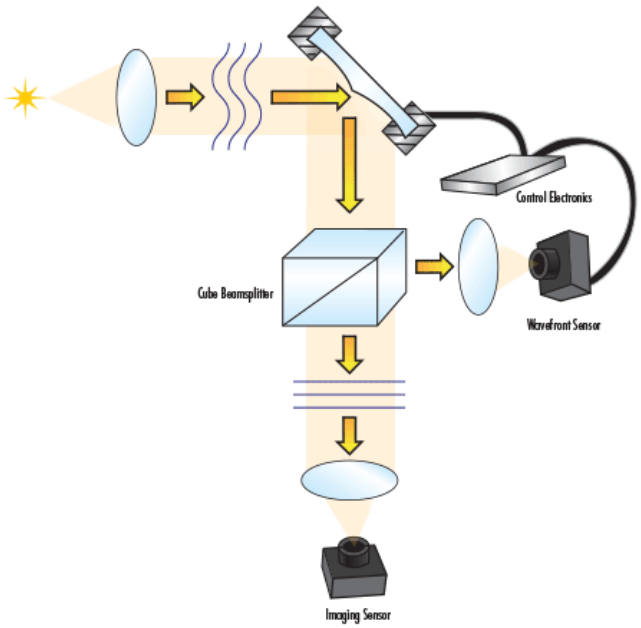

Figure 6 Closed looped AO system utilizing a wavefront sensor to provide feedback to a deformable mirror [8].

Closed-loop control is depicted in Figure 6, where a beam splitter is placed in the optical path to split off part of the beam and direct it towards the WFS. Systems such as this one continuously

sample and precisely measure the wavefront phase and correct for any aberrations within the system.

When constructing an AO system there are key DM parameters that must be considered. The first and simplest parameter is the desired dimension of the deformable mirror. DM's come in a wide range of sizes ranging from just a few millimeters in diameter to hundreds of centimeters. Matching the size of the DM to its desired performance in either micro or macro applications is the first step for success. DM's come in various surface types, such as segmented or continuous. Segmented mirrors are broken into a multitude of smaller mirror segments that are controlled individually, while continuous mirrors are comprised of a single surface membrane that is 'poked' at different locations to affect a surface shape. For segmented mirrors, the more segments a mirror has, the more precisely its shape is controlled. Likewise, the number of actuators a mirror has defines the quantity of unique correction maps that a mirror can produce. The more actuators a DM has, the more adaptable it is to correcting complex aberrations. The number of actuators in DMs range from tens to hundreds. Lastly, the type of actuation technology is an important parameter, as it controls the movement of each individual mirror segment. Most DMs are segmented deformable mirrors whose segments are moved by individual actuators that operate via piston and tip/tilt values or via Zernike coefficients. High performance AO systems commonly operate in an open-loop operation using precision linear piston and tip/tilt movement to allow for highly accurate corrections. This type of fully independent movement gives AO systems the ability to be used in applications such as beam shaping, fiber coupling and phased arrays. For continuous-surface deformable mirrors, mechanical actuator posts are used behind the reflective surface to form the membrane into the necessary shape. Other positioning methods include magnets or piezoelectric elements.

3.3.1 Single Shot Phase Retrieval

The concept of Adaptive Optics centers around using various optical elements to measure the phase of an aberrated wavefront such that a correction map is calculated and then applied to a deformable mirror in order to produce higher performance imaging. There are many methods used to measure the aberrated wavefront of a system, such as using a wavefront sensor, as described in the prior section. Phase retrieval is another technique used to measure unknown aberrated wavefronts or phase changes and is advantageous due to its simplicity when compared to more complicated methods such as the WFS. Phase retrieval has its own drawbacks in that it requires multiple image acquisitions and can suffer from low accuracy. These disadvantages led to the method of single-shot phase retrieval in which only a single image is necessary to reconstruct unknown extrinsic phase inconsistencies. This thesis reports on part of a larger project that involves using single-shot phase retrieval to detect data patterns in damaged optical storage media [26].

Most phase retrieval methods are derived from the Gerchberg-Saxton algorithm [9], which is an iterative phase retrieval algorithm that operates by retrieving the phase of an unknown wavefront from separate image acquisitions. Most commonly, the two image planes chosen are the image plane and the far-field diffraction plane, where the propagation of a wavefront between these two planes is described by the Fourier transform.

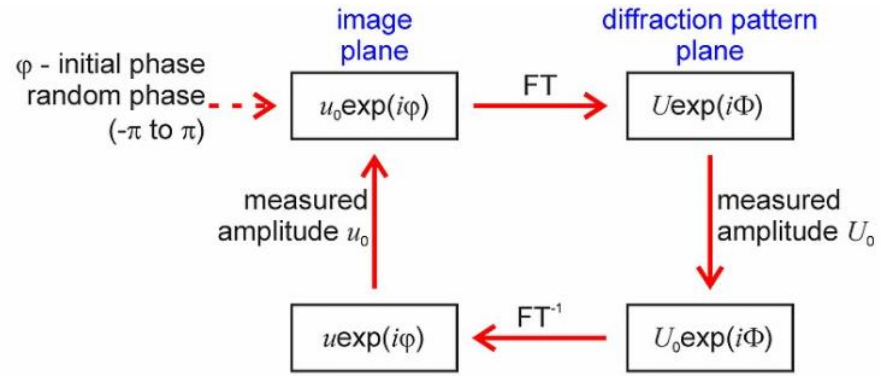

Figure 7 Iterative phase retrieval methods of the Gerchberg-Saxton algorithm. FT denotes Fourier Transform [9].

Using this algorithm, the phase distribution at one plane is known, and phase at the second plane is estimated by performing a Fourier transform. This algorithm has been improved upon since its creation and now holds enhanced accuracy and convergence through the implementation of various diversities such as defocus diversity, translation diversity, shifting illumination and random diversity. However, these methods do not overcome the limitation of requiring multiple image acquisitions in order to form a high-quality reconstruction. This challenge is conquered through the use of phase gratings and computer-generated holograms (CGHs). These optical elements are useful for their ability to distribute multiple images onto individual areas on a sensor, thus overcoming the 'single-shot' image acquisition limitation. In a single-shot acquisition, a diffractive element is used create multiple diffractive orders without significant power loss.

The method of single-shot phase retrieval this work centers around the use of complex diversity. Here, effective complex-number pupil filters that contain both phase and amplitude information are unrooted via numerical propagation from CGH design [10]. Multiple images are acquired from a single 'shot' image acquisition, and phase reconstruction is achieved through the use of a modified iterative Fourier algorithm. The designed CGH differs from other diversity techniques, as the data obtained through individual diffraction orders contain both real and

imaginary values. The single-shot phase retrieval technique produces multiple images at different positions on the image plane, as shown in Figure 8b, where each of the subimages is created by its own unique complex effective filter. Each image can easily be cropped from the original data such that multiple phasorgrams are obtained from a single image acquisition. Unlike the conventional diversity technique shown in Figure 8a, multiple image acquisitions are not required.

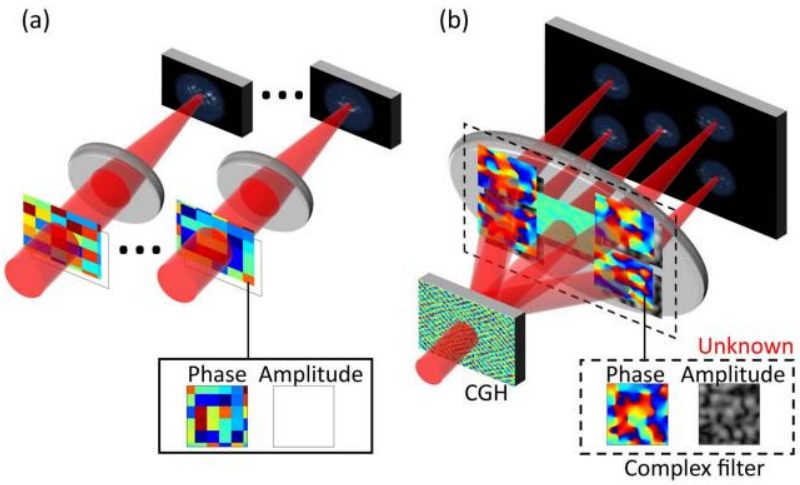

Figure 8 Comparison of (a) Conventional diversity and (b) complex diversity [10].

This thesis contains information regarding the fabrication of the CGH used in the single-shot technique shown in Figure 8b. The long-range goal from the sponsor of this work is to incorporate a single-shot measurement using complex diversity as feedback to the AO algorithm described in Section 2.2. Design of a complex diversity CGH is described in [11].

3.4 Replication

Once a pattern has been exposed onto a photoresist layer on a substrate, it then becomes necessary to form that exposed pattern into a more permanent optical element. Photoresist itself does not make a sound optical element as it is prone to smudging, changing refractive index under direct lighting conditions, and it does not have ideal transmissive properties. In short, exposing a

pattern into photoresist via photolithography only accomplishes the job of obtaining a physical pattern. The design then needs to be made into a usable element. There are many ways to accomplish this task, including etching, using an elastomeric mold for replication, and direct casting. These techniques are summarized below, and all of them have been tested in this work.

The most common method of forming a diffractive element from a photoresist pattern is etching the design into glass. Etching is a process by which regions of underlying material that are no longer covered by photoresist after development are removed from the substrate. This microfabrication process chemically removes layers from the surface of a sample. When used after a lithography exposure process, the resist acts as a mask and protects parts of the substrate from the etchant. The etching process results in a cavity in the material, the depth of which is controlled by the etching time and rate [12]. While very advantageous in mass-production applications due to its high repeatability, etching recipes can be troublesome to develop for iterative prototype processes and are costly. While many applications require a more robust surface than developed photoresist, the high-quality sample resulting from etched class can be excessively robust for some applications, like the prototype work described in this thesis.

Another method of transferring a lithographic exposure is to use a polymer mold and an optical adhesive transparent to the design wavelength in order to replicate the pattern onto a more permanent substrate [13]. Compared to the initial photoresist covered substrate, the replicated optical element offers much higher transmission and more robust mechanical properties. Furthermore, this process achieves a high-quality replication without the need for high-cost or complicated fabrication facilities. This fabrication process utilizes two main steps. First, a negative mold is created of the original exposed element. Next, the mold is used to create a replication out of UV- curing adhesive, as shown in Figure 9.

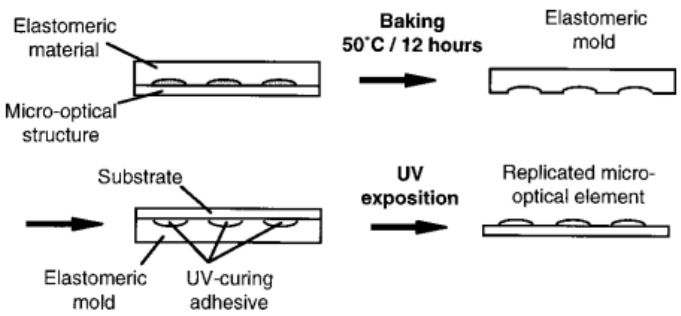

Figure 9 Replication of lithographic exposure using elastomer molds and optical adhesive [13].

One of the biggest advantages of this process is that the integrity of the original exposure master is preserved throughout the creation of the elastomeric mold. This quality is important if several molds need to be created from the same original master. Moreover, the flexible nature of the elastomer mold makes separation from the master and from the replicated element very simple. The use of a UV-curing adhesive to form the micro-structures of the exposed design gives very good results in terms of the final elements refractive and diffractive performance. Norland NOA 61 optical adhesive, for example, has high optical quality with a refractive index of 1.56 and high transmission. This replication process results in a semi-permanent optical element that performs very well for iterative prototype development.

The elastomeric mold replication process highlights the ability of micro-optical elements to be replicated with optical adhesives. While the intermediate step of creating an inverse elastomer mold allows the integrity of the original master to be preserved, it introduces a unique set of challenges in the fabrication process. For example, defects in the mold are directly transferred to the replicated element. Moreover, it is difficult to control the macro-level thickness of the optical adhesive when attempting to replicate larger patterns (larger than 1in by 1in in size). In the fabrication process, the optical adhesive is applied via a small droplet to the mold, and a substrate is applied to the top of the adhesive with a small amount of pressure in order to spread

the adhesive and provide a flat optical surface for the replicated element. For larger patterns and substrates, the distribution of the adhesive over the mold is very difficult to control in a precise manner (especially when considering that the reverse side of the mold may not have been baked entirely flat). For these reasons, it becomes advantageous to remove the elastomeric mold step entirely and perform replications via optical adhesive directly onto the original master itself, as described in the next paragraph [14].

The main advantage of a direct casting process over elastomeric replicaiton is the fast turnover rate, since the fabrication of an elastomer mold requires it to be baked overnight. Moreover, since both the original master exposure as well as the replication substrate are rigid glass substrates, spread of the optical adhesive between them is more likely to be uniform in thickness. The direct replication process it outlined in Figure 10.

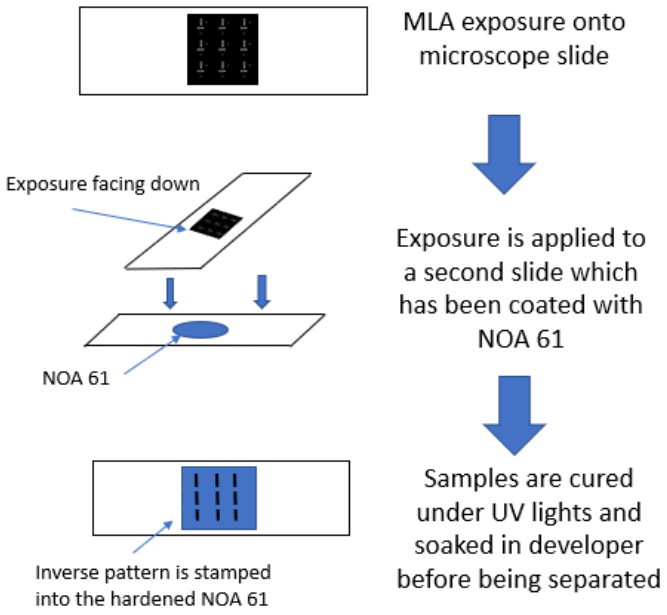

Figure 10. Outline of direct replication process

In contrast to using an elastomer mold that separates easily from both the original master as well as the replicated substrate, the separation of the original master from the replicated substrate in direct replication is more challenging. After the master is applied to a secondary sample and NOA 61 droplet, the two samples are then tightly contacted. The contacted samples require a short submersion bath (< 30s) in concentrated developer to dissolve the remaining photoresist on the original master exposure. After the photoresist is dissolved, the casted replication is removed from the master. The separation of the two samples results in a high tensile release force, which can be challenging to complete without breakage in fragile substrates. The process requires a robust substrate as well as mismatched mechanical orientation of the contracted substrates, such that there is enough leverage between them to separate them from each other. This mismatch in orientation is depicted in Figure 10, where the microscope slide containing the original master exposure is oriented at 90 degrees from the microscope slide with NOA 61 applied to it. This orientation allows leverage for the two samples to be separated once the adhesive is cured. Furthermore, since the original exposure is submerged in concentrated developer the original exposure pattern is destroyed. If multiple replications are required, then multiple exposures are fabricated.

Overall, the direct replication process results in the rapid fabrication of high quality micro-optic elements, the thicknesses of which are well controlled. The use of NOA 61 makes the optic highly transmissive and is stable enough to be handled repetitively. The final replicated element structures are measured using conventional white-light interferometry and integrated into existing experimental testbeds. The ability to 'stamp' an exposed lithography pattern into the NOA 61 lends itself perfectly to grayscale applications. Using this replication method, the replicated element is the direct inverse of the master that is exposed into photoresist.

4 TOOLS AND EQUIPMENT

4.1 MLA 150

The Heidelberg Instruments Maskless-Aligner 150 (MLA 150) is one of the primary instruments used for photolithography at the Wyant College of Optical Sciences at the University of Arizona. It is housed in the College's 8th floor cleanroom and is pictured below.

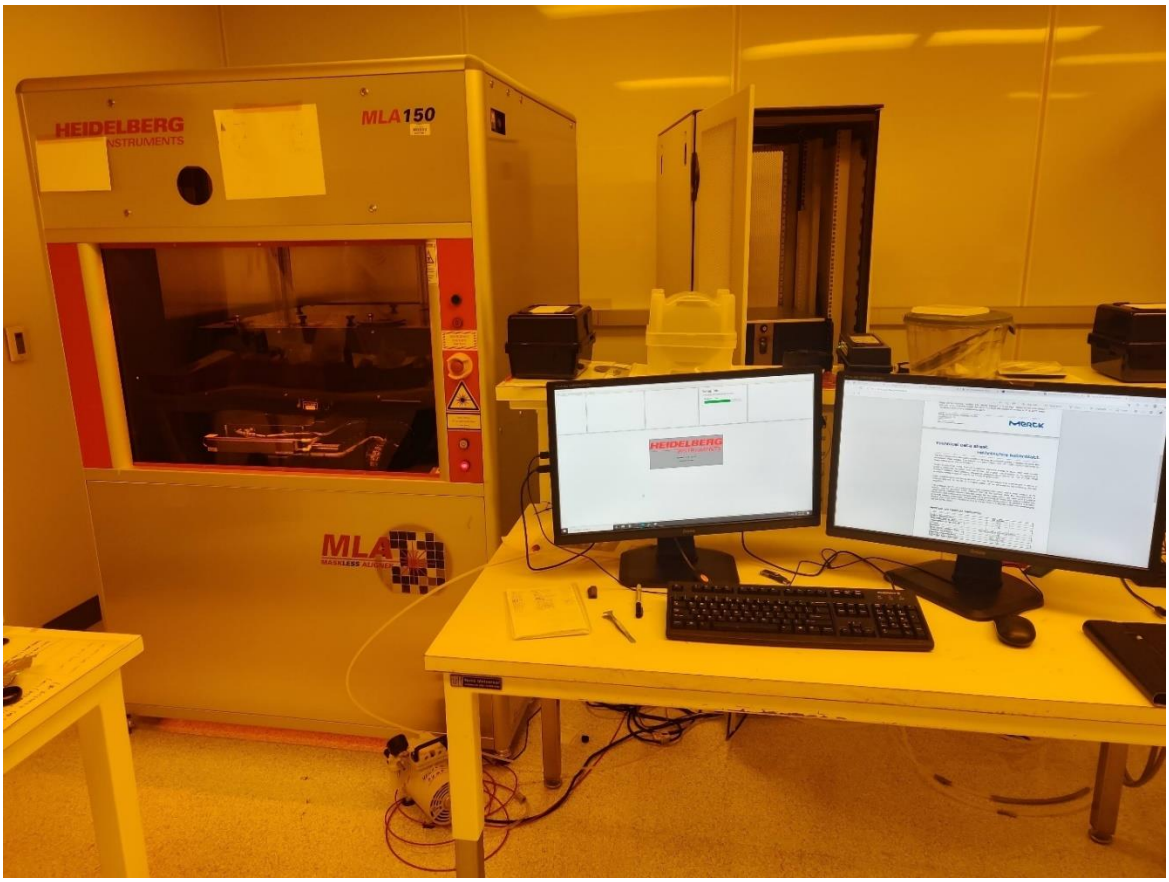

Figure 11 MLA 150 housed in the 8th floor cleanroom of the Wyant College of Optical Sciences.

The MLA 150 is a DMD based photolithography system capable of high-resolution grayscale printing on a large variety of substrate types and sizes. The instrument's intuitive alignment capabilities along with its user-friendly interface made it an ideal choice for grayscale process development. It is a comparatively new instrument, with first user-data being generated as recent

as 2014. This section contains a system overview, detailed operation processes, the procedures used and developed, as well as advanced grayscale techniques.

4.1.1 System Overview

The MLA 150 was developed with the goal of exposing patterns directly onto a substrate without the need of fabricating masks. This freedom allows the user to make direct improvements in exposure speed and ease of use in regards to both the user interface as well as the instrument's overall operation and flexibility. The MLA 150 exposes patterns onto a substrate using a raster-scan method depicted in Figure 12 [4] .

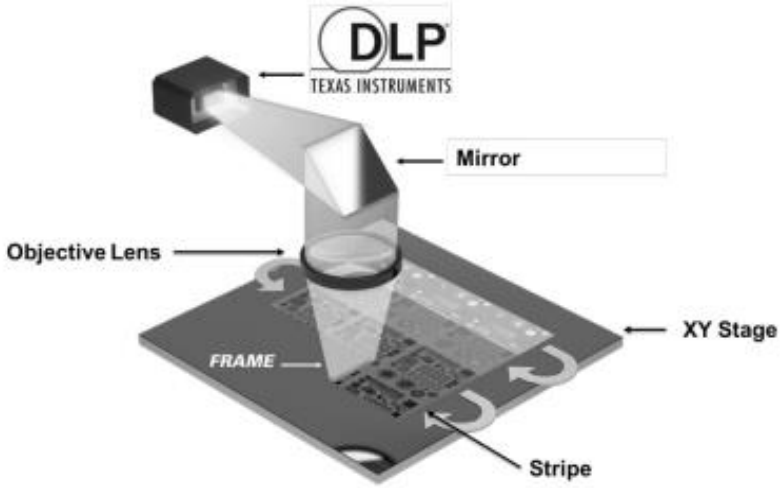

Figure 12 Depiction of raster-scan used by the MLA 150 to write patterns onto a substrate [4]

The sample is placed onto the XY-stage and fixed in place via vacuum. Each pattern is decomposed into stripes that are generated during the exposure. The XY- stage moves with a constant velocity under the optical fixture in order to generate each of these stripes. Stitching all of the stripes together results in a completed pattern. The MLA 150 writes a minimum feature size of 1 micron with alignment accuracy between layers of 500nm. Overall, the resolution is limited by the photoresist, wavelength and power stability of the system. The nominal resolution of 1 micron is achieved with a thin photoresist (less than 1 micron).

Optically, the operation of the MLA 150 centers around a DLP ® modulator from Texas Instruments. The DLP chip is a digital micromirror device (DMD), which is an array of micromirrors that are used for fast, reliable and efficient spatial light modulation. Notably, the DMD operates with an electrical input and optical output. The micro-display is made up of almost one million small mirrors, each of which is independently programmed and controlled. The array of mirrors is built on top of an associated CMOS memory cell [15]. As a whole, the array is changed with up to a 23 kHz frame rate [16]. Each memory cell is preloaded with a '1' or a '0' during operation. When a mirror reset is applied, each micromirror is electrostatically rotated about a hinge to a +/- 12° state. The +12° state corresponds to an 'on' pixel while the -12° state corresponds to an 'off' pixel. A physical stop on each mirror ensures that these two states are highly repeatable.

The MLA 150 utilizes fiber-coupled diode lasers for its light source. There are two options available, a 375nm and a 405nm version. Each user can choose which source is optimal for any given exposure and application. The MLA 150 has two main parameters which users need to set up for a given exposure. The Dose parameter controls the dose [mJ/cm2] and has a range from 40 [mJ/cm2] to 800 [mJ/cm2]. A high dose is necessary for thicker resists, and a low dose can easily clear through a thin photoresist coating. The Defocus parameter defines where the source focus is located along the optical axis. When set to 0, the focus is located at the top of the photoresist coating. A positive defocus value means that the focus shifts downward to inside the photoresist coating. The defocus has a range of -10 to +10 with a 10 being about a 6 micron shift. One of the biggest advantages of the MLA 150 is its user friendly interface. The tool can be operated very easily and with little training. The software guides the user though the process of loading and aligning the sample in order to minimize job start-up time.

As with most exposure tools, the XY stage is a crucial component. Since users expect a fast yet accurate exposure, the stage must provide high acceleration while still proving precise positioning and minimal vibration error. The MLA utilizes open-frame stages powered by linear motors. In order to position accurately, laser interferometers measure the stage location with a resolution of 20nm. Software furthermore corrects systematic position errors in real-time [16]. Samples are loaded onto the stage and affixed via a vacuum chuck. Samples of sizes 5mm to 8 inches in diameter are loaded with a wide variety of sample shapes and dimensions being supported. Substrate alignment is completed within software where a camera looks at the sample through openings in the chuck. Further alignment routines utilize integrated intensity diodes and photomultipliers to verify calibration. This alignment error compensation can correct for rotation, offset scaling and shearing.

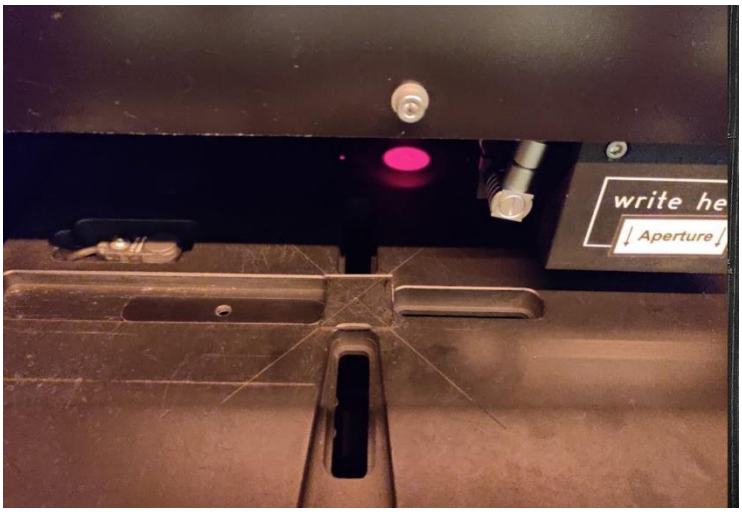

Figure 13 Mounting sample to vacuum chuck in the loading area of the MLA 150.

Once mounted on the vacuum chuck, the sample is protected by an enclosure. An automatic window is the only access to the system, and it is large enough to easily access the mounting area. The enclosure is equipped with a flow unit to monitor and guarantee stable temperature and clean air. This feature is commonly used to adjust the temperature within the flow unit to be comparable

to the outside temperature to avoid thermal expansion of the sample during the exposure. Overall, the MLA 150 is an effective lithographic instrument for quickly exposing three dimensional microstructures.

4.1.2 Grayscale lithography with the MLA 150

The MLA 150 has many capabilities, like its support of working with grayscale layered patterns. The main difference between normal operation and grayscale exposures is the utilization of different file types and a gray table. The MLA 150 supports the grayscale file types of .bmp and .dxf, although in this thesis only the .dxf file type was used. The .bmp file type was not successful in this work due to the large files necessary to print diffractive optics. The .dxf file type is derived from Drawing Interchange Format and is a CAD data file format commonly used for 2D or 3D drawings. Its use of layering gives it a great synergy for use with grayscale design. The need to use this specific file type was realized through trial and error and brought its own unique challenges to the design process, which are discussed in following sections. In order to upload a file to the MLA 150 software, it first needs to be converted into a format native to the software itself. In grayscale operation, this process includes assigning gray values to each layer of the pattern though the use of a pre- configured gray table. A gray table is a simple table, usually made in Microsoft Excel, which correlates each layer of the design with a corresponding gray value. Once an external gray table is created it is utilized in the MLA 150 software where it automatically applies the designated gray value to each corresponding layer. An example taken from the MLA 150 user interface is shown below in Table 16.

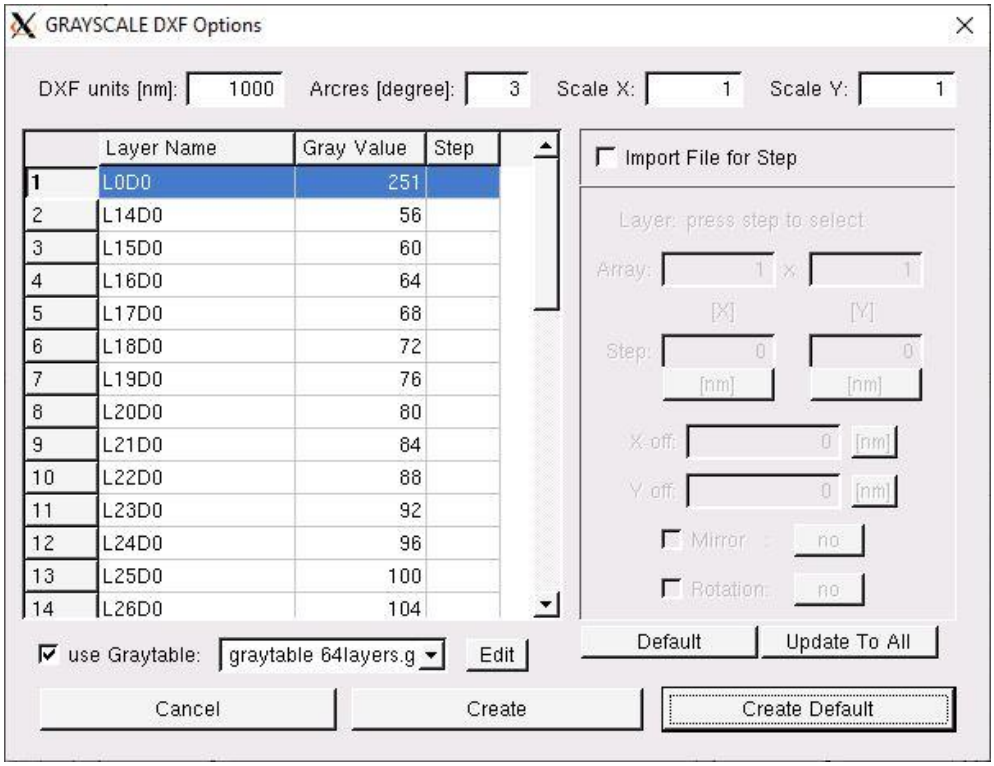

Figure 14 Utilization of a gray table when converting a file for grayscale exposure for the MLA 150.

The MLA 150 works with designs of up to 128 layers and uses 256 grayscale values. The shortest step between layers in a design is 2 grayscale values, where the grayscale value represents the percentage of the total dosage being applied. When a pattern is designed that uses less than the maximum number of layers, the gray values are split in equal iterations from 0 to 256 such that the entire dose range is used. In Figure 14, a design is converted that uses only 64 layers and the gray values are assigned to each layer with a step size of 4.

The assignment of gray value equally throughout each of a design's layers assumes a linear relationship between the relative dose being applied and the subsequent exposure depth. This relationship deviates from a linear scale due to the chemical and material response of the photoresist when exposed to UV light, as previously demonstrated in Figure 1. This non-linear response reveals the need to characterize a photoresist's depth response to varying dose such that

a calibration can be applied. This calibration process is further described in Chapter 6 ‘Grayscale Lithography Design’.

4.1.3 Materials and Chemistry

The process development of grayscale lithography on the MLA 150 centers around utilizing the given hardware such that the chemical response of a photoresist is manipulated in order to achieve a truly linear grayscale output. A linear output means that each layer of a grayscale design translates into an equally sized exposure depth. In pursuit of this goal, a fundamental understanding of the various materials and chemistry used during the lithography process is necessary. This section introduces the photoresists most commonly used in this work and their key parameters and responses.

4.1.3.1 S1813 and S1327 Photoresist

The MICROPOSIT S1800 Series of photoresists are positive photoresists optimized for use in binary applications due to their sharp response curves and high contrast. Their use here in grayscale applications is entirely due to ease of access and early signs of success. While exact process parameters are equipment and application dependent, these resists have well-developed specifications. The most pertinent characteristic of these photoresists is their relative contrast or the exposed thickness as a function of dose. The contrast curve for S1813 is given below, and all other photoresist specifications are given in Appendix B.

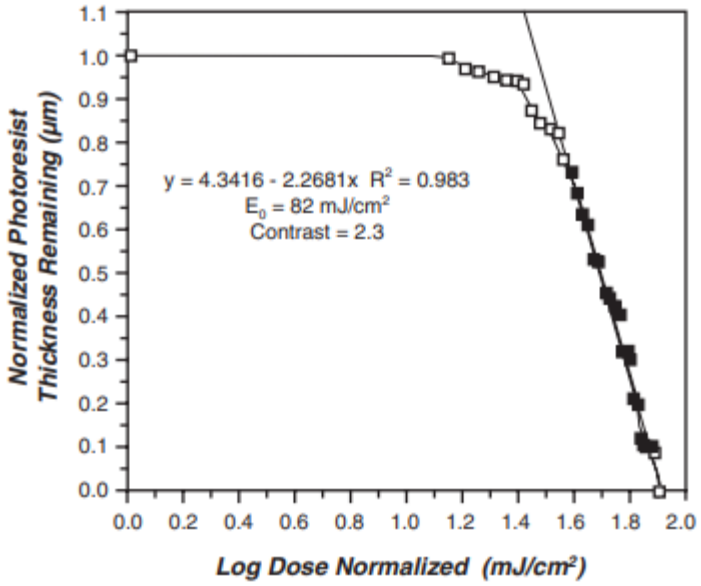

Figure 15 MICROPOSIT S1813 Photoresist Contrast Curve [17] **.**

S1813 is a very commonly used high-contrast photoresist. Photoresists that are high contrast have a small difference between the maximum and minimum depth in terms of the required dose to achieve each. The plot above demonstrates this quality as the curve moves from no thickness removed to all of the photoresist removed in a very short dose interval. While this change does happen drastically, it also occurs with a very linear relationship. The interval of 1.6 (mJ/cm2) to 1.9 (mJ/cm2) in normalized dose S1813 responds predictably when the dosage is increased. It is this characteristic that is taken advantage of for grayscale applications.

Both the S1813 and S1827 photoresists have very similar contrasts curves, the main difference between them being the viscosity of the resist. S1827 is a much thicker photoresist than S1318, which results in the possibility for a thicker photoresist layer when spin coating. The line of S1800 photoresists is manufactured in a variety of standard viscosities for the application of single-layer processing [17]. Both photoresists are developed using the same developer chemistry. The Microposit 351 developer is used for both photoresists in this work, although any metal-ion-

bearing Microposit developer will work. Furthermore, this line of photoresists is optimized for g-line (435 nm) exposure though they remain effective for broad-band exposure.

4.1.3.2 AZ P4620 Photoresist

The AZ P4000 line of photoresists are a positive resist series that have a lower photo-active compound concentration that allows for the application of thicker to very thick photoresist layers ranging from 3um – 30um. For a grayscale application, a thicker photoresist not only allows for larger feature depths, but also has the characteristic of having a more linear feature depth response to increasing dose. The line of AZ P4000 photoresists work best with the corresponding developer AZ4000K. Common processes for this resist include a 10um resist layer, baking at 115C for one minute and development for 2 minutes. The resist thickness as a function of spin speed is shown below.

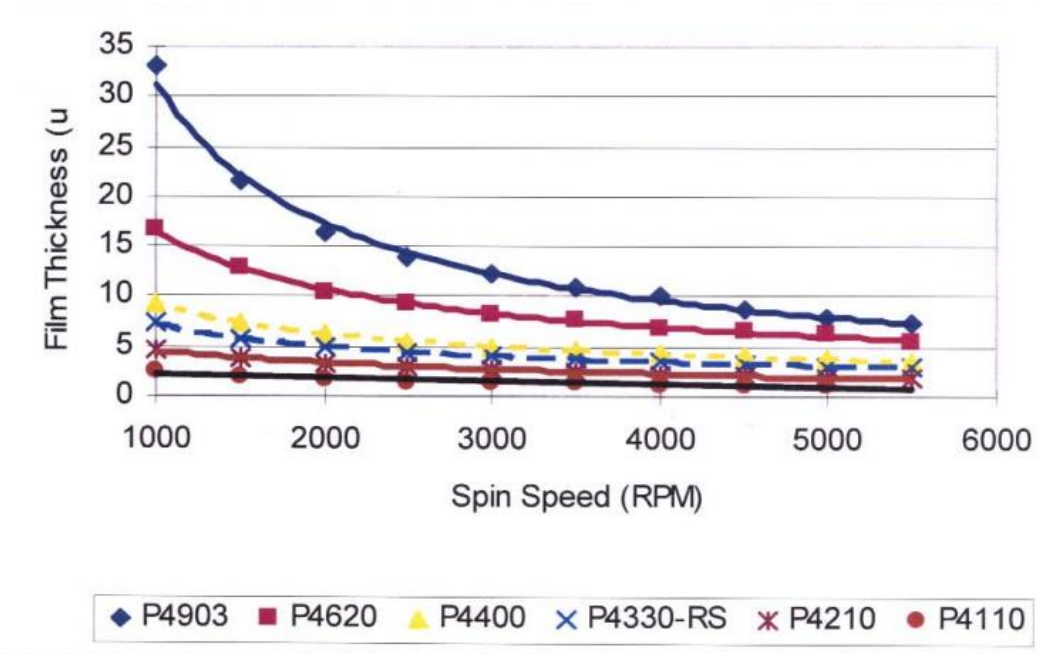

Figure 16 Spin speed curve for the AZ P4000 line of photoresists

For a spin speed of 4000rpm, it is expected that the AZ P2620 photoresist is around 6um thick.

4.2 NewView® White Light Interferometer

Throughout the process of creating an effective grayscale lithography fabrication methodology, it is necessary to have a consistent metrology instrument capable of accurately measuring the exposed and subsequently replicated features of the fabricated diffractive optical elements. A white light interferometer is used as the main metrology instrument, as it provided a non-contact optical method for precise surface height measurement on three dimensional microstructures. The surface profiles that are successfully measured on a white light interferometer vary from tens of nanometers to a few centimeters, depending on the magnification of the objective being used. White light interferometers utilize coherence scanning interferometry and use broadband, visible wavelengths as their source. The profile of the sample is measured when light interference occurs as the difference in distance traveled by the light of both the test and reference arms of the interferometer are nearly identical. An accurate positioning stage is necessary to scan the sample through a path length match. The vertical z-value a point on the surface of the sample imaged by a pixel then corresponds to the z-value of the vertical stage where the modulation of the interference pattern is greatest. When repeated for every pixel, a matrix of height values of the test sample surface is calculated [18].

4.2.1 System Overview

A NewView® 8300 white-light interferometer is utilized for the vast majority of measurements of lithographically printed samples in this work. The NewView® s used to produce ramp profile measurements for early calibration and linearization regimes. The instrument is also used to produce matrix surface profiles of test samples in order to compare fabricated samples to their original design, as well as many other applications.

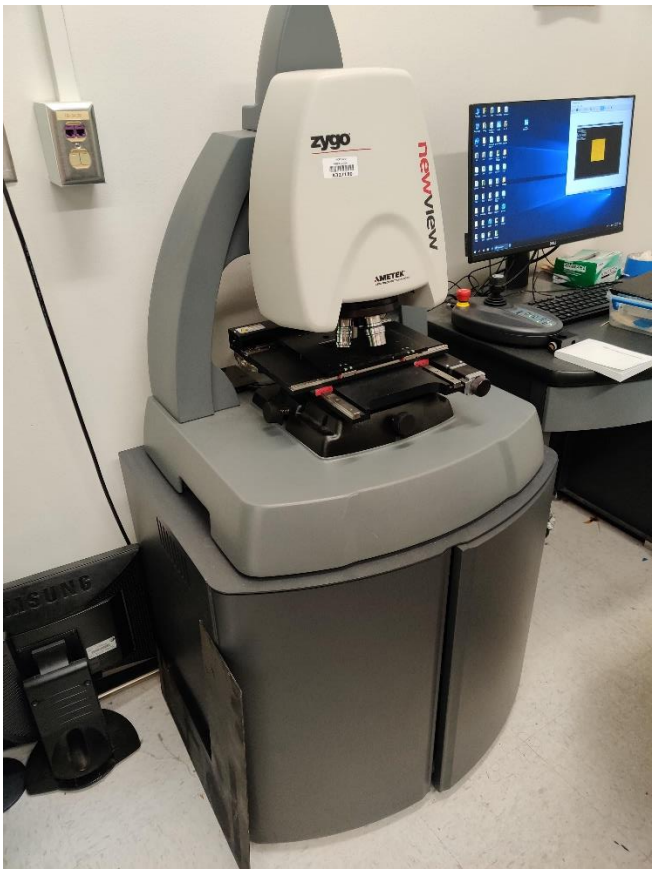

Figure 17 Zygo NewView® 8300 white light interferometer housed in the Wyant College of Optical Sciences

The Zygo NewView® 8300, shown above, uses 3D coherence scanning interferometry as its measurement technique. It uses a precision piezo driven stage with closed loop capacitance gauge control. It has the option to use a multitude of objective lens ranging from 1x to 100x, though specifically a 10x magnification objective is used throughout this work. A 10x magnification objective allows for ample imaging resolution and field of view while remaining easy to align and use. The field of view of the instrument ranges from 0.04mm to 16mm depending on the selected objective and zoom parameter. The instrument's z-drive focus stage has a 100mm range with 0.1um resolution. The system has a vertical scan range of 150um with a precision Piezo drive. Measurements are taken using the ZYGO Mx software under a windows environment. Other pertinent system performance specifications are summarized in the table below.

Zygo NewView 8300 Performance Specifications	
Surface Topography Repeatability	$0.2\ nm$
Repeatability of RMS	$0.01\ nm$
Maximum Data Scan Speed	$96\ um/sec$
Step Heat Repeatability	0.1%
Hight Response Linearity	$\leq 30nm$
FOV (10X obj.)	$0.83\ mm\ \times 0.83\ mm$
Optical Res Sparrow Criterion (10X obj.)	$0.95\ um$
Spatial Sampling	$0.82\ um$
Numerical Aperture	0.3

Table 1 Zygo NewView 8300 Performance Specifications [19]

5 EXPERIMENTAL PHOTORESIST CHARACTERIZATION

A main component of developing a comprehensive grayscale lithography procedure entailed characterizing various photoresists. This characterization regime includes identifying the dose-to clear value that is a key parameter used in all exposures. The dose-to-clear value is the dose value at which all the photoresist is cleared from the substrate after development. In order to identify this parameter, all other variables in the lithography process are kept constant, such as the sample preparation, photoresist spin speed and development time and conditions. An example sample preparation regime consists of a solvent wash of acetone and isopropyl alcohol followed by plasma cleaning. Microscope slides are used as substrates for all the initial experimentation and process development due to their acceptable quality and low cost. A spin recipe is created and kept constant for the entirety of testing consisting of 4 stages: 1) 5s increasing acceleration up to 2000rpm, 2) 5s increasing acceleration up to 3000rpm, 3) 5s increasing acceleration up to 4000rpm and 4) 5s at 4000rpm.

The dose parameter of the MLA 150 is the only variable adjusted and the 'series' print mode of the MLA 150 is utilized in order to perform this test.

Figure 18 'Series' exposure mode being chosen in the Job Setup menu on the MLA 150 in order to perform a dose series test on a given photoresist

In the series print mode, multiple iterations of the same design pattern are exposed at varying dosages. A standard ramp type pattern was utilized in order to perform this test, where the ramp progresses through the entirety of the thickness of the photoresist. It is beneficial to use a simple pattern that is small in size relative to the substrate, such that multiple patterns are exposed on a single substrate. A start and end dose are input parameters, as well as the number of intervals between those values. Each interval dose is then exposed onto the substrate as an individual pattern. The MLA 150 displays each pattern and interval before being exposed, as demonstrated below.

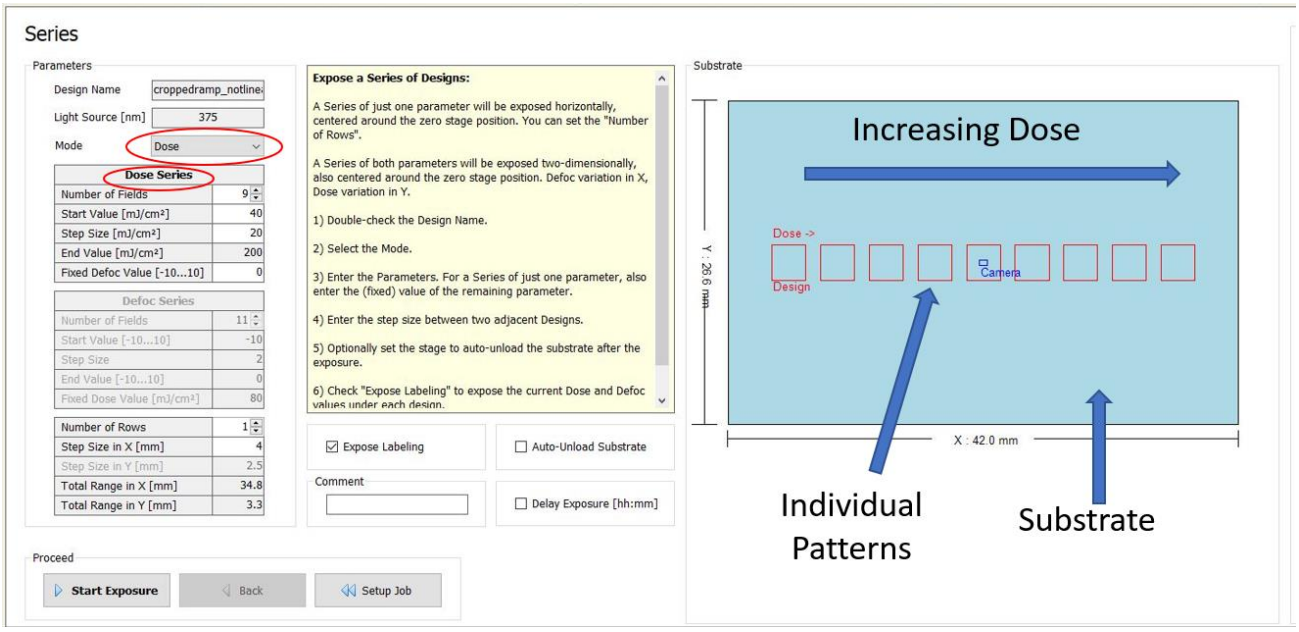

Figure 19 Exposure start menu on the MLA 150 demonstrating the layout and configuration of a series dose test. The options for dose values are given on the left and the layout of the patterns on the substrate is demonstrated on the right.

Once printed, the exposed samples are developed for a standard duration of 1 minute in a 1:4 ratio of 351 developer to DI water. The temperature of 21 degrees C and agitation methods is kept constant.

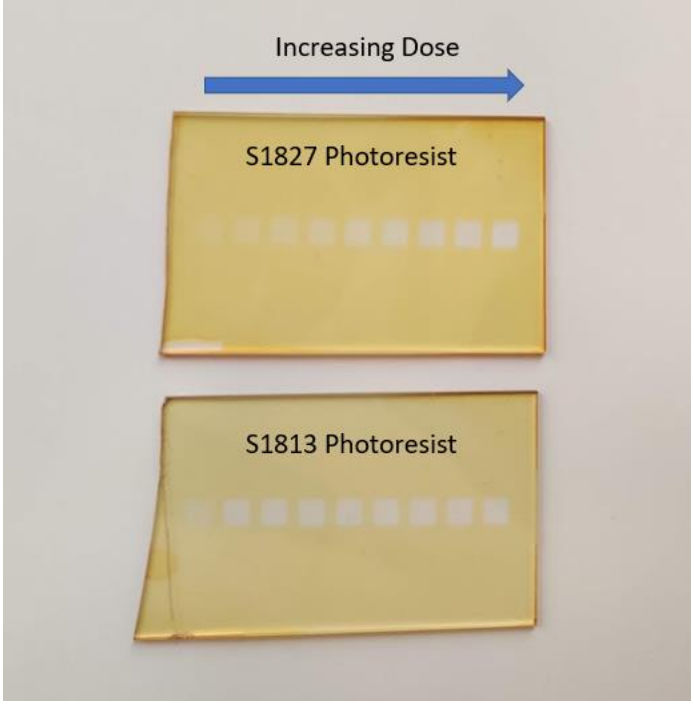

Figure 20 Example comparison of S1318 and S1827 photoresist exposures after an increasing dose series exposure

From Figure 20 it is seen that, for the same set of increasing dose exposures, the sample coated with S1813 cleared through the photoresist with a lower dose than with the sample coated with S1827 photoresist. Since both samples are spun at the same speed, these results are consistent with S1827 exhibiting a thicker photoresist. After development, the two samples are measured using a NewView® white light interferometer. The same feature is measured on each pattern, and the depth is measured. The dose at which the depth of the pattern equaled the total depth of the photoresist is the dose-to-clear for that photoresist. The detailed parameters of this dose series experiment as well as further results are discussed in the following sections.

5.1 S1813 Photoresist

A dose series test is performed using S1813 photoresist in order to characterize the behavior of the photoresist such that patterns are exposed using a consistent and repeatable procedure. As depicted in Figure 20, nine different dose values are tested, starting at a beginning dose of

$40\ mJ/cm^2$ up to $200\ mJ/cm^2$ with intervals of $20\ mJ/cm^2$. This set of doses are chosen because it covers a large range of values, but fits on a half microscope-slide substrate. The resulting ramp depths for each dose are given below.

Initial Dose Series Test for S1813 Photoresist	
Dose Value $[mJ/cm^2]$	Avg. Ramp Depth $[um]$
40	0.880
60	1.251
80	1.304
100	overexposed
120	overexposed
140	overexposed
160	overexposed
180	overexposed
200	overexposed

Table 2 Initial dose series experiment from $40\ mJ/cm^2$ up to $200\ mJ/cm^2$ with intervals of $20\ mJ/cm^2$. All doses above $80\ mJ/cm^2$ are severely overexposed.

From the measured ramp depths, the dose to clear value of S1713 under these processing conditions is $60\ mJ/cm^2$. This value is chosen, because all of the measurements done on patterns exposed with a dosage above this exhibit similar ramp depths as well as a completely smooth background. These characteristics show that all of the photoresist is cleared at the exposure's highest dose setting. Since S1813 is a relatively thin photoresist, it is not surprising that the dose-to-clear value is also very small. Only a small dose is necessary in order to clear all of the photoresist on the sample. Knowing the dose-to-clear value, it is then possible to complete further dose series experiments in order to determine the ramp depths at smaller intervals up to the maximum dose-to-clear value. The table below shows calculation of the average ramp depth for a sample size of 4 patterns per each dose interval.

Characterization of S1813 Photoresist					
Dose $[mJ/cm^2]$	Ramp Depth [um]				
	Trial 1	Trial 2	Trial 3	Trial 4	Average
40	0.809	0.791	0.741	0.773	0.7785
44	0.914	0.892	0.876	0.8001	0.870525
48	0.97	0.955	0.944	0.911	0.945
52	1.065	1.025	0.95	1.007	1.01175
56	1.139	1.107	1.034	1.051	1.08275
60	1.189	1.175	1.163	1.134	1.16525

Table 3 Further dose series experiments detailing smaller dose intervals below the dose to clear value. This table is used to choose a dose value based on a pattern's required feature depth.

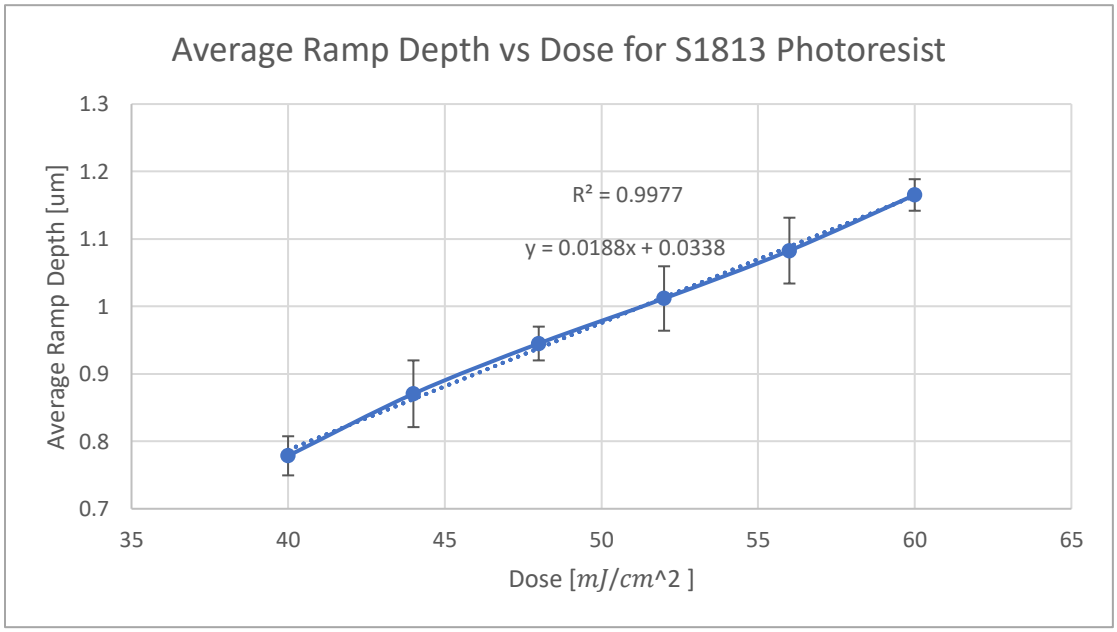

Figure 21 Average ramp height vs dose plotted using the data shown in Table 3. A linear trendline is plotted with equation and R squared value shown. Error bars show +/- one standard deviation of the data set.

The results shown in Table 3 are used to create linearization mappings for subsequent patterns and exposures. For exposure patterns, a maximum feature depth is first identified. From that desired feature depth, the dosage corresponding to the feature/ramp depth desired is chosen to

create a linearization mapping. That mapping is then applied to a specified design. When exposed with the same dose it is created from, the final exposure exhibit grayscale behavior with the specified feature depth. When this data is plotted as shown in Figure 21, a linear relationship is revealed between the MLA dose and resulting feature depth. From this data it is possible to extrapolate a dose value for any given feature depth within the bounds of the MLA dose and the photoresist dose to clear value.

5.2 S1827 Photoresist

A dose series test was carried out using S1827 photoresist in order to characterize the behavior of the photoresist, such that patterns are exposed using a consistent and repeatable procedure. As depicted in Figure 22, various dose values are tested starting at a dose of 40 mJ/cm^2 up to 240 mJ/cm^2 with intervals of 40 mJ/cm^2. This set of doses is chosen because it covers a large range of values but fits on a half microscope-slide substrate. The resulting ramp depths for each different dose are given below. The ramp data for patterns printed with a dose higher than 240 are severely overexposed.

Characterization of S1827 Photoresist					
Dose $[mJ/cm^2]$	Ramp Depth [um]				
	Trial 1	Trial 2	Trial 3	Trial 4	Average
40	0.625	0.6	0.622	0.627	0.6185
80	1.217	1.253	1.241	1.242	1.23825
120	1.73	1.773	1.73	1.712	1.73625
160	2.149	2.125	2.169	2.198	2.16025
200	2.451	2.509	2.486	2.419	2.46625
240	2.644	2.649	2.637	2.64	2.6425

Table 4 Initial dose series experiment from 40 mJ/cm^2 up to 240 mJ/cm^2 with intervals of 40 mJ/cm^2.

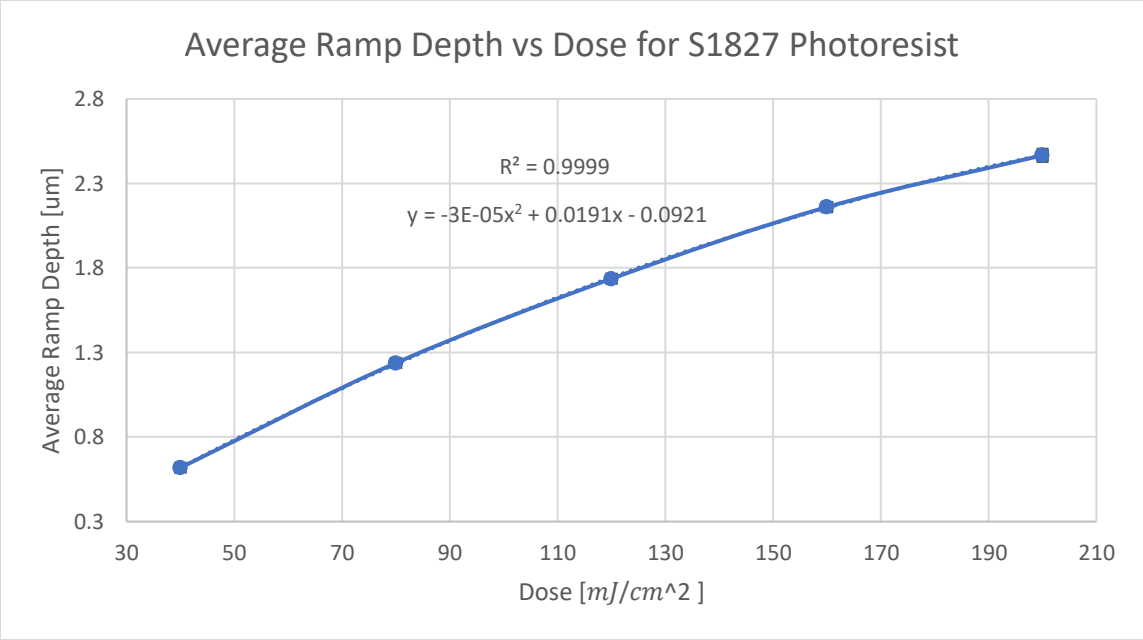

Figure 22 Average ramp height vs dose plotted using the data shown in Table 4. A quadratic trendline is plotted with equation and R squared value shown. Error bars show +/- one standard deviation of the data set though they are insignificant and do not display on the graph.

From the measured ramp depths, the dose-to-clear value of S1727 under these processing conditions is 240 mJ/cm^2. As with the previous photoresist, the dose to clear value is chosen as the dose value at which all of the photoresist is cleared from the sample during development. Since S1827 is a thicker photoresist than S1813, the feature depth has a much larger range over a larger interval of doses. When the average feature depth data is plotted as shown in Figure 22, a quadratic relationship is revealed between the MLA dose and resulting feature depth. From this data it is possible to extrapolate a dose value for any given feature depth within the bounds of the MLA dose and the photoresist dose-to-clear value.

The results shown in Table 4 are used to create a linearization mapping for patterns using the same methodology as outlined for S1813 photoresist. First, a maximum feature depth is identified. From that desired feature depth, the dosage corresponding to the feature/ramp depth

desired is chosen to create a linearization mapping. That mapping is then applied to a specified design. When exposed with the characterization dose, the final exposure exhibits grayscale behavior with the specified feature depth.

5.3 AZ4620 Photoresist

A dose series test is carried out using AZ4620 photoresist in order to characterize the behavior of the photoresist. All of the sample preparation processes are kept consistent for this photoresist, including the chemical clean and processing through the plasma cleaner. The spin recipe is also kept constant, though a different photoresist of AZ4620 is used. Since this resist is much thicker than S1813 or S1827, it does not work well with the syringe and filter application as the S- series resists did. Instead, The AZ4620 resist is applied by simply pouring the resist onto the slide in a thin stream until the surface is covered. Like the s-series resists, the sample is heated at 115C on a hotplate for 1 minute prior to being exposed. After exposure, the sample is developed using a P- series specific developer AZ4000K. A 4:1 ratio of developer to DI water is used, and the sample is developed for a total of 120 seconds. Developer temperature and agitation methods are also kept the same as with the S- series resists.

Like the S- series photoresist, a broad series of dose values are tested, starting at an initial dose of 40 mJ/cm^2 up to 320 mJ/cm^2 with intervals of 40 mJ/cm^2. This set of doses are chosen because it covers a large range of values while yielding an adequate amount of data points for analysis. The resulting ramp depths for each different dosage are given below. The ramp data for patterns printed with a dose lower than 80 are severely underexposed, and patterns printed with a dose higher than 250 are severely overexposed.

Characterization of AZ P4620 Photoresist					
Dose $[mJ/cm^2]$	**Ramp Depth [um]**				
	Trial 1	**Trial 2**	**Trial 3**	**Trial 4**	**Average**
40	underexposed				--
80	1.669	1.526	1.518	1.404	1.52925
120	2.134	2.225	2.328	2.411	2.2745
160	3.713	2.931	2.699	2.715	3.0145
200	3.563	3.356	3.513	3.658	3.5225
240	4.054	4.185	3.937	4.433	4.15225
280	5.063	4.974	4.64	5.238	4.97875
320	overexposed				--

Table 5 Results of dose series testing for AZ4620 photoresist. All doses tested below 80 and above 280 are severely under- or overexposed.

From the measured ramp depths, the dose-to-clear value of AZ4620 under these processing conditions is 280 mJ/cm^2. As with the previous photoresist, the dose to clear value is chosen as the dose value at which all of the photoresist is cleared from the sample during development. Since AZ4620 is a thicker photoresist than both of the s- series photoresists, the feature depth has a much larger range for a similar range of doses. The exposure series was printed 4 different times in order to average the data, as shown in the table above.

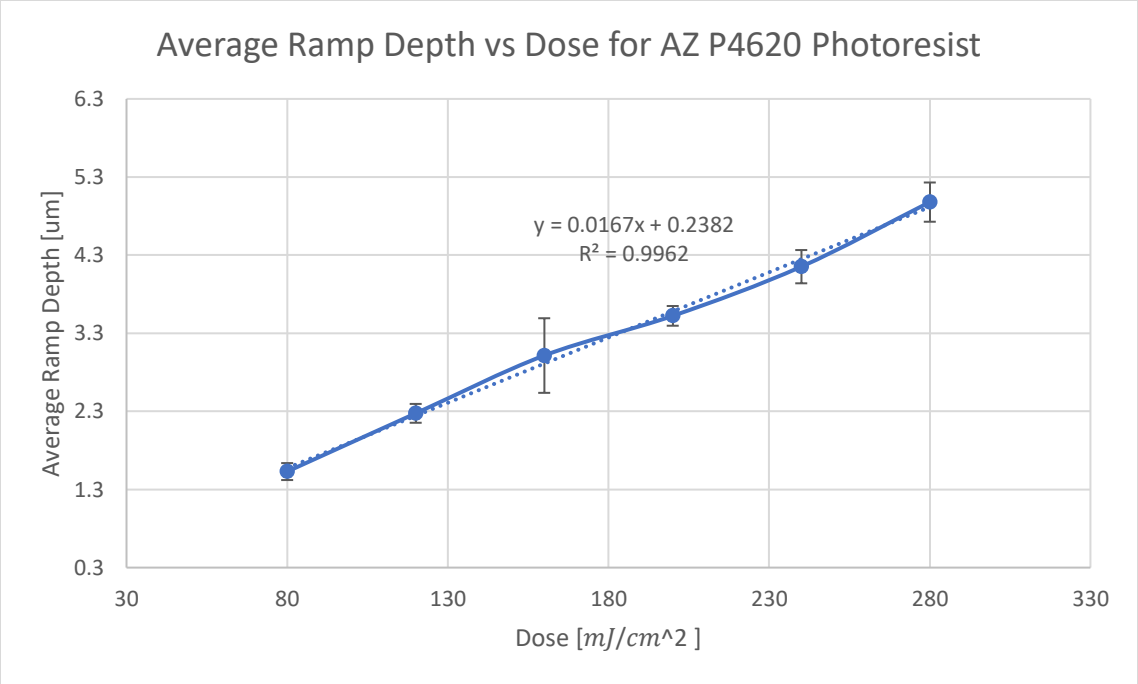

Figure 23 Average ramp height vs dose plotted using the data shown in Table 5. A linear trendline is plotted with equation and R squared value shown . Error bars show +/- one standard deviation of the data set.

When the average feature depth data is plotted as shown in Figure 23, a linear relationship is revealed between the MLA dose and resulting feature depth. From this data, it is possible to extrapolate a dose value for any given feature depth within the bounds of the MLA dose and the photoresist dose-to-clear value.

As with the S- series photoresist, the results shown in Table 5 are used to choose a dose from which to create a linearization mapping for patterns using the same methodology as outlined in previous sections. A maximum feature depth is first identified. From that desired feature depth, the dosage corresponding to the feature/ramp depth desired is chosen to create a linearization mapping. That mapping is then applied to a specified design. When exposed with the same dose it was characterized with, the final exposure exhibits grayscale behavior with the specified feature depth.

6 GRAYSCALE LITHOGRAPHY DESIGN

6.1 CGH Design via OptiScan

All of the computer-generated hologram (CGH) designs used are created in MATLAB. Some applications utilized their own MATLAB scripts to generate a design, such as the Adaptive Optics application discussed in Section 7.1. The Milster Research Group uses its own software, OptiScan, in order to create CGHs such as binary amplitude/phase transmission gratings, Fresnel lenses and CGHs using the Gerchberg-Saxton algorithm. Broadly, OptiScan is a tool for simulating the operation of optical systems. Unlike other simulation software, OptiScan incorporates a wide variety of wave-optic phenomena that are easily available through a user friendly interface.

Simple CGH's are made in OptiScan using the Gerchberg-Saxton beam shaper, which is an iterative phase retrieval algorithm. Opening up the software brings you to the DOE Calculator where the user adds/edits DOE elements.

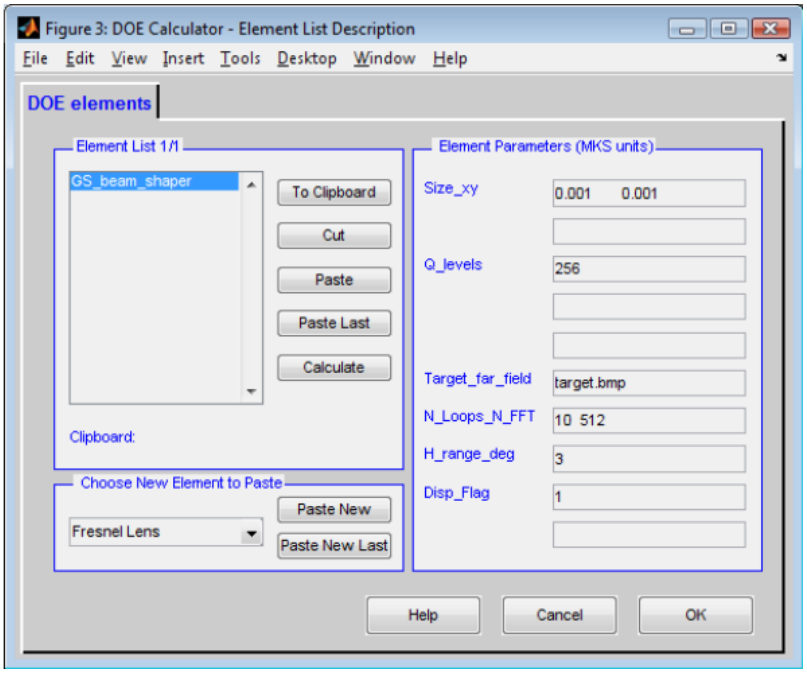

Figure 24 DOE Elements window specifying the Gerchberg-Saxton bean shaper as an element

Here, the Gerchberg-Saxton beam shaper is added as an element, and other element parameters specified. The software documentation files specify specifically what each parameter describes, as well as its units. The Gerchberg-Saxton beam shaper for example, is described in the documentation files as taking a bitmap image and creating a Fourier hologram for it using the Gerchberg-Saxton algorithm. A further example is the parameter H_range_deg, which is given as the full angular range corresponding to the input Target_far_field bitmap file demonstrated below [20].

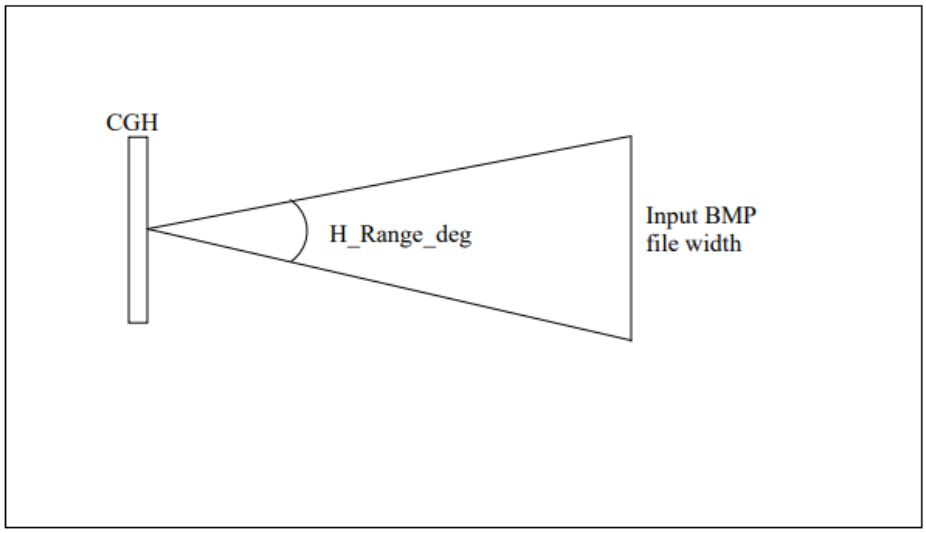

Figure 25 Description of the Gerchberg-Saxton beam shaper element parameter H_range_deg [20]

All other parameter descriptions for the Gerchberg-Saxton beam shaper as well as all other elements are found in the documentation files on the Milster Group website. Overall, OptiScan is a very useful software tool that allows users to create simple CGH designs quickly and efficiently.

.

6.2 Ramp Calibration Process

Throughout the process of developing a grayscale lithography procedure, it is necessary to have a consistent calibration pattern that can be fabricated and lithographically exposed in order to determine the relative success of the developing procedures. A calibration ramp pattern is developed in OptiScan using the 'Ramp' element and a Q_level value of 64 (a detailed description of the OptiScan design process is given in Appendix A). The Q_level value specifies the number of quantization levels in an exposure, where a value of 2 indicates a binary exposure and a higher value indicates differing amounts of gray levels. Multiple 'ramp' elements are added to the design in different sizes and orientations in groupings over the entire exposure area, such that the behavior of the exposure and fabrication process is verified over both the x- and y- axis and in differing feature sizes. The base calibration ramp file is depicted below.

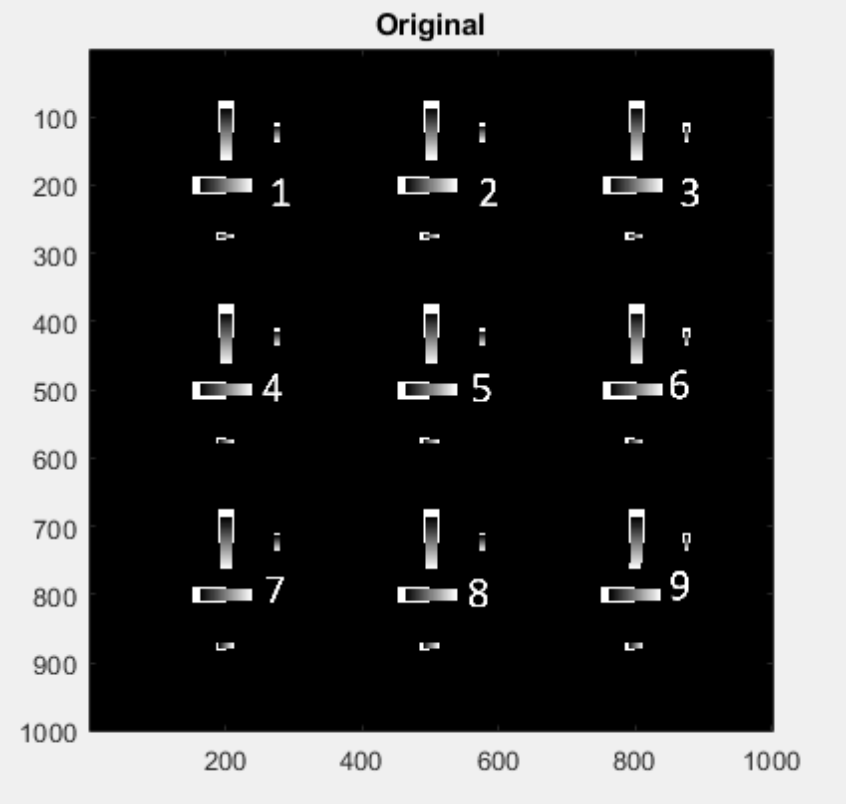

Figure 26 Calibration ramp design via OptiScan. All ramp groupings are numbered to ensure similar features are compared when experimenting with different exposure parameters.

All MATLAB designed CGHs are output as bitmap files and converted individually into .dxf files. Separate MATLAB software is created and tested to convert CGH designs from bitmap to .dxf, as shown in Appendix D. The above ramp file served as an efficient method for observing the progress of the grayscale lithography procedures. The nine large vertical and horizontal ramps are useful in determining whether the process results in a grayscale output. This file is used to characterize each different photoresist used throughout this project. As explained in previous sections, a dose series test is first performed on the ramp pattern in order to determine the proper dosage parameter for the given photoresist. Next, the development process is refined such that the ideal developer concentration, time, temperature and agitation methods are determined. Once the correct ramp depth is obtained from finalizing the development process, the ramp calibration pattern is calibrated, such that the resulting exposure exhibits a linear progression grayscale response.

6.3 Linearization Methods

Although the MLA 150 is capable of exposing patterns in grayscale, the outcome does not demonstrate truly linear grayscale performance. Due to the chemical response of the photoresist to the instrument's source irradiance, the initial ramp calibration patterns show a large shoulder in with linearly increasing exposure, where the photoresist does not react linearly at small dose levels.

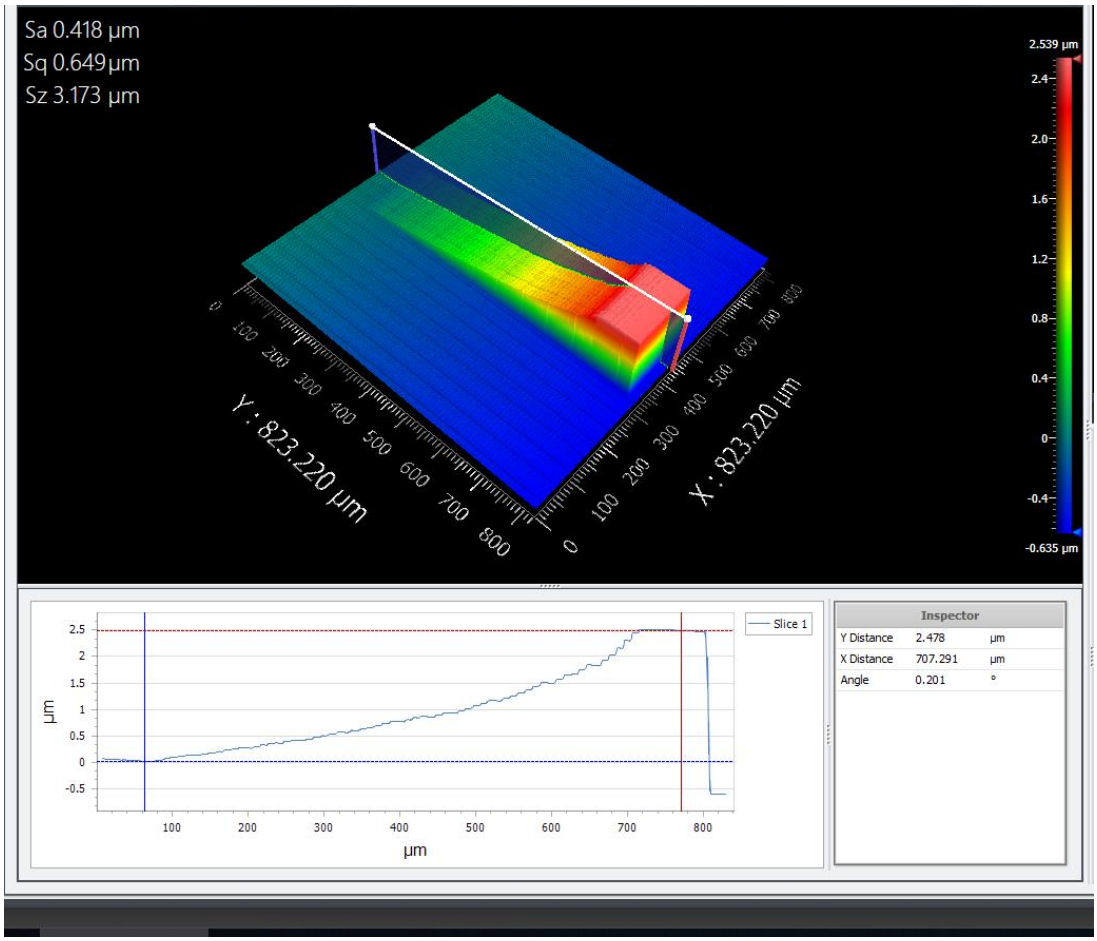

Figure 27. Profile scan of a calibration ramp exposed with S1827 photoresist prior to being calibrated and linearized. The ramp shows a non-linear progression.

In order to prevent this characteristic response, as shown in Figure 27, the ramp pattern needs to be calibrated and linearized such that when exposed, the resulting pattern has equally exposed grayscale layers. The profile data depicted in the NewView white light interferometer scans is exported as a .cvs file, and the ramp data are isolated. Once input into MATLAB, the data is flipped left/right in order to accommodate the linearization software.

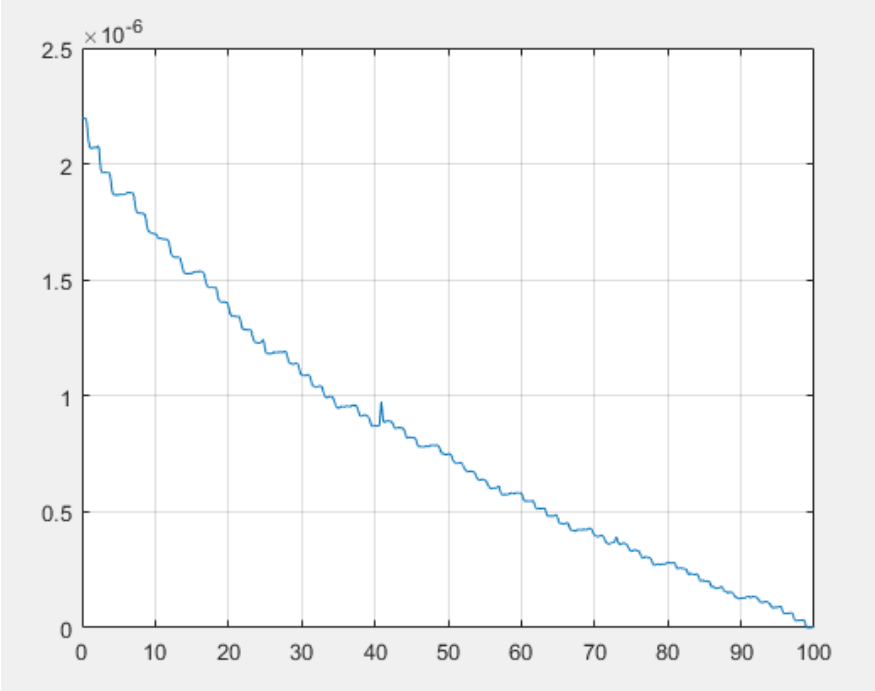

Figure 28 Ramp profile data isolated and flipped left/right in order to accommodate software requirements

Next, a curve fit is applied to the data, such that the curve fit close resembles the behavior of the measured data. The curve fitting results for the above set of data is shown below.

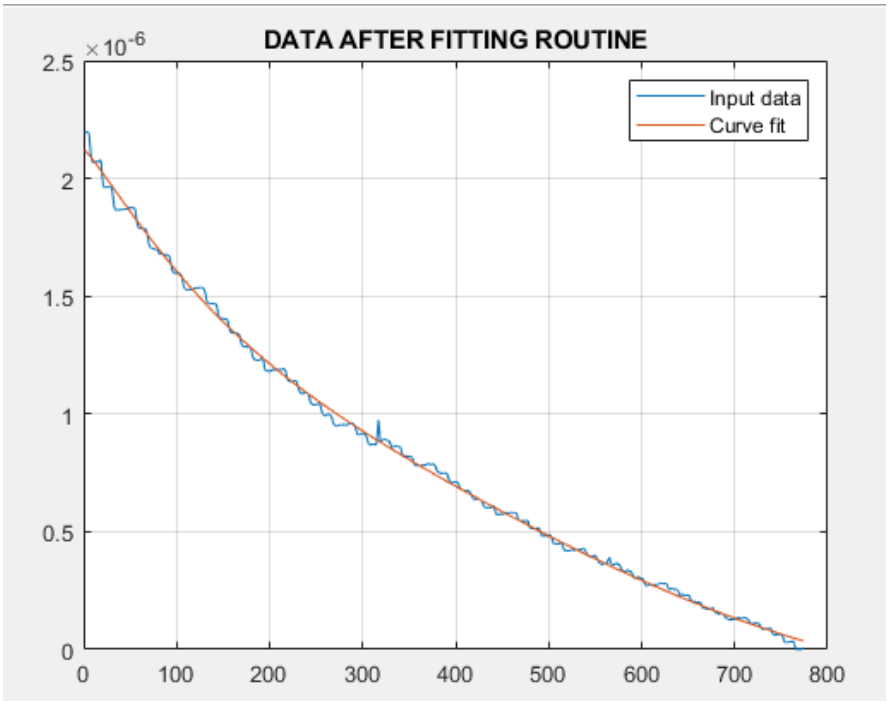

Figure 29 Curve fitting regime applied to raw profile data

Once an appropriate curve fit is found, an exposure range is chosen. The exposure range is chosen around the most linearly behaving section of the curve. Commonly, the low-end and high-end dose values are not used. These areas have the characteristic of behaving non-linearly. The height difference between the top and bottom point of the exposure range shown in green corresponds to the final maximum depth of the final exposed pattern.

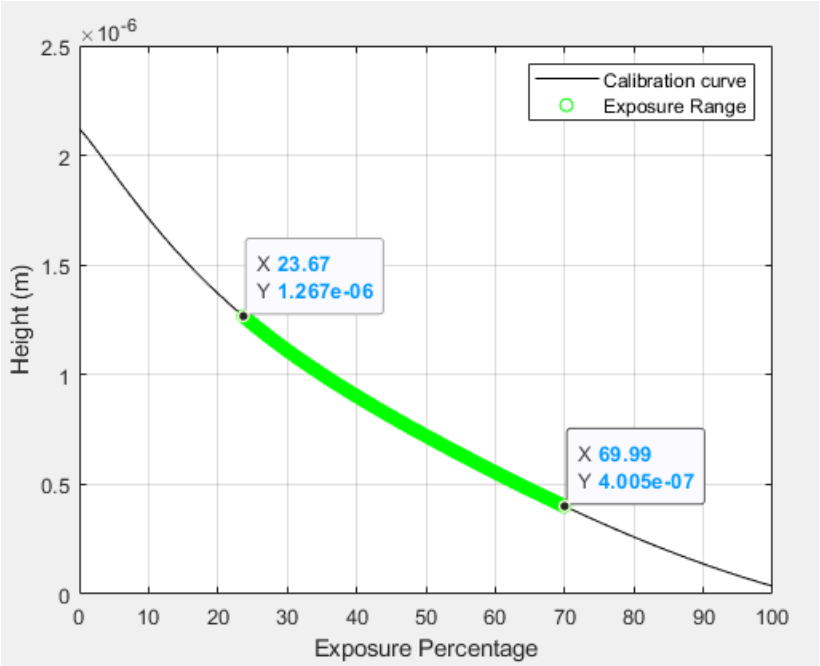

Figure 30 Choosing exposure range from curve fit data

Once an exposure range is chosen with the user's specific depth requirement, it is then mapped as an input/output table shown below. This mapping table visually correlates the output dosage required to obtain the input design.

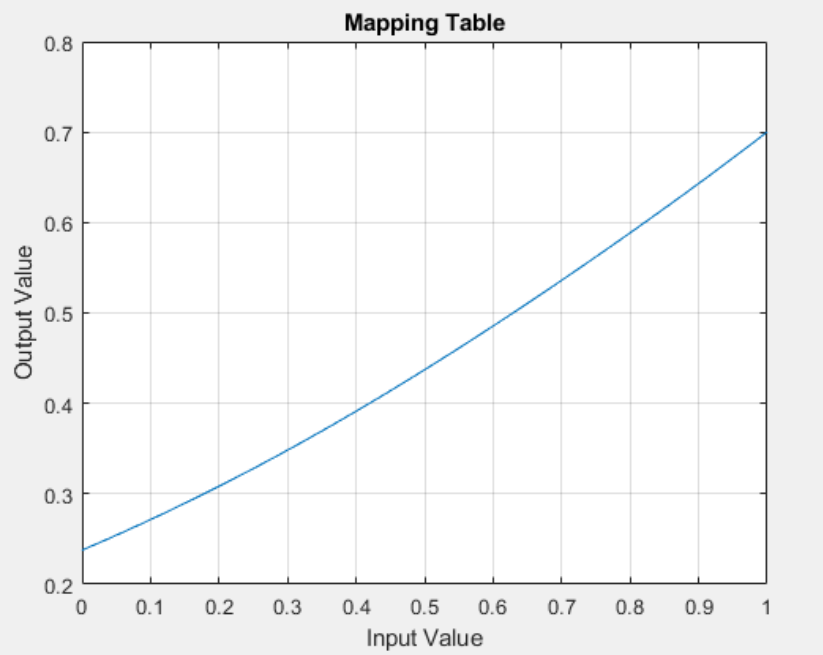

Figure 31 Linearization mapping table

The mapping table relationship is applied to exposure pattern and will result in a linear output. All other variables such as photoresist, dosage, and developer processes must be kept constant throughout the use of a single mapping calibration. The calibration ramp pattern below is been calibrated using the above table mapping.

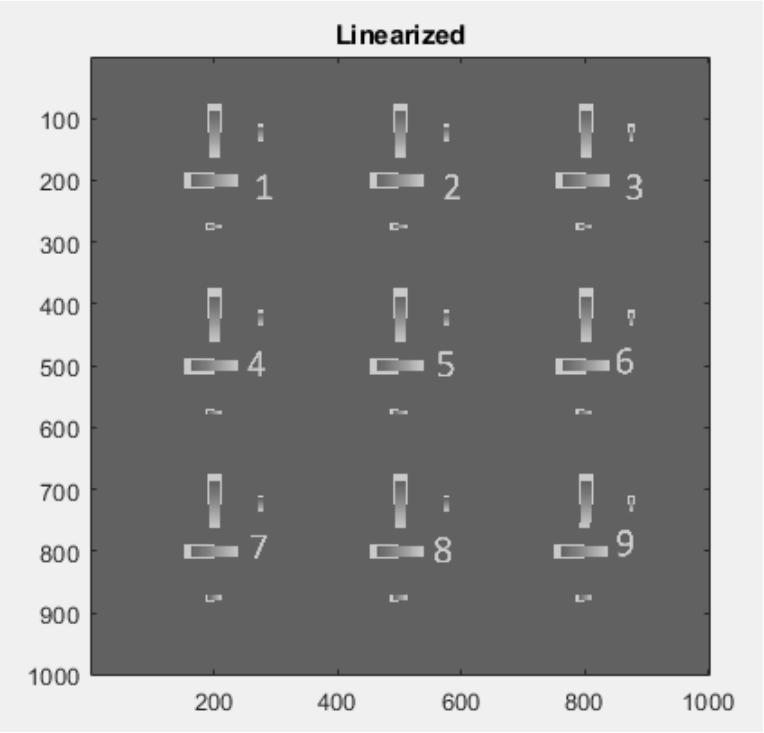

Figure 32 Final linearized ramp calibration design once the linearization mapping has been applied

Visually, the design appears to have a more grayed background than the original due to the exposure range chosen and subsequent mapping table discarding the maximum and minimum exposure doses. The middle gray values have a much more linear progression in response to a linearly increasing dosage. Due to this process, the number of grayscale layers of the linearized pattern after the mapping is decreased by a factor of two. The original calibration ramp pattern is created with 64 grayscale layers, such that all of the designs applied with a linearization mapping have 32 grayscale layers. A user manual of the linearization software used for this project is given in Appendix A.

One of the biggest challenges in working with the MLA 150 is the aspect of the instrument being used by numerous students throughout the college. While the instrument is housed in stable and consistent conditions, even very slight changes to its environment and usage results in

drastically different exposure responses. The above linearization regime needed to be redone and updated frequently throughout the project, as the instrument went through updates and down times that affected its exposure characteristics. Many of the linearized examples given throughout this report are linearized using different mappings dependent upon the required feature depth as well as through different calibrations done to the instrument throughout its usage.

7 FABRICATION RESULTS

7.1 Grayscale Lithography via MLA 150

In order to form a direct comparison of the effect of the linearization technique on the exposures, all parameters are kept constant except for the design file itself. Microscope slides are used as test substrates, as their quality is good enough to demonstrate consistent and comparable results while still being cost effective. The samples are prepped through a process of chemical solvent cleaning of acetone and isopropyl alcohol followed by 5 minutes in a plasma cleaner. The specified photoresist (S1827 in this example) is spun onto the sample after being applied through a 0.45 micron filter following the same recipe as used in the original exposure. The spin recipe specifies 5s of acceleration increasing up to 2000rpm, 5s of acceleration increasing up to 3000rpm, 5s of acceleration increasing up to 4000rpm and finally 5s at 4000rpm. The coated samples are then baked on a hotplate at 115C for one minute. After being exposed, the sample is immersed in a 1:4 concentration of 351 developer to water for a total of 1 minute. The sample is agitated every 5 seconds for the duration of the bath and rinsed in DI water after being removed.

The linearization regime discussed in the previous section yields very successful results. A direct comparison is made of the calibration ramp pattern exposed both before and after calibration, with the linearization mapping demonstrating drastic improvement. The same feature of the calibrated and linearized ramp pattern is shown below.

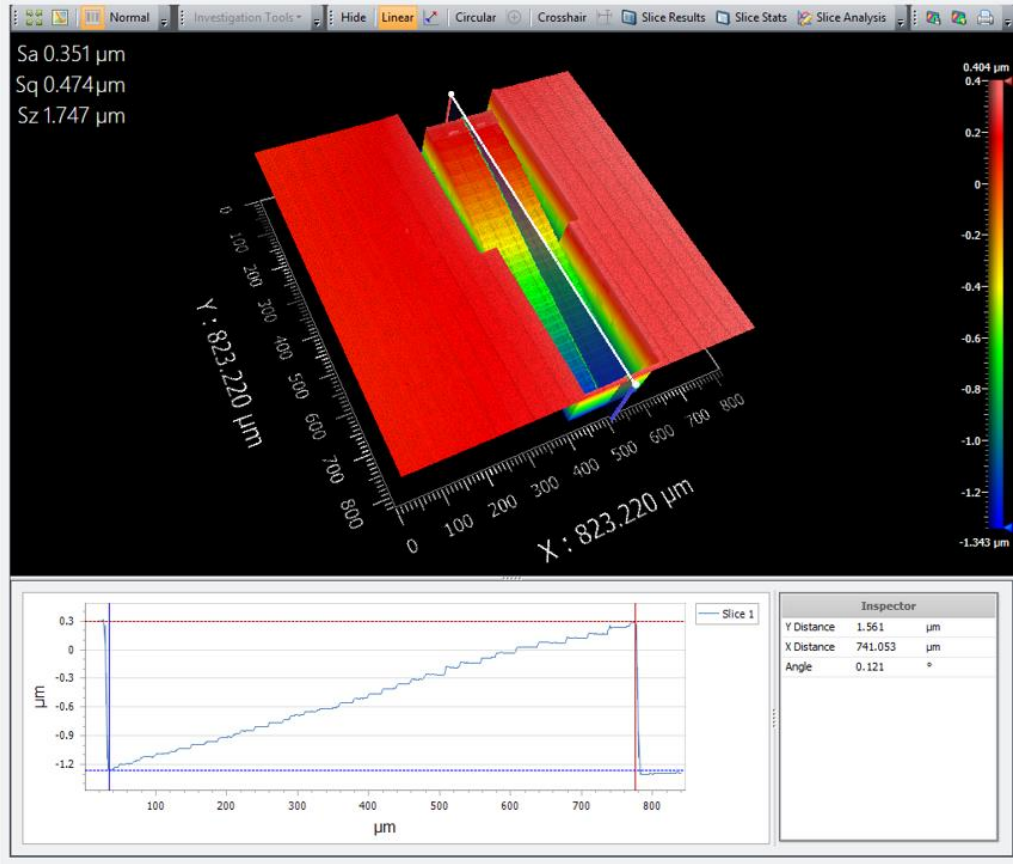

Figure 33 Resulting performance of linearization on the calibration ramp pattern, comparable to the feature shown in Figure 27 that was measured before a linearization regime was applied.

Figure 33 in comparison to Figure 27 demonstrates that the linear performance of the lithographic exposure is greatly improved as a result of applying a calibrated linearization mapping. The use of the calibration ramp pattern enables experimental proof of the quality of the linearization technique. Once the calibration ramp pattern demonstrates a cleanly linear response post-exposure, the linearization mapping is then applied to grayscale patterns for improved grayscale performance.

Further variables were tested to verify the fabrication process, such as exposing calibration ramps across both the x- and y- axis of the MLA in order to ensure proper performance.

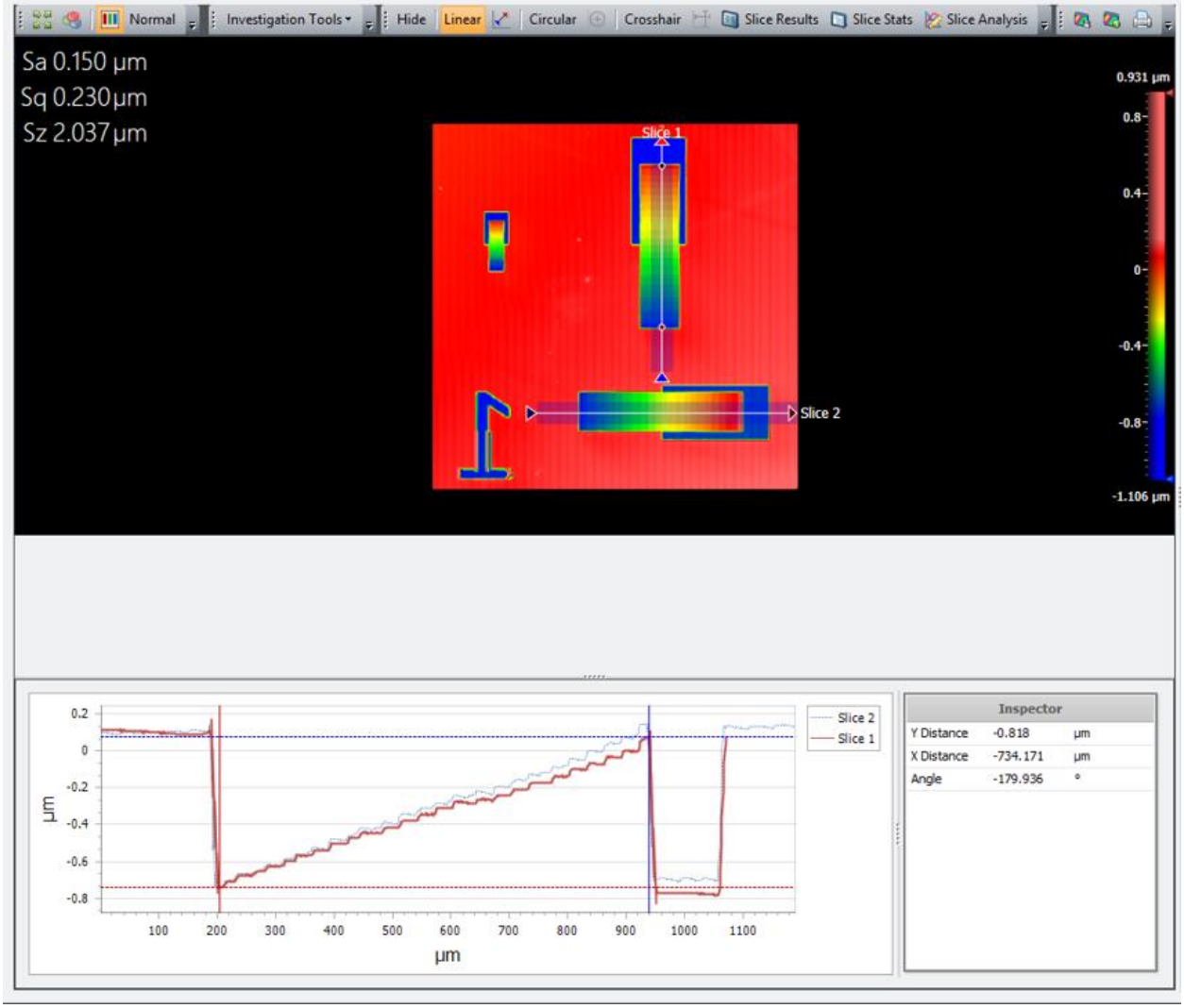

Figure 34 Verification of linearized MLA exposure of the calibration ramp pattern over the x- and y- axis. The average profile of two 100um thick slices are shown overlapping.

Figure 34 above demonstrates that the calibration ramp pattern exposes evenly and accurately in both directions. Since the MLA 150 utilizes a stitching regime in order to print over large areas, it is important to ensure that the stitching is accurate over both axes. Overall, it is found that the DMD pixel width setting on the MLA 150 had a large impact on whether both axes printed with high quality. When using the innermost 400 DMD pixels, the stitching between the MLA exposures as the stage moves is much less visible in the resulting patterns. For this reason, the

DMD width is kept constant at 400 pixels, rather than the nominal setting of 1000 pixels. This 400-pixel setting increased the exposure time by a factor of two, but it greatly increased the quality of the resulting exposures.

One example of the linearization mapping being applied to any specified grayscale design is the use of a very complex pattern detailing the facial profile of a person. The original grayscale pattern as well as the linearized pattern is shown below.

Figure 35 Original grayscale pattern and linearized grayscale pattern of a person's image.

While not significant for its ability to observe any one qualitative feature or aspect of the exposure, this pattern enables the testing of the linearization regime as well as the bitmap to .dxf conversion software on larger and more complex files (15x larger file size). This exposure utilized S1813

photoresist and is developed for 45s. Interferometer scans of the linearized exposure are shown below.

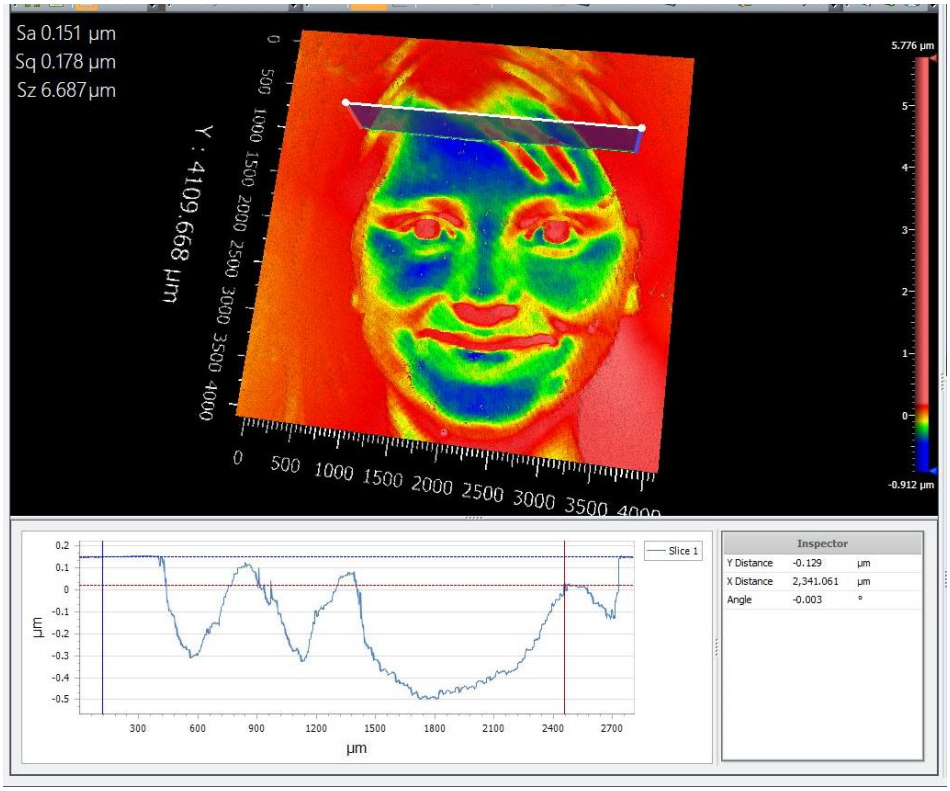

Figure 36 Linearized exposure of a person's image in order to test the usage of a large and complex file. The profile shown is not significant, except to demonstrate the grayscale characteristics of the exposure. 4x4 stitched image using a 10x magnification objective.

The above exposure demonstrates the success of the linearization regime on much larger and complex files. This test was also a successful demonstration of the conversion software such that the image of the person was preserved. A user manual and overview of the conversion software used in this project are given in Appendix A.

7.2 Replication via NOA61

Once a consistent high quality grayscale lithographic produce is finalized, the pattern is replicated as a more permanent and useful optical element. Unlike photoresist, NOA61 has

advantageous transmissive properties. Once cast and hardened under UV lights, the resulting optical element is an exact inverse of the original exposure pattern. The replication process is chosen over more in-depth etching processes due to its quick turnover time that enables multiple iterations over a short time period. This is advantageous when testing multiple variables and parameters over the course of the project.

Samples are replicated first onto microscope slides that are prepared using the same methodology as for lithographic exposures. Substrates are cleaned using a chemical solvent rinse of acetone and isopropyl alcohol before being rinsed with DI water and cleaned in a plasma cleaner for 5 minutes. It is necessary for the samples to be completely dry before applying a drop of NOA61 onto the center of the substrate. The exposed pattern is then placed facedown onto the NOA61 droplet, such that the NOA61 spreads under the weight of the sample to cover the entire exposed pattern. Both samples are then transferred to a UV oven and cured for 10 minutes. The curing process bonds the NOA61 to the secondary substrate. The cured samples are placed in a bath of concentrated developer for 15s. Immersion in concentrated developer helps to dissolve the original photoresist exposure, such that the two samples can be separated. Separation of the samples is done carefully, as the samples will snap apart suddenly when adequate force is applied. On some occasions the photoresist on the exposure sample is cleared due to incorrect development, such that the NOA61 bonds to both glass substrates. In this scenario, the samples do not separate and will likely break when separation is attempted. The replication process is depicted previously in Figure 10. Once separated, the replicated optical element has the inverse pattern of the original exposed sample. In many instances, the replicated sample also exhibits small bubbles on the surface of the NOA61. While the exact cause of these air bubbles are unknown, it is likely due to air pockets in the original droplet of NOA61 before the exposed sample is applied or from the

replicated sample not being complexly dry before NOA61 is applied. In this application where the replicated samples are small in size (not greater than 10x10mm), any air bubbles that remain throughout the process did not pose a significance source of error to the resulting pattern.

Furthermore, the replicated patterns preserve the depth of the original exposures. When tested with a linearized calibration ramp pattern, the exposure is designed with a feature depth of 0.8um. This depth corresponded to about one wavelength of optical path difference at 405nm. As shown below, both the linearized MLA exposure and the subsequently replicated pattern are fabricated very close to this specified depth.

A) Linearized MLA Exposure, Depth of 0.780um

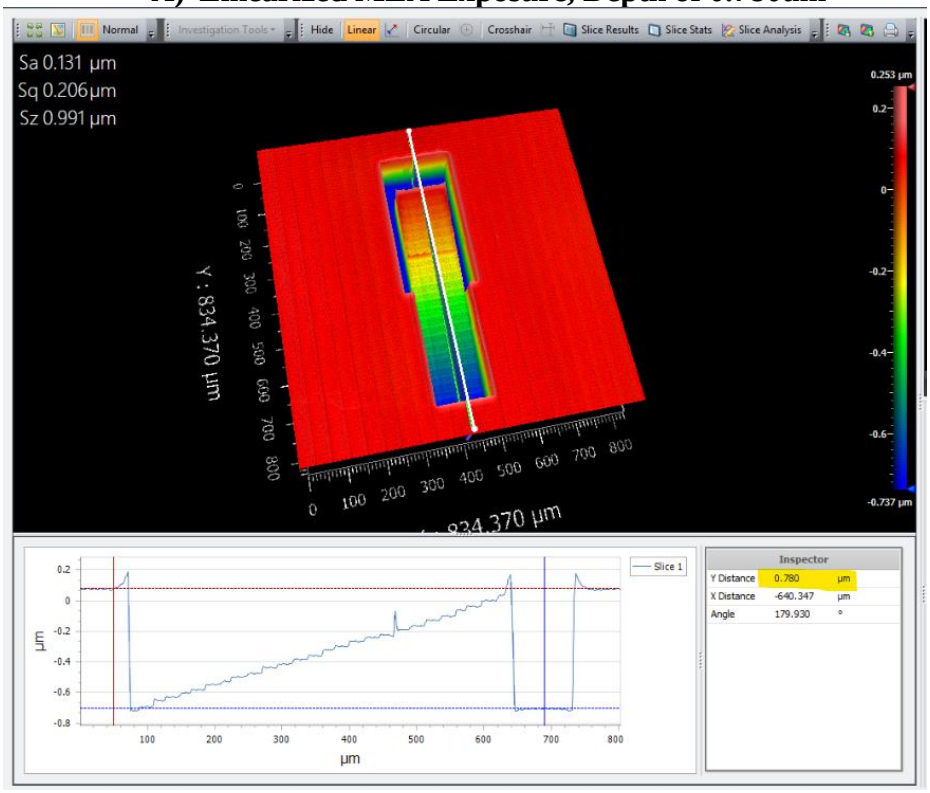

B) Pattern Replicated in NOA61, Depth of 0.784um

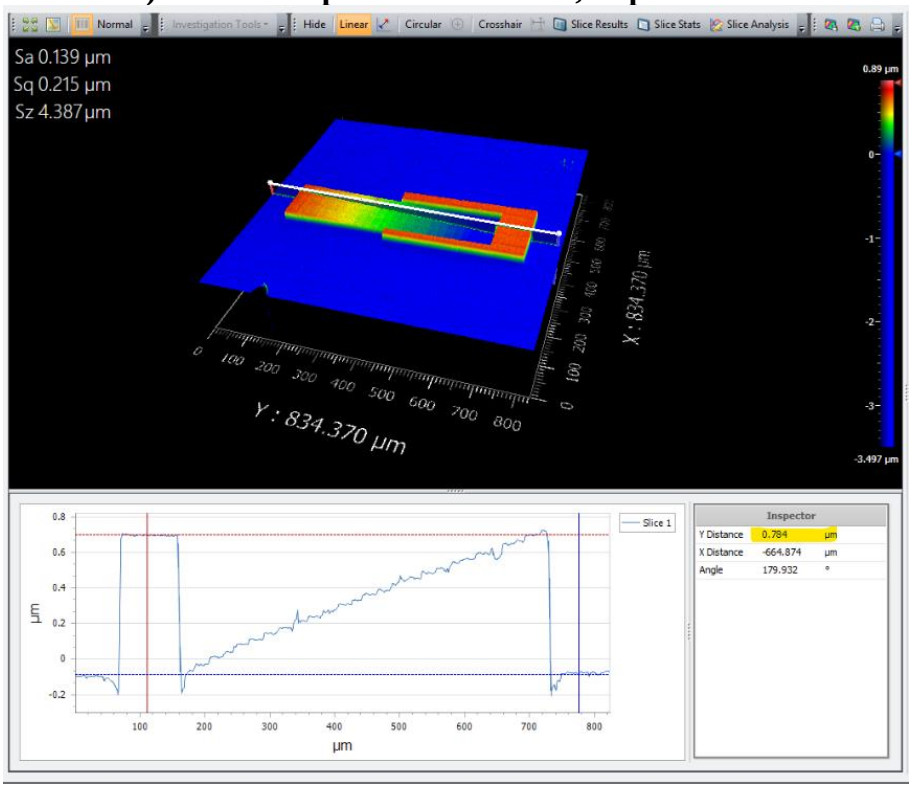

Figure 37 Direct comparison of a linearized exposure (A) and its replication (B) with the depth of the pattern (~0.78um) being preserved throughout the replication process.

An example of a replicated element is shown below.

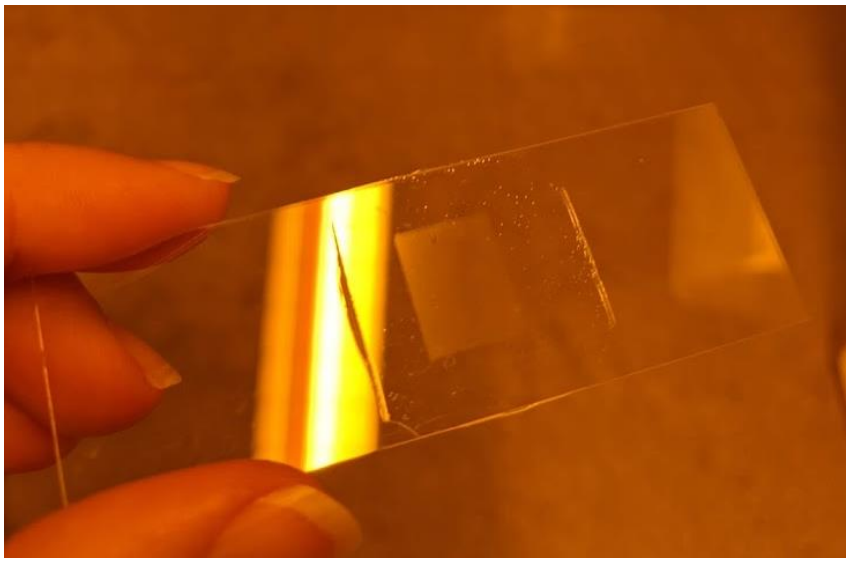

Figure 38 Example of a replicated element with an 8X10mm diffractive pattern on a microscope slide.

An example replicated optical element is shown rather than an example of a replicated calibration ramp pattern simply because the ramp pattern is difficult to discern visually as a replicated element. The sample shown in Figure 28 is a replicated CGH pattern designed for an adaptive optics application, to be discussed in the following section. The CGH itself is the seemingly diffuse rectangle in the center of the microscope slide, with the cured NOA61 shown as the raised clear section surrounding it.

8 APPLICATIONS

8.1 Adaptive Optics - Single Shot Phase Retrieval

The biggest application of grayscale lithography throughout the duration of the project is in the continued progression towards creating a CGH for single shot phase retrieval. The design and use of the CGH is coordinated through a fellow student Emily Finan, whose dissertation centers around this topic. The main contribution of this work is in the fabrication and testing of the proposed CGH as described in the following sections.

Once the proposed CGH design is linearized according to the MLA 150's specific exposure characteristics, it is fabricated. The CGH's are designed to be about 11X10mm in size and are designed to a specific wavelength and beam size. They are further designed with calibration ramps in a single corner for metrology and quality control purposes. The original and linearized CGH design is shown below.

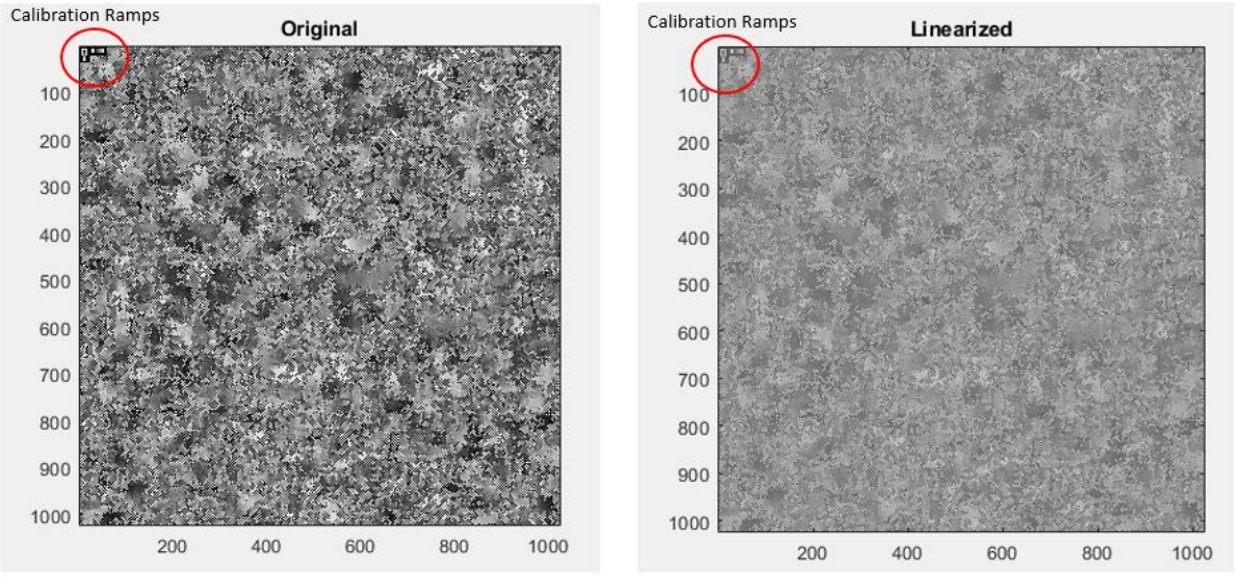

Figure 39 Original and Linearized CGH design for applications in adaptive optics for single shot phase retrieval

The linearization mapping for this design is created using the same process outlined in Section 6.3 Linearization Methods. The CGH is exposed in S1318 photoresist and subsequently replicated in NOA61. The linearized lithographic exposure and replicated samples are both measured via white-light interferometer. Profiles of the calibration ramps are measured on both samples and are compared below.

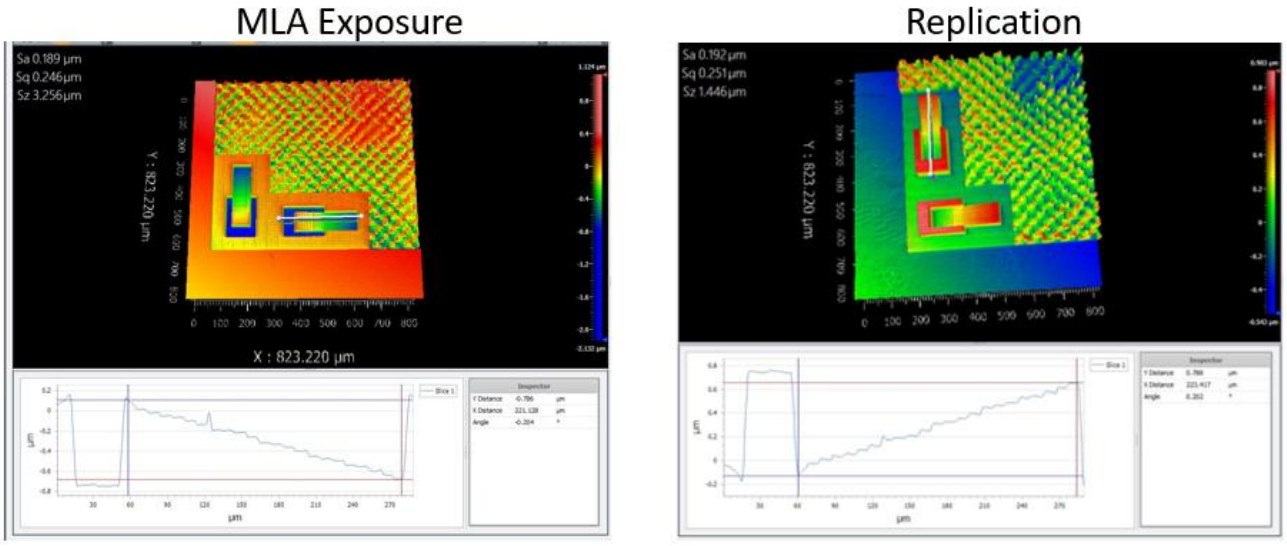

Figure 40 Comparison of a similar feature (calibration ramp) of the original linearized exposure and the replicated element. The depth of the MLA Exposure ramp (0.786um) is very similar to its replication (0.788um).

The comparison of each sample's calibration ramps shows that the exposure meet the depth requirement of $\sim 0.78um$ with acceptable error. Furthermore, the linear characteristic of the calibration ramps gives confidence that the remainder of the CGH pattern itself is printed with a linearly progressing grayscale profile. Though these measurements are a great indication of a successful fabrication process, further measurements are made in order to investigate the CGH's application in adaptive optics for single shot phase retrieval.

8.1.1 CGH Test Setup

A CGH test setup was created specifically for this application in order to image the CGH for comparison against simulated results. This project focuses on the assembly, alignment and metrology aspects of the testbed, rather than the simulation itself. Comparisons against the simulated images are made with contributions from Emily Finan. The assembled testbed and corresponding diagram of labeled components are shown below.

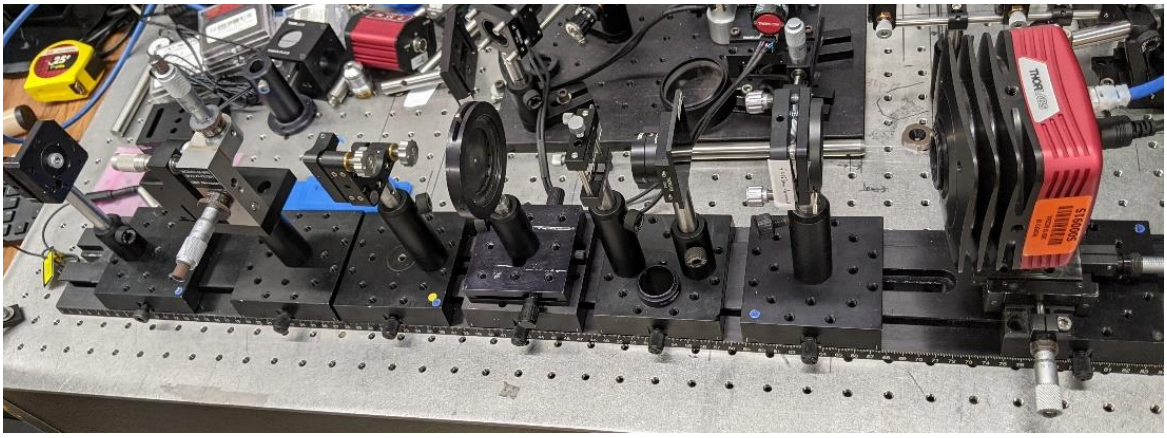

Figure 41 Experimental CGH Testbed

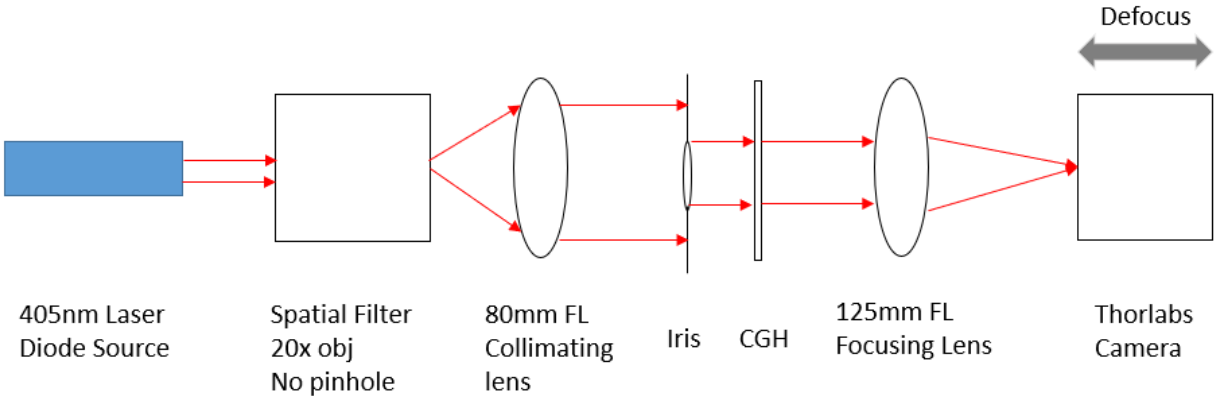

Figure 42 Diagram of CGH testbed with labeled components and light path

The test uses a 405nm laser diode source. The source is known to be non-uniform from previous experiments, which necessitates the use of a spatial filter in order to 1) expand the beam

and 2) clean up higher frequencies. An 80mm focal length collimating lens is used to collimate the beam. The collimation is checked using an appropriately sized shear plate. The beam is known to be collimated when the interference lines seen on the observation screen of the shear plate are parallel with the indication line. An iris is used to ensure a specified beam size incident onto the next component, the CGH. The image of the CGH is then focused onto the detector, which is a Thorlabs 8050-GE-TE- 8 Megapixel Monochrome CCD camera whose specifications are listed below.

Specification of Thorlabs 8050-GE-TE- 8 Megapixel Monochrome CCD Camera	
Sensor	Monochrome
Number of Active Pixels	3296 x 2472 (horizontal x vertical)
Pixel Size	5.5um x 5.5 um
Digital Output	14 Bit
Cooling	Cools to -10C at 20C ambient temp

Table 6 Specification of Thorlabs 8050-GE-TE- 8 Megapixel Monochrome CCD Camera

As described in Section 3.3.1 'Single Shot Phase Retrieval', the image of the CGH results in four diffracted images at the edge of the image with a separate center image. It is the four corner images that are used in the reconstruction regime (not discussed as a part of this work). An initial comparison of the experimental image and the simulated result are made, as demonstrated below.

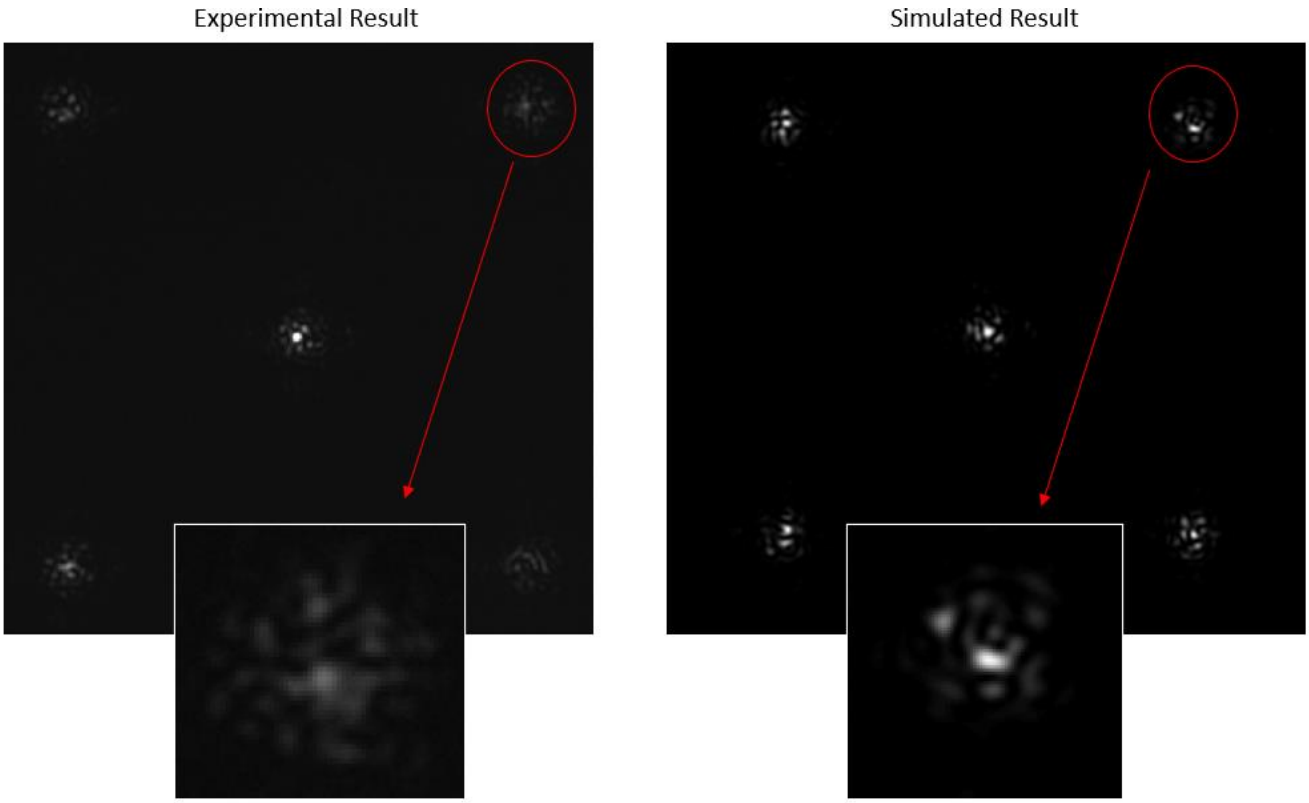

Figure 43 Comparison of the experimental image of the CGH taking using the CGH testbed and the simulated result.

Visually, the experimentally imaged CGH exhibits the appropriate pattern of a central image with an image in each of the sensor's 4 corners. When compared to simulated results, there is a difference in intensity and general shape of the four diffracted images of the experimental results. The figure above enlarges and compares a similar diffracted image between the two data sets to highlight this difference. In order to further investigate the success of the grayscale lithography and replication process in fabricating this CGH, the initial design was compared to the fabricated element. This comparison is done by extracting the 3D data from the NewView White Light interferometer and comparing it to a similar section of the original design file, as shown below.

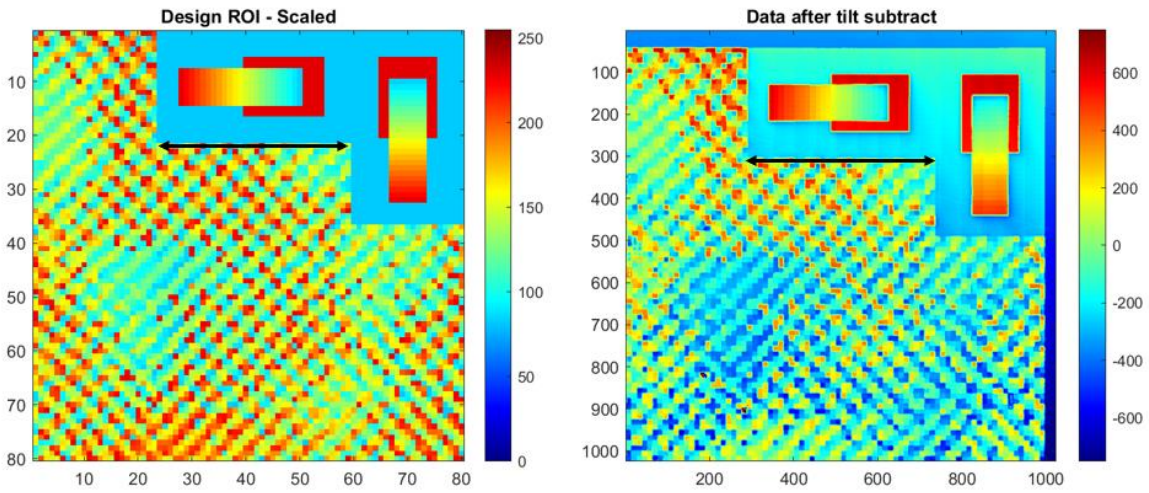

Figure 44 Comparison between the scaled design (left) and the fabricated element with tilt removed (right)

This comparison verifies that the fabrication process is a success. There are many possible reasons why the CGH images did not match the simulated images, even though the element was fabricated correctly. One possible explanation is that the placement of the incident beam onto the CGH is uncertain throughout the experiments. The beam diameter through the CGH is only 3mm, while the CGH itself is 11mm by 10m. The beam is directed through the center of the CGH, but even small displacements have a large effect on the resulting diffracted images. These factors are considered as possible areas for redesign and improvement. Overall, the fabrication of this CGH is a success and resulted in promising experimental data that helps future designs.

9 CONCLUSIONS

Optical lithography is a powerful method for creating small features in a very effective way. Developing a lithography process depends on the overall project parameters such as feature size, feature depth, sample size, and the use case for the final optical element. This project details the process development for grayscale optical lithography through the use of three different types of photoresist. Two of those photoresists come from the Microposit S1800 series and are classified as a binary photoresist, meaning that their contrast curves display sharp changes of feature depth in response to an increasing dose. The third photoresist is a classic grayscale photoresist, meaning that its contrast curve displays a gradual and linear change of feature depth in response to an increasing dosage. Binary photoresists are initially used for grayscale lithography development in this project due to the resist being readily available to students though it has proven to be very effective for grayscale applications of feature depths up to $1.5um$. Both S1800 series photoresists of S1318 and S1827 are analyzed, and their dose-to-clear values observed for a standardized grayscale process. The feature depth is also analyzed as a function of dose up to the dose-to-clear value for both photoresists. The AZ P4620 photoresist is used in order to have a diverse data set including the characterization of a photoresist with a much thicker resist layer of up to $6um$. Like the S1800 series photoresist, the AZ P4620 photoresist is analyzed, and its dose-to-clear value observed for a standardized grayscale process. The feature depth is also analyzed as a function of dose up to the dose-to-clear value in order to demonstrate a full characterization of the resist's behavior.

A linearization technique is developed that makes use of each photoresist's characterization and results in a drastic improvement in the quality of the grayscale exposures from the MLA 150. The linearization process makes use of the initial feature height vs. dose analysis of each

photoresist to control the output feature depth of the final linearized patterns. The linearization regime includes a calibration of the MLA 150's effect on various photoresist via MATLAB computation. Mapping tables are created that correlate the dose of the MLA 150 with the output dose that is needed for an improved grayscale output. While effective, any slight changes to the operating conditions of the instrument or changes to the sample preparation process result in the need for a new linearization mapping at any given dose. The software utilized in the grayscale lithography processes are extensively detailed, and software user manuals are created. Example uses of the various software are outlined, such that they can be referenced for future use.

In order to create an optical element from the lithography exposures, a fabrication process is developed in which the exposure pattern is replicated into NOA 61. This process is utilized in favor of other conventional fabrication processes, such as etching, due to the improved efficiency and lower cost. The durability of the replicated optical elements is satisfactory for their in-lab uses, such that a more permanent fabrication process is not required. Results show that the replication process used to fabricate a diffractive optical element preserves the feature depth of in the photoresist pattern. This process is used to create optical elements, such as CGH's for use in adaptive optics.

The overall success of the developed grayscale lithography process, as well as the subsequent replication of exposed patterns, is highlighted when the processes are used for an adaptive optics application. A computer-generated hologram is successfully exposed and replicated such that its output is compared to simulated results. A CGH test setup is constructed using a 405nm diode source in order to image the CGH. Analysis shows that the fabricated CGH matches its design requirements very well, though its comparison images to simulated results are inconclusive.

Changes to the design may need to be made in order for the fabricated element to better match simulated image results.

Overall, the work done for this project is cumulated in an effective and consistent baseline grayscale lithography process using the MLA 150. This work is focused on the characterization of multiple photoresists such that a specific photoresist is chosen based on the design parameters required of an exposure. The effect of the instrument's dose setting on the feature depth of subsequent exposures is thoroughly investigated, such that the relationship between them is well understood. Future work could further investigate this relationship on various other photoresists, such as negative-tone resist types. Other sample preparation parameters such as spin speed (which control the thickness of the initial resist layer), hotplate baking temperatures or even developer concentration and temperature could be further investigated. Other future work could look into using the MLA's native ability to assign gray values to every grayscale layer of an exposure as a method of intrinsic linearization. If successful, it may be more effective to calibrate the instrument via assigning calibrated gray values rather than calibrating the design pattern itself.

10 APPENDIX A

10.1 Software Manuals

10.1.1 OptiScan

The creation of DOE an CGH designs for lithographic exposure are done through OptiScan's DOE and CGH Calculator. It is a tool used to help design different diffractive optical elements and computer generated holograms to be written in photo-resist. It can be found under Accessories in the man OptiScan project window. The software is too detailed to be covered here. More information about the DOE and CGH Calculator can be found in "The DOE and CGH Calculator Help" file posted on the OptiScan website which can be found via a simple google search. This help file is reference 24 and can be used to find further information.

The calibration ramp pattern was formed using OptiScan and the 'Ramp' function within the DOE and CGH calculator. This option is found under accessories in the Main Project Workspace as shown below.

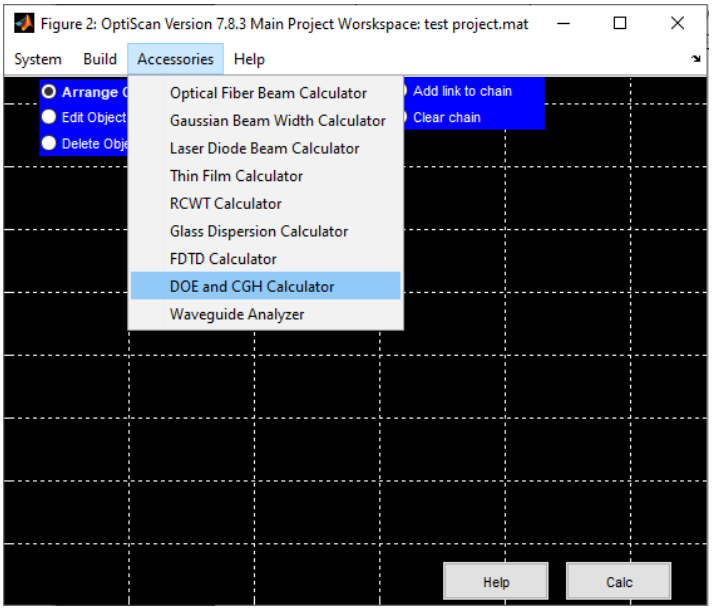

Figure 45 Choosing the DOE and CGH calculator within the Main Project Workspace

The DOE Calculator then opens and has the option to manipulate various elements within the DOE calculator as well as set the main DOE Master Definition values, shown below.

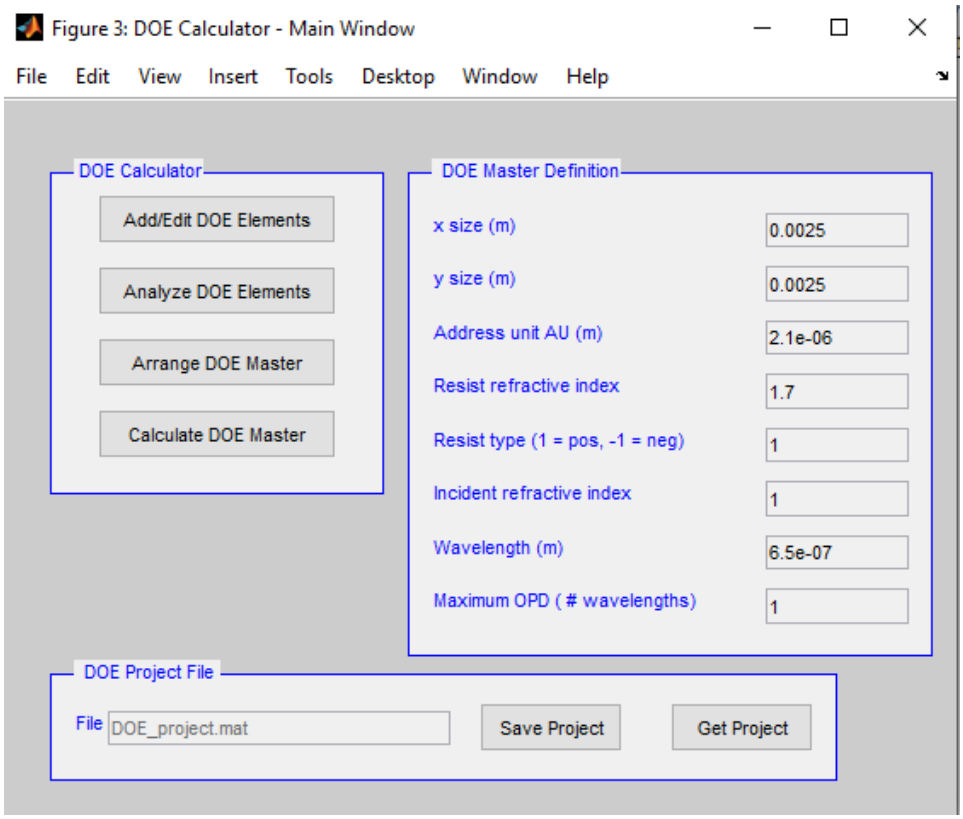

Figure 46 DOE Calculator main window

The function descriptions for the DOE Calculator options are given below.

DOE Calculator – Main Window - Buttons	
Parameter	Description
Add/Edit DOE Elements	Used to change the element list containing separate DOE elements, which are part of the Master DOE.
Analyze DOE Elements	**Not completed option/under construction**
Arrange DOE Master	Used to arrange separate Elements in the Element List as to their positins and tiling in the Master DOE.
Calculate DOE Master	Opens a panel which specifies type of linearization, border and function for generating the Master DOE.

Table 7 DOE Calculator Main Window button descriptions.

Selecting “Add/Edit DOE Elements” brings up the Element List Description where a ramp element can be added.

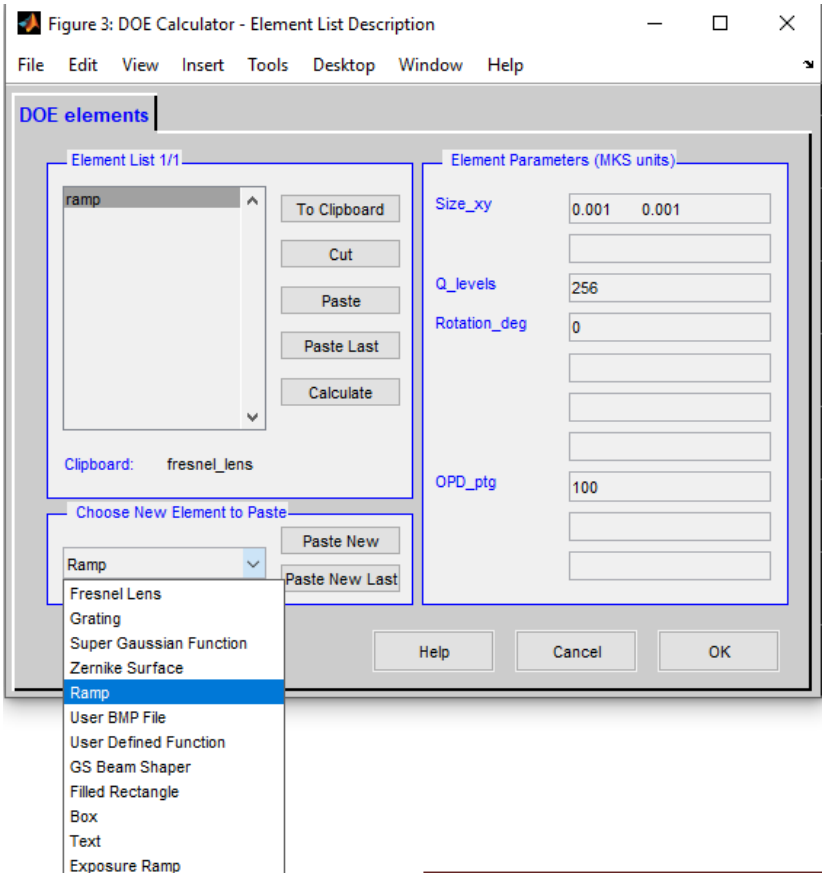

Figure 47 Adding a Ramp element to the Element List

The element parameters are listed to the right on the Element List Description page when the ramp element is highlighted. A description of these parameters is given below.

Ramp – Element Parameters	
Parameter	Description
Size_xy	Horizontal and vertical dimensions of the element with units of meters.
Q_Levels	Number of quantization levels in exposure. 2 indicates binary resist, 256 indicates 256 gray levels.
Rotation_deg	The angle which the element is rotated about the center with units of degrees.
OPD_ptg	The percentage of the total OPD for the total thickness of the element.

Table 8 Ramp Element parameter descriptions

Using OptiScan a ramp was created on a DOE Master which was 5mm by 5mm in size. The ramp has 256 gray values and is 3mm by 1mm in size centered on the DOE Master. This simple example design is shown below.

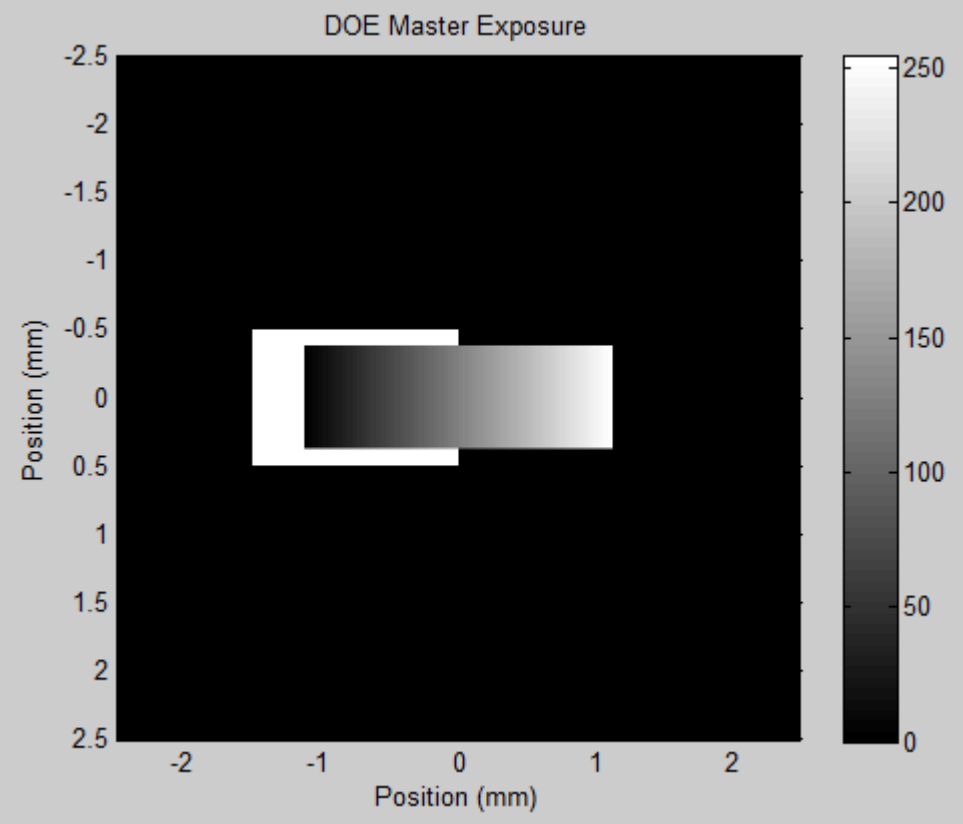

Figure 48 Example Ramp exposure pattern detailing a simple exposure ramp.

Multiple Ramp Elements of varying sizes and orientations can be added to the Element List and their position within the DOE Master can be changed via the Arrange DOE Master button in the Main DOE Window.

10.1.2 File Conversion Software

All exposure patterns were designed in OptiScan as bitmap files. The MLA 150 worked best with grayscale exposure which were of the .dxf file type. In order to use the designed patterns on the MLA 150, the patterns needed to be converted from the .bmp to the .dxf file type. Bitmap

is a file type which contains raster graphics data and is independent of display devices. This file type contains uncompressed image data which supports either monochrome or color images at variable color bit depths. The .bmp format includes a file header which holds the file identifier, size, width, height, data compression method, color and data starting point. The header is followed by the raw pixel image data. A .dxf file on the other hand is a file extension deduced from Drawing Exchange Format developed by Autodesk as a universal format for storing CAD models. This file type is text-based ASCII format. The .dxf file type is formatted with a Header, classes, tables, blocks, entities, objects, thumbnailimage, and end of file sections [25].

Multiple different processes were attempted in order to perform this conversion, since it is a very unusual conversion to need to make. Commercial conversion software existed such as LinkCAD but proved to be much too expensive to be feasible for use on this project. The need for an effective and low-cost solution resulted in a conversion software being hand-coded in MATLAB by the Milster Research Group. This software is further detailed in Appendix D. The only input from the user is a .bmp file and a desired number of gray levels. The file location is set as the variable 'fname_in' and the number of grayscale levels is set as the variable 'Nlevels'. The output is a .dxf file of the same pattern with the given number of gray levels. The output file name and location is set as the variable fname_out. The MATLAB code for this software is given in Appendix D.

10.1.3 Linearization Process Software

The Linearization Process Software is the workhorse of the grayscale linearization regime. It takes an exposure ramp raw data and isolates a linear-behaving portion of the data in which to make a mapping table of power vs. exposure depth. When the software is first run, it will prompt

the user to select a data set to use. For this project all raw data was exported from the NewView White Light Interferometer as a .cvs file. This file is then displayed as a plot to the user.

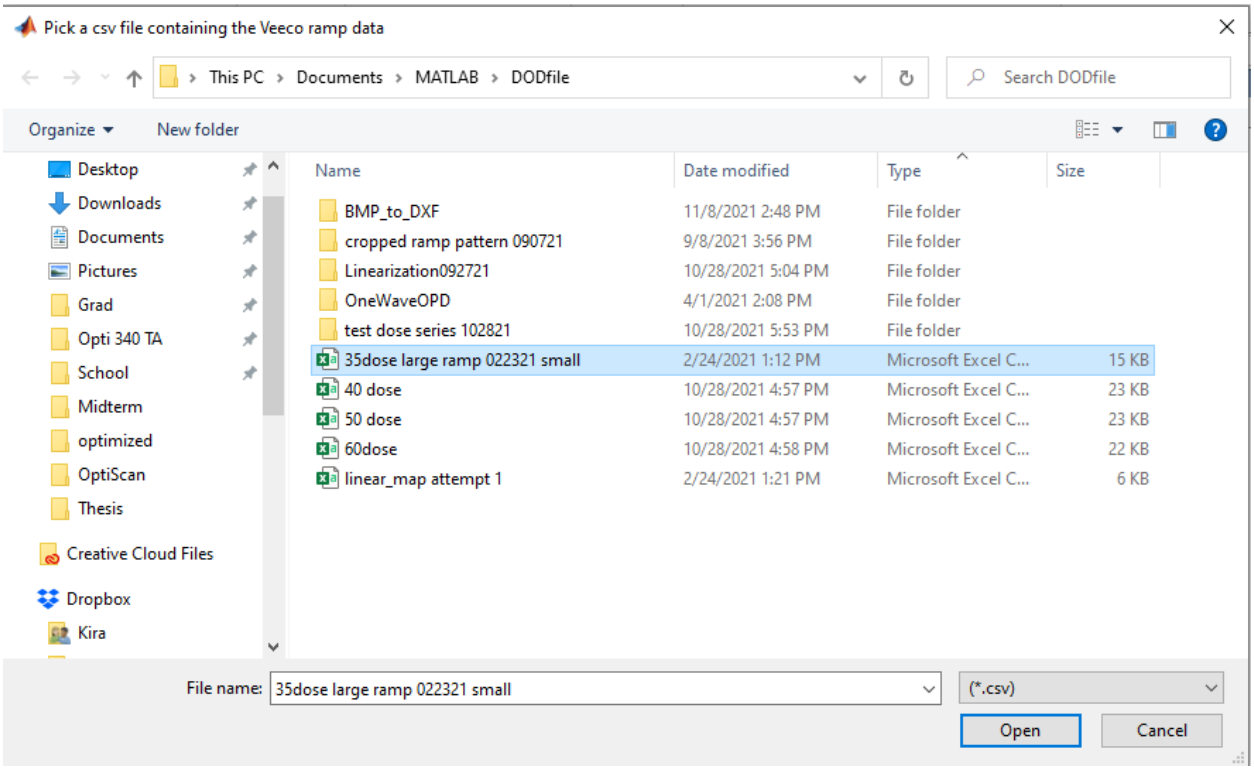

Figure 49 Prompting the user to select a profile data file

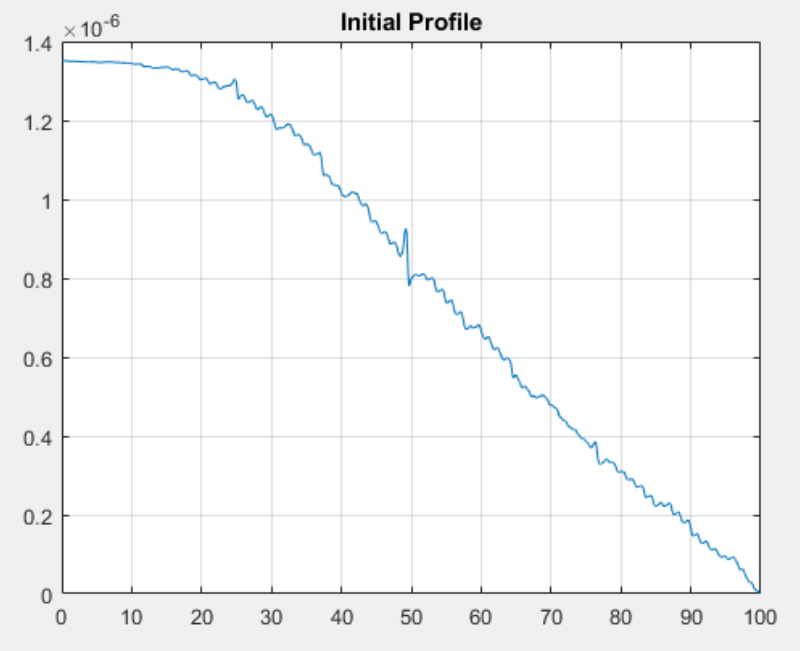

Figure 50 Display of selected raw data. Axis are position in units of microns.

The user is then prompted on what they would like to do with the presented data. In order to perform a linearization mapping, a curve fit must be applied to the data. This is done by entering in '2' for the second option as demonstrated below.

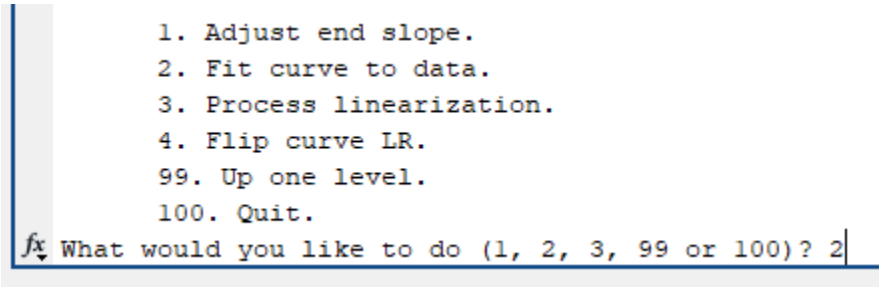

Figure 51 User selecting 2nd option to apply a curve fit to the data.

A curve fitting routine is then performed and overlayed on top of the data before being displayed to the user. The minimum error of the fitting routine's iterations are also displayed. The user has the option to move forward with the fitted curve or to perform the fitting routine again.

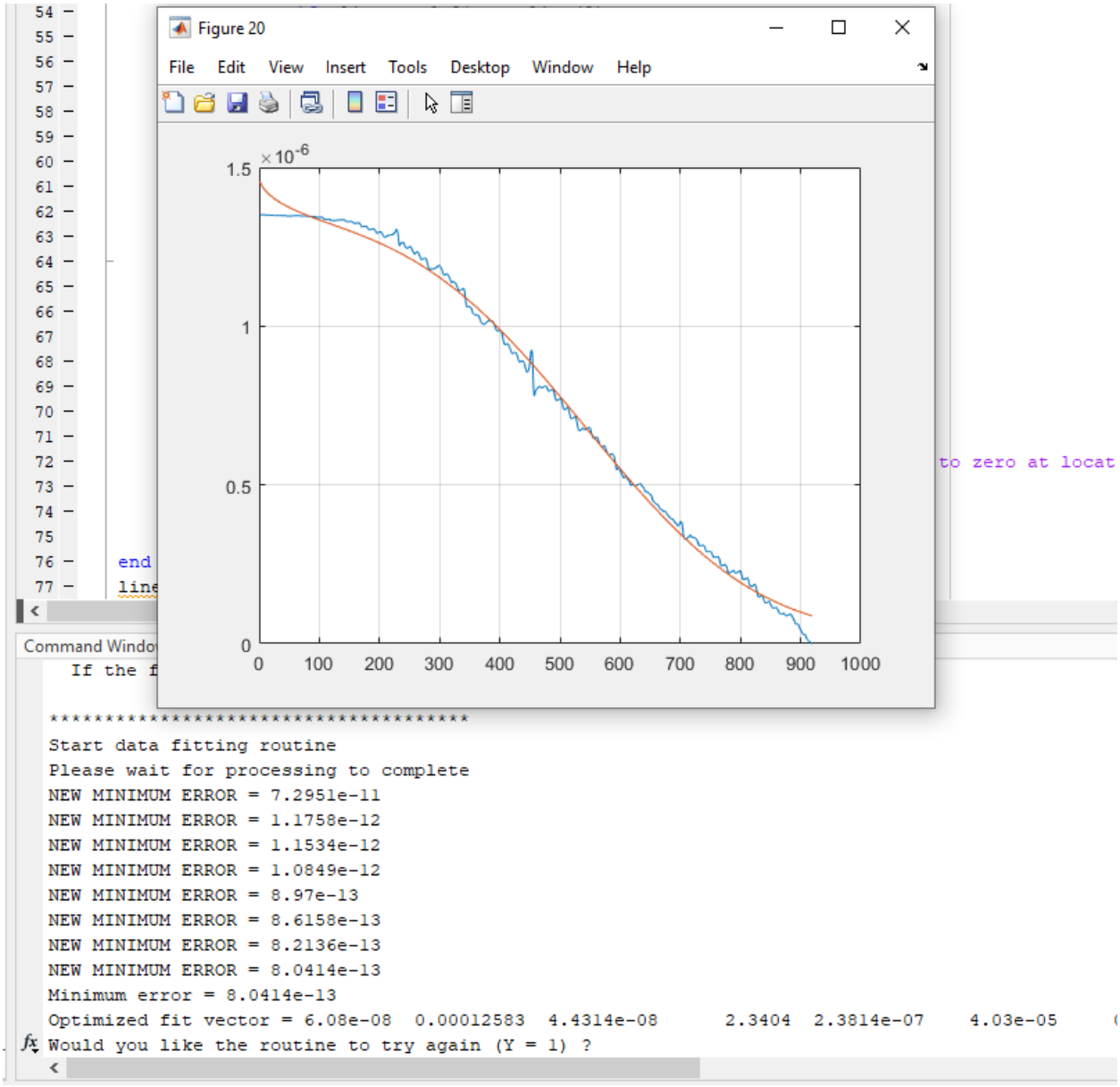

Figure 52 Curve fitting routine in progress.

In the case shown above, the curve fit does not capture the characterists of the profile data as well as it could and so it is performed again by entering in the value ‘1’ in to the command line. The fitting routine can be repeated as many times as needed. Once an appropriate curve fit is found as demonstrated below, the fitting routine can be exited by entering in any value other than ‘1’ into the command line.

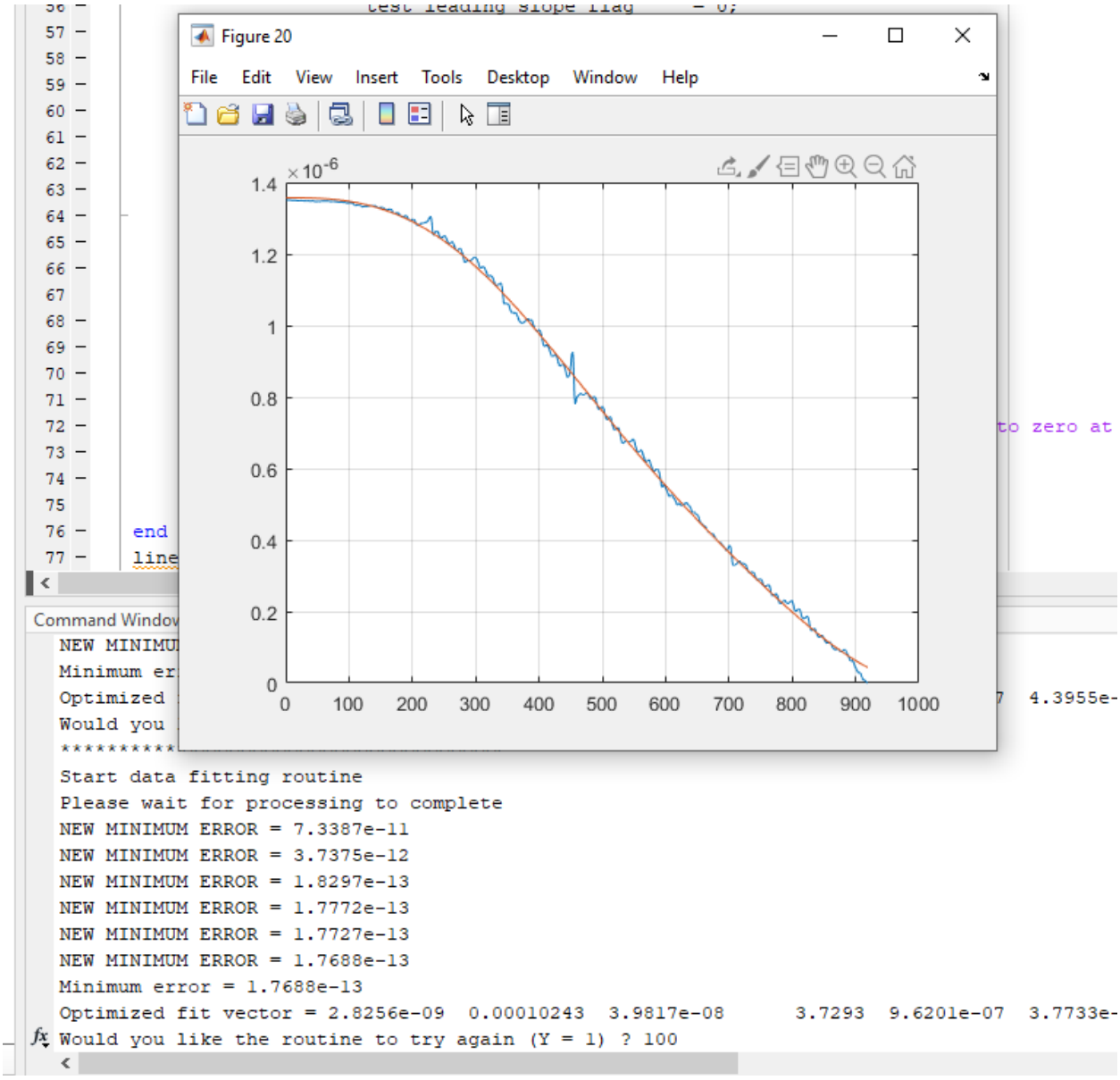

Figure 53 Successful curve fitting routine.

The curve fit data is then displayed in a labeled plot and options are given to the user on how they would like to proceed. The next step is to process the linearization by entering option '3' in to the command line.

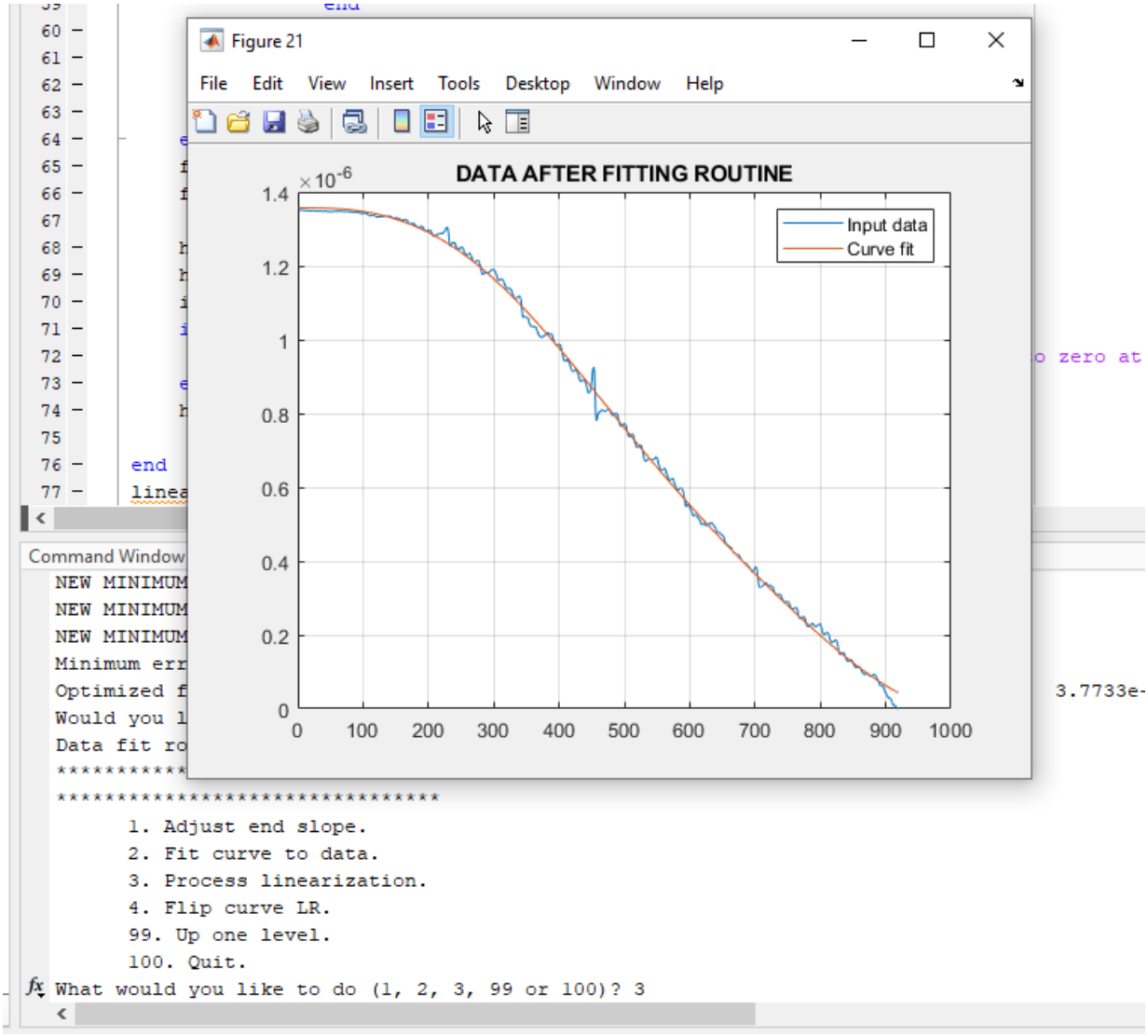

Figure 54 Curve fitting routine complete, selecting option 3 to move on and process the linearization.

The software will then display an Exposure range overlaid on the calibration curve of curve fit data. The options provided allow the user to change the offset and range of the exposure curve. The resist characteristics such as the refractive index as well as the wavelength used can also be input.

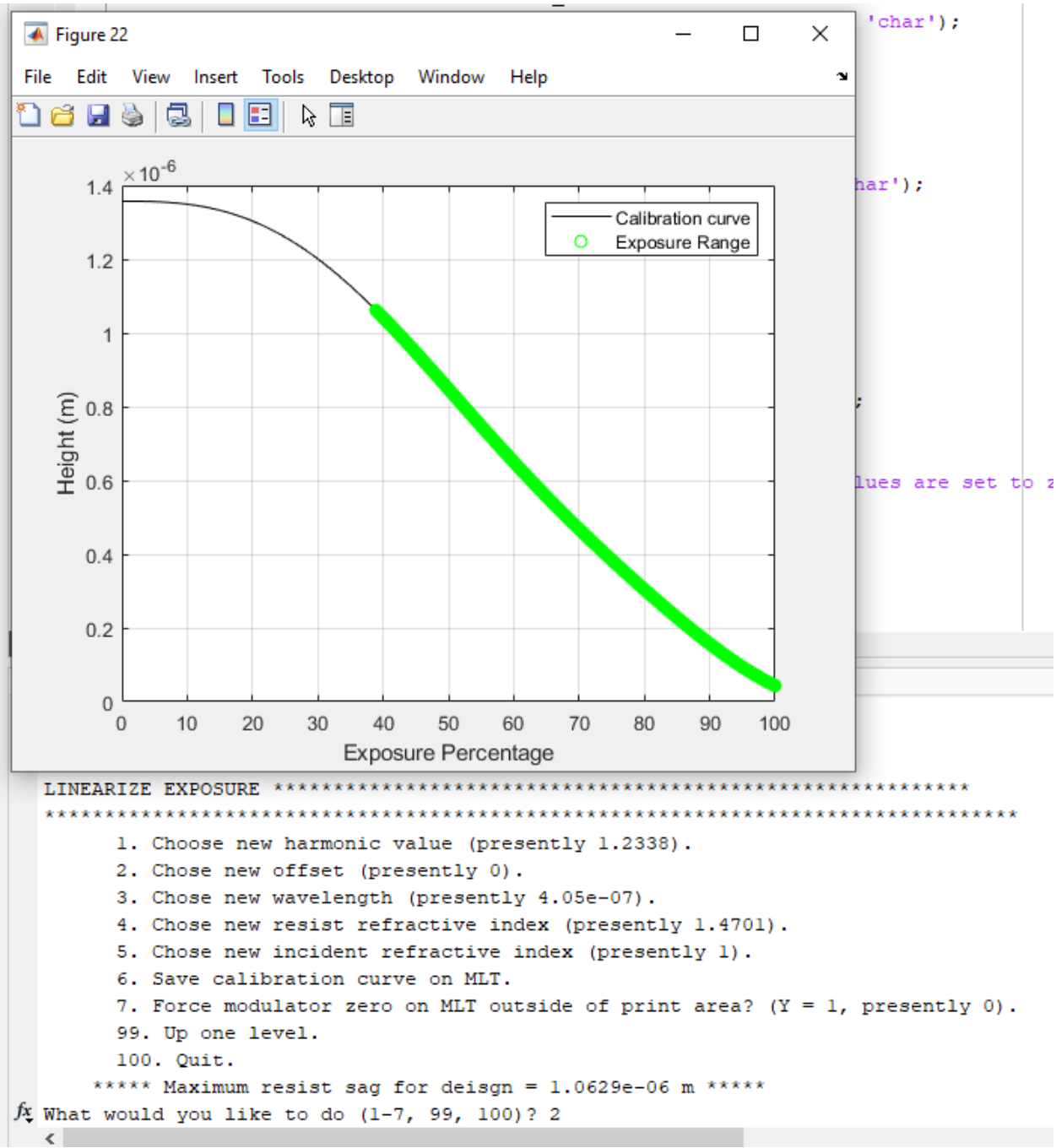

Figure 55 Initial processing of the linearization given curve fit data.

Choosing option ‘2’ will allow the user to indicate a new offset value. The offset value changes where the exposure curve begins, starting from the zero value on the calibration curve (in units of

meters). In this example, an offset value of 2×10^{-7} is chosen. The goal is to relocate the exposure range to the most linear-behaving section of the calibration curve.

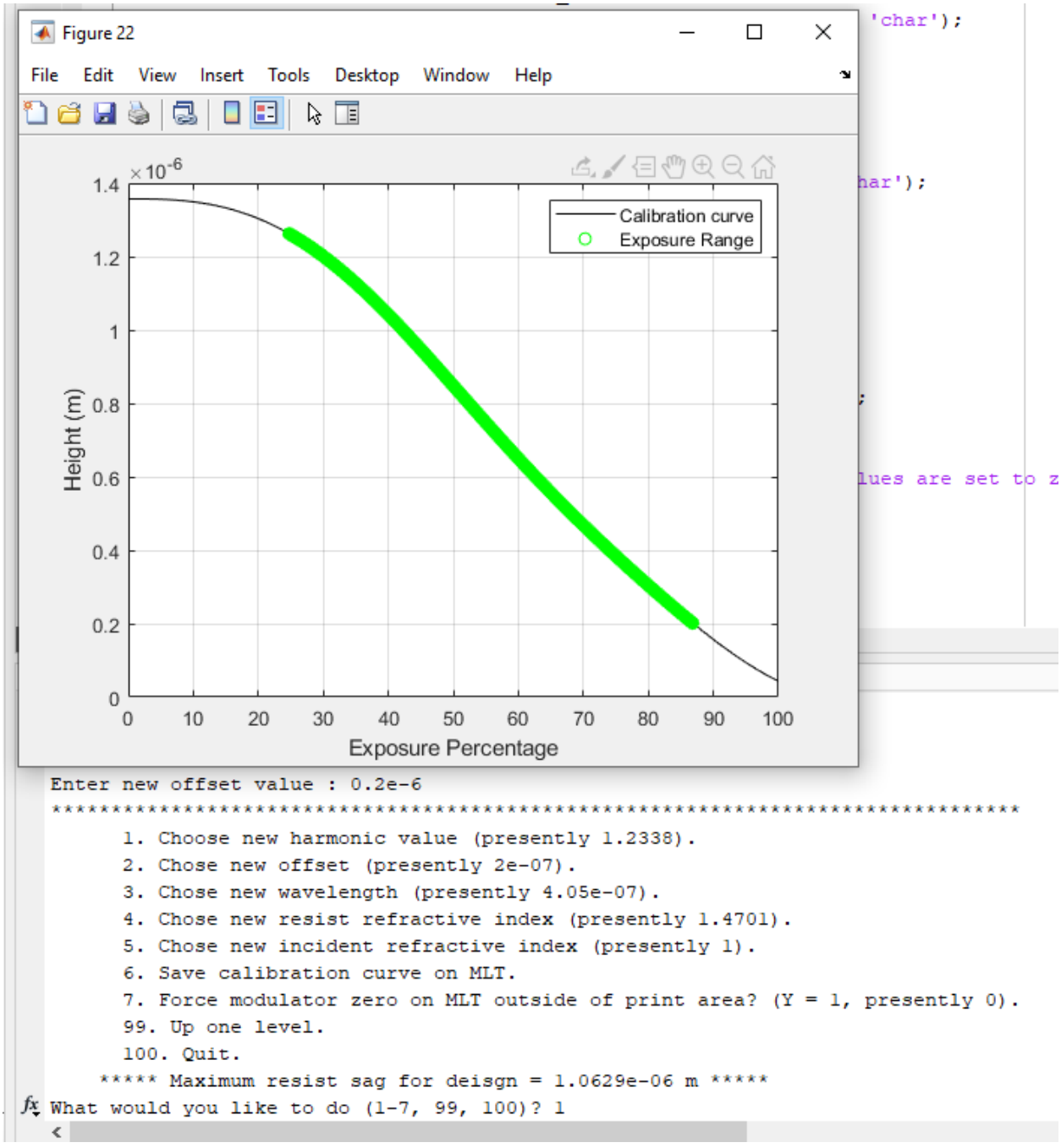

Figure 56 Resulting change on the location of the exposure range after changing the offset value.

Next the harmonic value can be changed by selecting option ‘1’ in the command line. The harmonic value changes the overall length of the exposure range over the width of the calibration curve. In this example the harmonic value is decreased to a value of 1. Choosing the value centers the exposure range over the linear region of the calibration curve and excludes the initial and ending regions of the calibration curve which act non-linearly.

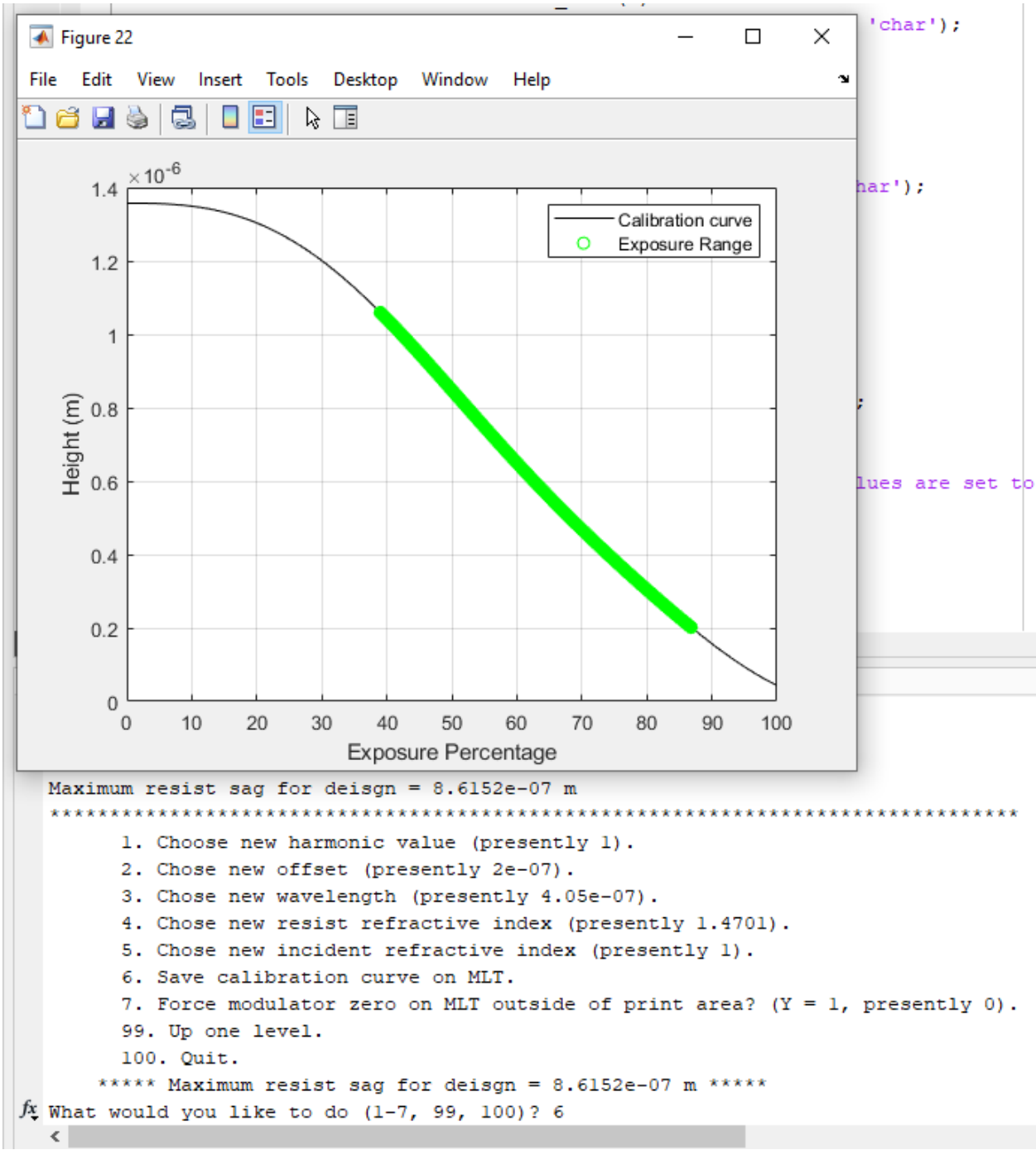

Figure 57 Choosing a new harmonic value. The exposure range is now correctly positioned.

Once the exposure curve is positioned to the users satisfaction over the calibration curve, the exposure has been linearized and a mapping table can now be created. This is done by selecting

option ‘6’ in the command line. The software will then display the Mapping Table and prompt the user to choose a file name and location for the mapping.

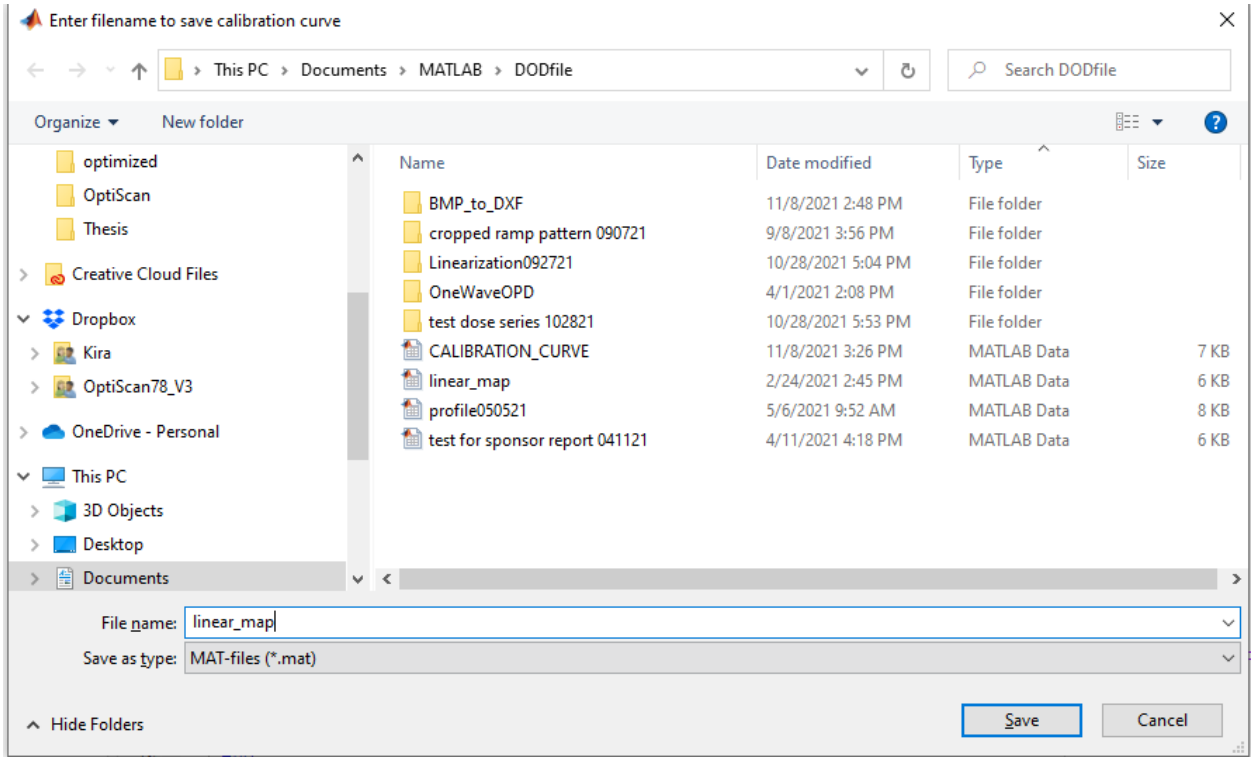

Figure 58 Prompting the user to choose a file name and location

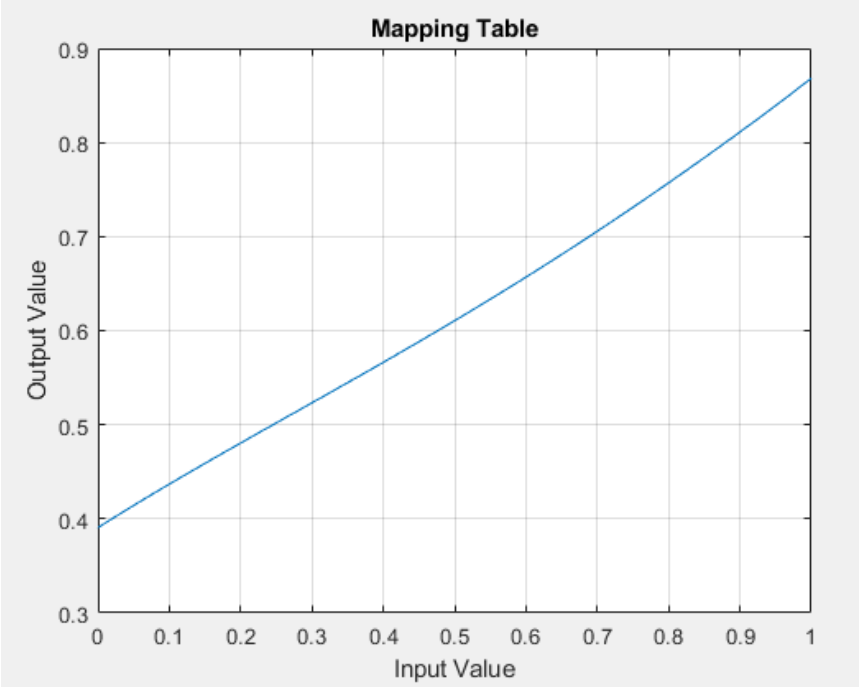

Figure 59 Final Mapping Table output from the Linearization Process. The table correlates an original dose value (x-axis) with a calibrated dose value (y- axis)

The mapping table can then be used with the Linearization Mapping Software to be applied to future exposure patterns. The resulting pattern will be calibrated for the photoresist and instrument characteristics such that the resulting exposure exhibits equal depth grayscale levels. The MATLAB code for this software is given in Appendix C.

10.1.3.1 Linearization Mapping Software

The use of the Linearization Process Software results in the output a Mapping table (in the form of a MATLAB .mat file) which correlates an instrument power (or dose) for a desired pattern height. This mapping is a calibration of the MLA 150 and can be applied to any grayscale .bmp image. Once applied the resulting exposure pattern will be calibrated to the MLA 150's dose characteristics as well as to the specified photoresist being used. This software features a simple scaling of pixel values in the input design in order to apply the Mapping table. The input design

to be calibrated is input as the variable ‘BMPfname’ and the Mapping Table is input as the variable “S”. The output is given as a linearized .bmp file. This linearized file can then be directly uploaded to the MLA 150 and converted on the instrument’s native software for use.

11 APPENDIX B

11.1 Photoresist Data Sheets

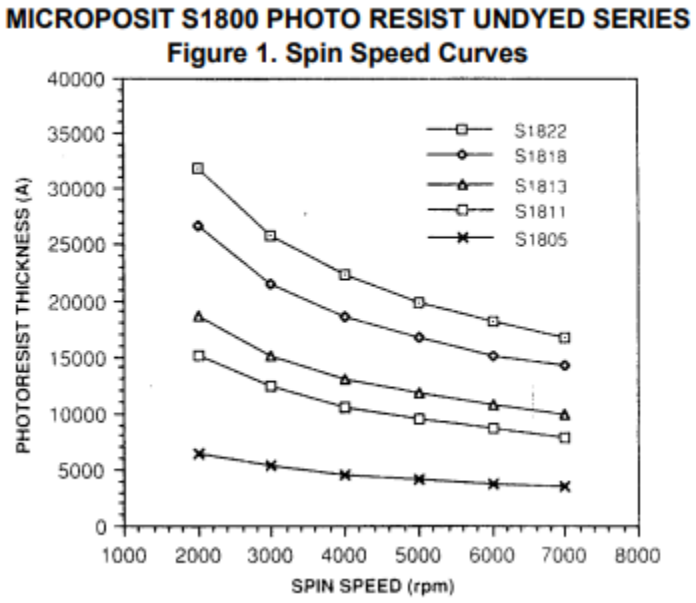

Figure 60 Photoresist thickness vs. Spin Speed for the S1800 series photoresist. S1813 and S1827 photoresists are included.

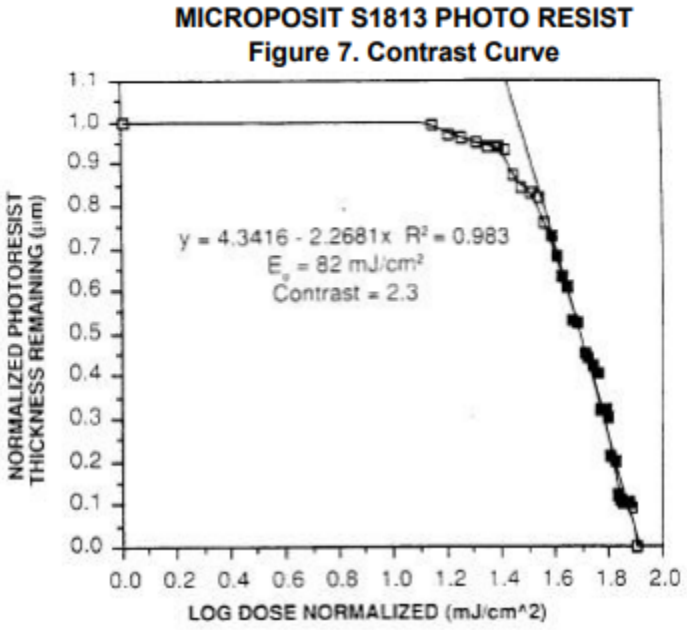

Figure 61 Normalized photoresist thickness vs. normalize dose (log) for S1813 photoresist.

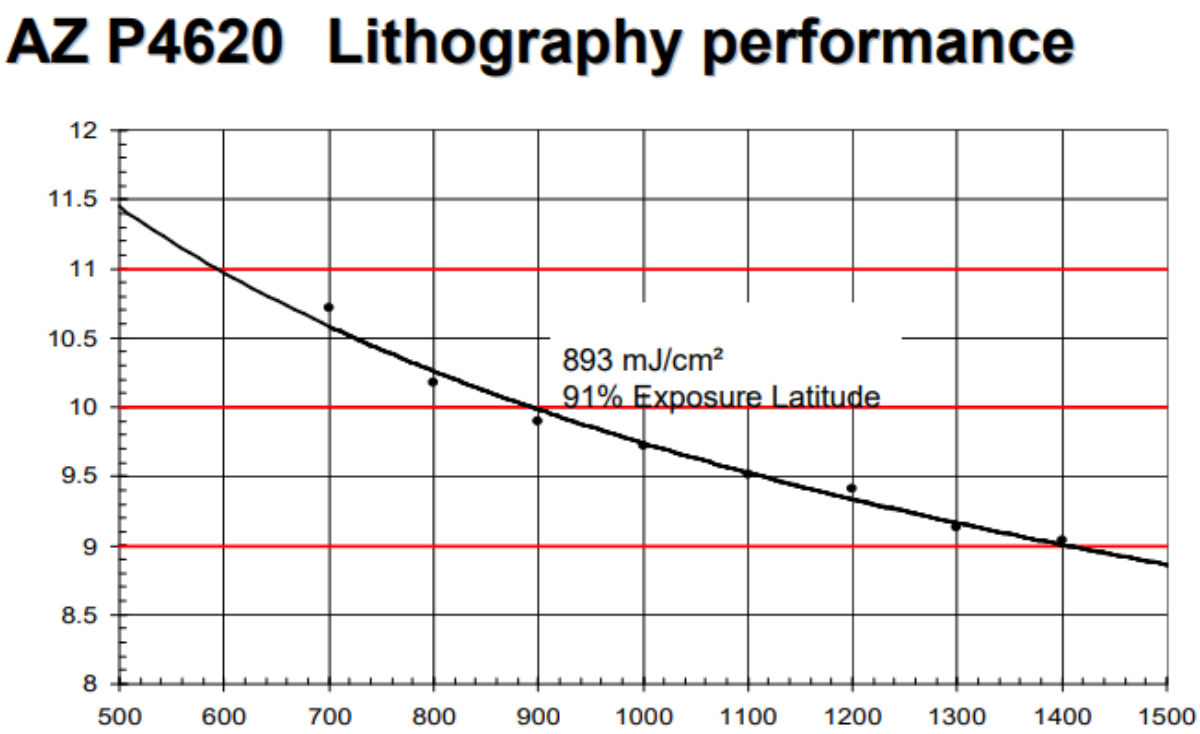

Figure 62 AZP4620 Lithography contrast curve. Photoresist depth vs. Dose

12 APPENDIX C

12.1 Linearization Process Code

```
%Linearization Process
%Created by Milster Research Group 2007
%Most recent revision 092721

function    [height_data, interface_flag_out] =
process_linearization_022321(varargin)

parameters          = varargin_to_struct( varargin{:} );

height_data         = eval('parameters.height_data',            '[]');
LAMBDA              = eval('parameters.lambda',                 '405e-9');
n_resist            = eval('parameters.n_resist',               '1.4701');
n_incident          = eval('parameters.n_incident',             '1.0');
differential_etch   = eval('parameters.differential_etch',      '1');
resist_type         = eval('parameters.resist_type',            '1');
harmonic_value      = eval('parameters.harmonic_value',         '1.2338');
zero_bmp_flag       = eval('parameters.zero_bmp_flag',          '0');
t_max               = eval('parameters.t_max',                  '0');
start_dir_Veeco     = eval('parameters.start_dir_veeco',
'''C:\Users\kpurv\Documents\MATLAB\DODfile''');
start_dir_MLT       = eval('parameters.start_dir_mlt',
'''C:\Users\kpurv\Documents\MATLAB\DODfile''');
project_directory   = eval('parameters.project_directory',
'''C:\Users\kpurv\Documents\MATLAB\DODfile''');
resist_dispersion_file = eval('parameters.resist_dispersion_file',
'''D:\MILSTER GROUP\Students - Vis scholars\Kira
Purvin\Linearization\resist_dispersion.dat''');
length_end_slope_calc = eval('parameters.length_end_slope_calc','40');
fig_id              = eval('parameters.fig_id',                 '20');
save_pname          = fullfile(start_dir_MLT,'linear_map.mat');
save_hd_pname       = fullfile(start_dir_MLT,'CALIBRATION_CURVE.mat');

if isempty(height_data)
    [filename, pathname] = uigetfile('*.csv', 'Pick a csv file containing the
Veeco ramp data',start_dir_Veeco);
    if isequal(filename,0)
        disp('User selected Cancel')
        return
    else
        pname           = fullfile(pathname, filename);
        disp(['User selected ', pname])
    end

    %process csv file
    fid1                = fopen(pname,'r');
    fid2                = fopen([pname(1:(end-4)) '.txt'],'w+');
```

```
    EOF_indicator      = 0;
    line               = fgetl(fid1);
    line               = fgetl(fid1);
    line               = fgetl(fid1);
    line               = uint8(0);
    test_leading_slope_flag     = 1;
    test_line         = 0;
    while test_line ~=-1
        test_line      = fgetl(fid1);
        index           = strfind(test_line,'---');
        for ii = 1:length(index)
            test_line(index(ii):(index(ii)+2))='NaN';
        end
        if isstr(test_line)
            test_line  = str2num(test_line);
        end
        if test_line ~=-1
            if test_leading_slope_flag
                if  line >= 0.9*test_line(2)
                    fwrite(fid2, [num2str(test_line(2)) ','], 'char');
                    test_leading_slope_flag     = 0;
                else
                    line        = test_line(2);
                end
            else
                fwrite(fid2, [num2str(test_line(2)) ','] , 'char');
            end
        end
    end
    fclose(fid1);
    fclose(fid2);

    height_data        = load([pname(1:(end-4)) '.txt']);
    height_data        = (height_data- min(height_data))*1e-6;
    index              = find(isnan(height_data));
    if ~isempty(index)
        disp(['*****WARNING: NaNs located in height data.  Values are set to
zero at locations ' num2str(index)])
    end
    height_data(index) = 0;

end
linearize_thickness= height_data;

interface_flag  = 1;
while interface_flag
    xvec        = linspace(0,100,length(height_data));
    figure(fig_id);plot(xvec,height_data);grid
    disp('********************************')
    disp('      1. Adjust end slope.')
    disp('      2. Fit curve to data.')
    disp('      3. Process linearization.')
    disp('      4. Flip curve LR.')
    disp('      99. Up one level.')
    disp('      100. Quit.')
```

```
    go_flag        = input('What would you like to do (1, 2, 3, 99 or 100)?
');
    if ~isempty(go_flag) & any(go_flag==[1 2 3 4 99 100])

        if go_flag  == 1

            %take out end slope
            end_slope       = sum(diff(height_data((end-
length_end_slope_calc):end)))/(length_end_slope_calc-1);
            height_data     = height_data -
end_slope*(1:length(height_data));
            height_data     = height_data- min(height_data);
            xvec            = linspace(0,100,length(height_data));
            figure(fig_id);plot(xvec,height_data);grid

        elseif go_flag == 2

            height_data         = fit_hight_data_curve(height_data,fig_id);

        elseif go_flag == 3

            save CALIBRATION_CURVE height_data
            save(save_hd_pname,'height_data')
            [harmonic_value,t_offset,interface_flag] =
choose_offset(harmonic_value,LAMBDA,n_resist,n_incident,differential_etch,t_m
ax,...

fig_id,save_pname,[],height_data,resist_type,resist_dispersion_file,zero_bmp_
flag);
            if interface_flag == 0
                interface_flag_out  = 0;
            end

        elseif go_flag == 4

            height_data         = fliplr(height_data);
            figure(fig_id);plot(xvec,height_data);grid

        elseif go_flag == 99

           interface_flag       = 0;
           interface_flag_out   = 1;

        elseif go_flag == 100

           interface_flag       = 0;
           interface_flag_out   = 0;

        end

    end
end

end
```

```
%*************************************************************************
%*************************************************************************
%                           Subroutines
%*************************************************************************
%*************************************************************************

%*************************************************************************
%                   Choose offset
%*************************************************************************
function [harmonic_value,t_offset,interface_flag_out] =
choose_offset(harmonic_value,LAMBDA,n_resist,n_incident,differential_etch,t_m
ax,...

fig_id,save_pname,xvec,height_data,resist_type,resist_dispersion_file,zero_bm
p_flag)

if t_max == 0
    t_max           = LAMBDA*harmonic_value/(n_resist-
n_incident)*differential_etch;
end
show_flag                       = 1;
fid                             = fig_id;
disp('LINEARIZE EXPOSURE
**********************************************************')
if ~exist('t_offset')
    t_offset                    = 0;
end
if ~exist('xvec') | isempty(xvec)
    xvec                = linspace(0,100,length(height_data));
end

interface_flag_out  = 1;
interface_flag = 1;
while interface_flag
    indx                        = find(height_data>=t_offset &
height_data<=(t_max+t_offset));

figure(fig_id+2);plot(xvec,height_data,'k',xvec(indx),height_data(indx),'go')
    xlabel('Exposure Percentage')
    ylabel('Height (m)')
    legend('Calibration curve','Exposure Range')
    grid;pause(0.1)
    if (t_max+t_offset)>max(height_data)
        disp('*****WARNING: Requested height too large for calibration.
Reduce offset and/or harmonic value.')
    end
    diff_height             = diff(height_data(indx));
    if any(diff_height)==0
        disp('*****WARNING: Non-unique height data in requested range.
Increase offset.')
    end


disp('**************************************************************************
**********')
```

```
    disp(['      1. Choose new harmonic value (presently '
num2str(harmonic_value) ').'])
    disp(['      2. Chose new offset (presently ' num2str(t_offset) ').'])
    disp(['      3. Chose new wavelength (presently ' num2str(LAMBDA) ').'])
    disp(['      4. Chose new resist refractive index (presently '
num2str(n_resist) ').'])
    disp(['      5. Chose new incident refractive index (presently '
num2str(n_incident) ').'])
    disp('      6. Save calibration curve on MLT.')
    disp(['      7. Force modulator zero on MLT outside of print area? (Y =
1, presently ' num2str(zero_bmp_flag) ').'])
    disp('      99. Up one level.')
    disp('      100. Quit.')
    disp(['    ***** Maximum resist sag for deisgn = ' num2str(t_max) ' m
*****'])
    go_flag        = input('What would you like to do (1-7, 99, 100)? ');
    if ~isempty(go_flag) & any(go_flag==[1 2 3 4 5 6 7 99 100])

        if go_flag  == 1

            %choose new harmonic value
            new_harmonic_value  = input('Enter new harmonic value : ');
            if ~isempty(new_harmonic_value)
                harmonic_value  = new_harmonic_value;
            end
            t_max               = LAMBDA*harmonic_value/(n_resist-
n_incident)*differential_etch;
            disp(['Maximum resist sag for deisgn = ' num2str(t_max) ' m'])

        elseif go_flag == 2

            new_t_offset        = input('Enter new offset value : ');
            if ~isempty(new_t_offset)
                t_offset        = new_t_offset;
            end

        elseif go_flag == 3

            %choose new wavelength value
            new_wavelength_value  = input('Enter new wavelength value (m) :
');
            if ~isempty(new_wavelength_value)
                LAMBDA  = new_wavelength_value;
                resist_index_mat = load(resist_dispersion_file);
                n_resist         =
interp1(resist_index_mat(:,1),resist_index_mat(:,2),LAMBDA);
            end
            t_max               = LAMBDA*harmonic_value/(n_resist-
n_incident)*differential_etch;
            disp(['Maximum resist sag for deisgn = ' num2str(t_max) ' m'])

        elseif go_flag == 4

            %choose new resist refractive index value
```

```
            new_resist_refractive_index_value  = input('Enter new resist
refractive index value : ');
            if ~isempty(new_resist_refractive_index_value)
                n_resist  = new_resist_refractive_index_value;
            end
            t_max               = LAMBDA*harmonic_value/(n_resist-
n_incident)*differential_etch;
            disp(['Maximum resist sag for deisgn = ' num2str(t_max) ' m'])

        elseif go_flag == 5

            %choose newincident refractive index value
            new_incident_refractive_index_value  = input('Enter new incident
refractive index value : ');
            if ~isempty(new_incident_refractive_index_value)
                n_incident  = new_incident_refractive_index_value;
            end
            t_max               = LAMBDA*harmonic_value/(n_resist-
n_incident)*differential_etch;
            disp(['Maximum resist sag for deisgn = ' num2str(t_max) ' m'])

        elseif go_flag == 6


process_data_and_save(height_data,t_max,t_offset,fig_id,save_pname,resist_typ
e,zero_bmp_flag);

        elseif go_flag == 7

            %choose zero bmp flag
            zero_bmp_flag  = input('Force zero bmp level outside of print
area (Y == 1)? : ');
            if isempty(zero_bmp_flag)
                zero_bmp_flag   = 0;
                disp('Modulator zero will not be forced outside of print
area.')
            elseif zero_bmp_flag ~= 1
                zero_bmp_flag   = 0;
                disp('Modulator zero will not be forced outside of print
area.')
            else
                disp('Modulator zero will be forced outside of print area.')
            end

        elseif go_flag == 99

            interface_flag      = 0;
            interface_flag_out  = 1;

        elseif go_flag == 100

            interface_flag      = 0;
            interface_flag_out  = 0;

        end
```

```
    end

end

end
%*************************************************************************
%                           exposure_fit_error
%*************************************************************************
function error_result = exposure_fit_error(x,xvec,height_data)

% exposure_curve      = @(x) x(1)*exp(x(2)+x(3)*0  - (x(4)*xvec.*xvec).^x(5))
+ x(6)*0*xvec.*exp(-(x(7)*xvec.*xvec).^x(8) + 0*x(9));

difference_data     = exposure_curve(x,xvec) - height_data';
if min(difference_data)~=difference_data(end)
    error_result    = 1000;
    %disp('E1')
end

if min(difference_data)~= min(height_data)
    error_result    = 1000;
    %disp('E2')
end

error_result        = sum( (difference_data).^2 );
if ~isreal(error_result)
    error_result    = 1000;
end

if any(diff(exposure_curve(x,xvec))>0)
    indx            = find(diff(exposure_curve(x,xvec))>0);
    error_result    = error_result + sum(difference_data(indx).^2);
end
end
%*************************************************************************
%                           exposure_curve
%*************************************************************************
function y = exposure_curve(x,xvec)

y           = x(1)*exp(x(2) - (x(3)*xvec.*xvec).^x(4)) + x(5)*exp(x(12)-
(x(6)*xvec.*xvec).^x(7)) + x(8)*exp(x(13)-(x(9)*xvec.*xvec).^x(10)) + x(11);
index       = find(y<0);
y(index)    = 0;
end
%*************************************************************************
%                           fit_height_data_curve
%*************************************************************************
function   height_data         = fit_hight_data_curve(height_data,fig_id);

%now fit curve
disp('This program calculates a fit to the height_data vector in a mat file
according to:')
disp(' fit function =  x(1)*exp(x(2) - (x(3)*xvec.*xvec).^x(4)) +
x(5)*exp(x(12)-(x(6)*xvec.*xvec).^x(7)) ...')
```

```
disp('               + x(8)*exp(x(13)-(x(9)*xvec.*xvec).^x(10))')
disp('The program uses the fminsearch Matlab function, so it has a tendency
to get ')
disp('  stuck in local minima.  Twenty five random perturbations of the
starting vector ')
disp('  are used to attempt a more global optimum.  The user can input a
starting ')
disp('  vector, if desired.  The height_data vector corresponds to resist
thickness, and it  ')
disp('  starts at zero exposure and ends at 100% exposure.  Thickness has
units of meters.')
disp('  There is no restriction on vector length, but it should have at least
50 points.')
disp('  If the fit is not very well, you can rerun the routine
automatically.')
pause(1)
disp(' ')

if ~(exist('height_data')==1)
    disp('*****ERROR: mat file does not contain a vector named height_data.')
    return
elseif any(~isreal(height_data))
    disp('*****ERROR: Imaginary data in height_data.')
    return
elseif length(height_data(:)) < 3
    disp('*****ERROR: Please use more data points for height_data.')
    return
end

height_data         = height_data(:);

x0_default          = [1.6e-007 7e-005 7e-008   3 4.5e-007 3e-005  1.4  9e-
007  1.5e-005  4 -1.6e-007 0 0];

repeat_flag         = 1;

new_x0_flag         = 0;
x0                  = x0_default;

xvec                = 1:length(height_data);
height_data_scaled  = height_data;

fval_min_base       = 1.1*exposure_fit_error(x0_default,xvec,height_data);
fval_min            = fval_min_base;
while repeat_flag == 1

    %exposure_curve      = @(x) x(1)*exp(x(2)+x(3)*0  -
(x(4)*xvec.*xvec).^x(5)) + x(6)*0*xvec.*exp(-(x(7)*xvec.*xvec).^x(8)
+0*x(9));
    x                   = x0;
    disp('************************************')
    disp('Start data fitting routine')
    disp('Please wait for processing to complete')
    %     keyboard
```

```
    for jj = 1:1
        front_factor            = 0.25;
        for ii = 1:25
            x0_trial            = x + front_factor*(0.5*rand(1,length(x0)) -
1).*x;
            indx                = find(x0_trial <0);
            x0_trial(indx)      = zeros(1,length(indx));
            [x_trial, fval, exitflag] = fminsearch(@exposure_fit_error,
x0_trial,...
                optimset('TolX',1e-
7,'MaxFunEvals',500,'Display','off'),xvec,height_data_scaled);
            if fval < fval_min & isreal(fval)
                fval_min        = fval;
                x_min           = x_trial;
                x               = x_trial;
                y_test          =  exposure_curve(x,xvec);
                figure(fig_id);plot([height_data';y_test]');grid
                disp(['NEW MINIMUM ERROR = ' num2str(fval)])
                front_factor    = front_factor*0.5;
            end
        end
    end

    disp(['Minimum error = ' num2str(fval_min)])
    disp(['Optimized fit vector = ' num2str(x_min)])
    repeat_flag             = input('Would you like the routine to try again
(Y = 1) ? ');
    if repeat_flag
        %reset_flag          = input('Would you like to reset the coefficient
vector (Y = 1) ? ');
        if 1 %reset_flag
            %new_x0_flag         = input('Would you like to enter your own
starting values (Y = 1) ? ');
            new_x0_flag     = 0;
            if ~isempty(new_x0_flag) & new_x0_flag == 1
                disp('Enter the starting vector')
                x0(1)           = input('Enter x1:');
                x0(2)           = input('Enter x2:');
                x0(3)           = input('Enter x3:');
                x0(4)           = input('Enter x4:');
                x0(5)           = input('Enter x5:');
                x0(6)           = input('Enter x6:');
                x0(7)           = input('Enter x7:');
                x0(8)           = input('Enter x8:');
                x0(9)           = input('Enter x9:');
            else
                %x0_default      = x0.*(0.1*rand(1,length(x0_default)));
                fval_min        = fval_min_base;
            end
        end
    end


end
disp('Data fit routine complete')
disp('*****************************************')
```

```
figure(fig_id+1);plot([height_data';y_test]');grid
title('DATA AFTER FITTING ROUTINE')
legend('Input data','Curve fit')
height_data           = y_test;

end
%************************************************************************
%                            process_data_and_save
%************************************************************************
function
process_data_and_save(height_data,t_max,t_offset,fig_id,save_pname,resist_typ
e,zero_bmp_flag)
if ~exist('linearize_thickness')
    linearize_thickness = height_data;
end
disp(['Thickness modulation range = ' num2str(t_offset) ' to '
num2str(t_max+t_offset) ' with amplitude = ' num2str(t_max)])

work_indx           = find( (linearize_thickness <= (t_offset + t_max)) &
(linearize_thickness >= t_offset) );

lin_xvec            = (-linearize_thickness(work_indx) +
linearize_thickness(work_indx(1)))/...
    (linearize_thickness(work_indx(1)) -
linearize_thickness(work_indx(end)));
lin_yvec            = work_indx/length(linearize_thickness);

indx                = find(lin_xvec>=0);
lin_xvec            = lin_xvec(indx);
lin_yvec            = lin_yvec(indx);

figure(fig_id+3);plot(lin_xvec,lin_yvec);grid
xlabel('Input Value')
ylabel('Output Value')
title('Mapping Table')

% output_map(index)   = uint8(255);
    [filename, pathname] = uiputfile('*.mat', 'Enter filename to save
calibration curve',save_pname);
    if isequal(filename,0)
        disp('User selected Cancel')
        return
    else
        save_pname       = fullfile(pathname, filename);
        disp(['User selected ', save_pname])
    end

save(save_pname,'lin_xvec','lin_yvec')

end
```

12.2 Application of Linearization Mapping Code

```
%Application of linearization mapping to .bmp exposure patterns
%Created by Milster Reserach Group 022421


%initial parameters
fignum      = 10;
BMPfname    = 'DOE_project_A_final.bmp';


%get map file
S           = load('linear_map2_040121.mat');
lin_xvec    = S.lin_xvec;
lin_yvec    = S.lin_yvec;

%get BMP
X           = double(imread(BMPfname));
[nr, nc]    = size(X);

%scale linear map
lin_xvec    = 255*lin_xvec;
lin_yvec    = 255*lin_yvec;

%linearize
Xout        = interp1(lin_xvec,lin_yvec,X(:),'spline');
indx        = find(isnan(Xout));
Xout(indx)  = zeros(1,length(indx));
Xout        = uint8(round(reshape(Xout,nr,nc)));

%Set min/max pixels for scaling
Xout(1,1)=uint8(1);
Xout(nr,nc)=uint8(255);

%view results
figure(fignum)
imagesc(X);colormap(gray);axis image
title('Original')
caxis([min(X(:)) max(X(:))])
figure(fignum+1)
imagesc(Xout);colormap(gray);axis image
title('Linearized')
caxis([min(X(:)) max(X(:))])

%Write image as .bmp and .png
imwrite(Xout,'onewaveOPDramp2_040121.bmp')
imwrite(Xout,'onewaveOPDramp2_040121.png')
```

13 APPENDIX D

13.1 File Conversion Code

```
%Bitmap to .dxf file conversion software V3
%Created by Milster Research Group 060921
%asumes DXF is set for scale of 0.010mm

%parameters
fignum          = 10;
%Input File and Location
fname_in        = 'C:\Users\kpurv\Documents\MATLAB\DODfile\test dose series
102821\lin102821_60d_s1827.bmp';
%Output File and Location
fname_out       = 'C:\Users\kpurv\Documents\MATLAB\DODfile\test dose series
102821\lin102821_60d_s1827.dxf';
fname_Header    = 'Header060321.mat';
fname_Closing   = 'Closing060321.mat';
scale           = 10;  %This scales each pixel to 10 microns
Layerheading    = 'L';
Layerending     = 'D0';
Polylinehead    = [{'0'} {'POLYLINE'} {'8'}];
% Polylinemid     = [{'70'} {'0'} {'40'} {'25'} {'41'} {'25'} {'66'} {'1'}
{'0'} {'VERTEX'} {'8'}];
Polylinemid     = [{'70'} {'0'} {'40'} {'10'} {'41'} {'10'} {'66'} {'1'}
{'0'} {'VERTEX'} {'8'}];
Nlevels         = 64;  %Number of grayscale levels - also number of layers

%load image file
X           = imread(fname_in,'bmp');
X           = round(double(X)/4);  %scale to 0:63
indx        = find(X==64);
X(indx)     = 63*ones(1,length(indx));
[nr, nc]    = size(X);

%Setup structs and vectors
Tablevec        = [{'0'} {'SECTION'} {'2'}  {'TABLES'} {'0'} {'TABLE'} {'2'}
{'LAYER'} {'70'} {'63'}];
Entitiesvec     = [{'0'} {'SECTION'} {'2'} {'BLOCKS'} {'0'} {'ENDSEC'} {'0'}
{'SECTION'} {'2'} {'ENTITIES'}];

%load header info (saved as cell vector)
S               = load(fname_Header);
Headervec       = S.Headervec;

%load closing info (saved as cell vector);
S               = load(fname_Closing);
Closingvec      = S.Closeingvec;

%make Tables section
```

```
for ii = 1:Nlevels
    layer_name  = [Layerheading num2str(ii-1) Layerending];
    Tablevec    = [Tablevec {'0'} {'LAYER'} {'70'} {'0'} {'62'} {num2str(ii-
1)} {'6'} {'CONTINUOUS'} {'2'} {layer_name}];
end
Tablevec        = [Tablevec {'0'} {'ENDTAB'} {'0'} {'ENDSEC'}];

%At this point, need to start writing DXF file, becuase the length of
%Polyline is so long
fileID          = fopen(fname_out,'w');
for ii = 1:length(Headervec)
    fprintf(fileID,[Headervec{ii} '\n']);
end
for ii = 1:length(Tablevec)
    fprintf(fileID,[Tablevec{ii} '\n']);
end
for ii = 1:length(Entitiesvec)
    fprintf(fileID,[Entitiesvec{ii} '\n']);
end

%Main Conversion Process
for ii = 1:nr
    disp(['Processing image line ' num2str(ii) ' out of ' num2str(nr)])
    imageline   = X(ii,:);  %Scan one line
    for jj = 0:(Nlevels-1)   %test for each level from 0:63
        indxjj  = find(imageline == jj);  %find which pixels have the value
        layer_name  = [Layerheading num2str(jj) Layerending];
        if ~isempty(indxjj) && (length(indxjj) > 1)  %process pixels with
that value when more than just one pixel
            Polylinevec     = [];
            [position_vec, length_vec]  = process_line(indxjj);
            for kk = 1:length(position_vec)
                xvalue_start    = scale*(position_vec(kk) - nc/2);
                xvalue_end      = scale*(position_vec(kk) + length_vec(kk) -
nc/2);
                yvalue          = scale*(ii-nr/2);
               Polylinevec = [Polylinevec Polylinehead {layer_name}
Polylinemid ...
                    {layer_name} ...
                    {'10'} {num2str(round(xvalue_start))} {'20'}
{num2str(round(yvalue))} ...
                    {'0'} {'VERTEX'} {'8'} {layer_name} ...
                    {'10'} {num2str(round(xvalue_end))} {'20'}
{num2str(round(yvalue))} ...
                    {'0'} {'SEQEND'} ...
                    ];
            end
            for kk = 1:length(Polylinevec)
                fprintf(fileID,[Polylinevec{kk} '\n']);
            end
        elseif ~isempty(indxjj) && (length(indxjj) == 1) %process pixels with
that value when just one pixel
            Polylinevec     = [];
            xvalue      = scale*(indxjj-nc/2);
            yvalue      = scale*(ii-nr/2);
            Polylinevec = [Polylinehead {layer_name} Polylinemid ...
```

```
                {layer_name} ...
                {'10'} {num2str(round(xvalue-scale))} {'20'}
{num2str(round(yvalue))} ...
                {'0'} {'VERTEX'} {'8'} {layer_name} ...
                {'10'} {num2str(round(xvalue))} {'20'}
{num2str(round(yvalue))} ...
                {'0'} {'SEQEND'} ...
                ];
            for kk = 1:length(Polylinevec)
                fprintf(fileID,[Polylinevec{kk} '\n']);
            end
        end
    end
end


%Print closing to file
for ii = 1:length(Closingvec)
    fprintf(fileID,[Closingvec{ii} '\n']);
end
fclose(fileID);


function [position_vec, length_vec]  = process_line(indxjj)

length_vec  = [];
for ii = 1:length(indxjj)
    if ii == 1
        position_vec    = indxjj(1);
        length_count    = 1;
    else
        DELTAindx   = indxjj(ii)-indxjj(ii-1);
        if DELTAindx == 1 && ii ~= length(indxjj)
            length_count    = length_count +1;
        elseif DELTAindx == 1 && ii == length(indxjj)
            length_count    = length_count +1;
            length_vec      = [length_vec length_count];
        elseif DELTAindx > 1  && ii ~= length(indxjj)
            length_vec      = [length_vec length_count];
            length_count    = 1;
            position_vec    = [position_vec indxjj(ii)];
        elseif DELTAindx > 1  && ii == length(indxjj)
            length_vec      = [length_vec length_count 1];
            position_vec    = [position_vec indxjj(ii)];
        end
    end
end
end
```

14 REFERENCES

[1] M. J. Madou, *Fundamentals of Microfabrication*. 2018. doi: 10.1201/9781482274004.

[2] M. McLean, "Encyclopedia of materials science and technology," *International Materials Reviews*, vol. 31, no. 1, 2012, doi: 10.1179/095066086790324285.

[3] Lee Craig Johnson, "Fabrication of Diffractive Optics using Grayscale and Binary Lithography," 2018.

[4] A. Grushina, "Direct-write grayscale lithography," *Advanced Optical Technologies*, vol. 8, no. 3–4, 2019, doi: 10.1515/aot-2019-0024.

[5] A. Rammohan, P. K. Dwivedi, R. Martinez-Duarte, H. Katepalli, M. J. Madou, and A. Sharma, "One-step maskless grayscale lithography for the fabrication of 3-dimensional structures in SU-8," *Sensors and Actuators, B: Chemical*, vol. 153, no. 1, 2011, doi: 10.1016/j.snb.2010.10.021.

[6] Claire E. Max, "Adaptive Optics: An Introduction."

[7] J. Porter, H. M. Queener, J. E. Lin, K. Thorn, and A. Awwal, *Adaptive Optics for Vision Science: Principles, Practices, Design, and Applications*. 2005. doi: 10.1002/0471914878.

[8] edmundoptics.com, "Introduction to Adaptive Optics and Deformable Mirrors," Feb. 29, 2016.

[9] R. W. Gerchberg and W. O. Saxton, "PRACTICAL ALGORITHM FOR THE DETERMINATION OF PHASE FROM IMAGE AND DIFFRACTION PLANE PICTURES.," *Optik (Stuttgart)*, vol. 35, no. 2, 1972.

[10] A. Eguchi and T. D. Milster, “Single-shot phase retrieval with complex diversity,” *Optics Letters*, vol. 44, no. 21, 2019, doi: 10.1364/ol.44.005108.

[11] R.W. Gerchberg, “System and method for recovering phase information of a wavefront,” 6,906,839, Jun. 14, 2005

[12] M. Köhler, *Etching in Microsystem Technology*. 1999. doi: 10.1002/9783527613786.

[13] P. Nussbaum, “Simple technique for replication of micro-optical elements,” *Optical Engineering*, vol. 37, no. 6, 1998, doi: 10.1117/1.601799.

[14] M. T. Gale, M. Rossi, and H. Schutz, “Fabrication and replication of continuous-relief does,” in *IEE Conference Publication*, 1993, no. 379.

[15] Mouser Electronivs, “Texas Instruments DLP Devices,” Aug. 03, 2021.

[16] S. Diez, “The next generation of maskless lithography,” in *Emerging Digital Micromirror Device Based Systems and Applications VIII*, 2016, vol. 9761. doi: 10.1117/12.2211052.

[17] Rohm and Haas, “Microposit S1800 G2 Series Photoresists For Microlithography Applicaions.”

[18] P. de Groot, “Principles of interference microscopy for the measurement of surface topography,” *Advances in Optics and Photonics*, vol. 7, no. 1, 2015, doi: 10.1364/aop.7.000001.

[19] Zygo Corporation, “NewView 8300 Specifications,” Mar. 2014.

[20] Tom D. Milster, “The DOE and CGH calculator,” Tucson, Arionza, 2012.

[21] AutoCAD, “DXF Reference,” 2012.